L-TYPE CA^{2+} CHANNEL MEDIATED CA^{2+} TRANSIENT DISCRIMINATES DIFFERENT FIRING PATTERNS IN HIPPOCAMPAL CA1 NEURONS: A MODELING STUDY.

by

JIHONG REN

B.E., Huazhong University of Science and Technology, 1995
M.E., Huazhong University of Science and Technology, 1998

A THESIS SUBMITTED IN PARTIAL FULFILMENT OF THE REQUREMENTS FOR THE DEGREE OF

Master of Science

in

THE FACULTY OF GRADUATE STUDIES

Graduate program in neuroscience

We accept this thesis as conforming to the required standards

The University of British Columbia

July 2000

In presenting this thesis in partial fulfilment of the requirements for an advanced degree at the University of British Columbia, I agree that the Library shall make it freely available for reference and study. I further agree that permission for extensive copying of this thesis for scholarly purposes may be granted by the head of my department or by his or her representatives. It is understood that copying or publication of this thesis for financial gain shall not be allowed without my written permission.

Department of Neuroscience

The University of British Columbia
Vancouver, Canada

Date Aug. 28th, 2002

Abstract

Evidence suggests an important role for L-type voltage sensitive Ca^{2+} channels (VSCCs) in activating immediate early genes (Murphy et al. 1991). To understand how L-type VSCCs regulate somatic and nuclear Ca^{2+} dynamics in response to different synaptic bursting waveforms that might be associated with unique forms of plasticity, we have modeled hippocampal CA1 neuron electrophysiology and intracellular Ca^{2+} dynamics. The model reproduces most of the eletrophysiological properties of hippocampal CA1 neurons, such as bursting vs. nonbursting behavior, AP frequency accommodation and AP back propagation. We examined Ca^{2+} influx through L-type VSCCs, and the resulting intracellular Ca^{2+} transient in response to simulated waveforms obtained with different presynaptic firing frequencies, active conductances and synaptic conductances. Simulation results suggest that L-type VSCCs prefer synaptic stimuli and conditions that result in a high depolarization plateau over other types of waveforms including repetitive APs, subthreshold EPSPs, or bursting firing. It was found that low activation potential and slow activation rate of L-type VSCCs contribute to the selective response of L-type VSCCs to firing patterns.

Pharmacological experiments and simulation results suggest an important role of intracellular Ca^{2+} stores in nuclear Ca^{2+} elevation in response to either single AP or tetanic synaptic stimulus. Moreover, previous studies in muscle suggest a specific spatial relationship between the L-type VSCCs and the ryanodine receptor. Therefore, we sought to determine whether a similar coupling between Ca^{2+} channels and stores would facilitate Ca^{2+}-induced Ca^{2+} release (CICR) action. Moving the Ca^{2+} stores away from the

Ca^{2+} channels (from 50 nm to 2 μm) resulted in a large reduction in the elevation of Ca^{2+} transient.

TABLE OF CONTENTS

ABSTRACT ii

TABLE OF CONTENTS iv

LIST OF TABLES vii

LIST OF FIGURES viii

ACKNOWLEDGEMENT x

CHAPTER 1 INTRODUCTION 1

1.1 Ca^{2+} channels 6

1.2 Ca^{2+} store 9

1.3 Co-localization of VSCCs with Ca^{2+} store 10

1.4 Research Hypothesis 11

CHAPTER 2 METHODS 14

2.1 Experimental procedure 14

2.2 Modeling hippocampal CA1 neuron 15

2.2.1 Introduction to NEURON simulator 16

2.2.2 Modeling hippocampal CA1 neuron eletrophysiology 17

2.2.2.1 Structure of model cell and electrotonic parameters 17

2.2.2.2 Ionic channel kinetics 19

2.2.3 Modeling intracellular Ca^{2+} dynamics 38

2.2.3.1 Ca^{2+} buffering 41

2.2.3.2 Diffusion of Ca^{2+} 42

2.2.3.3 Ca^{2+} Store 44

2.2.3.4 Ca^{2+} pumps and leak channels 45

CHAPTER 3 RESULTS **47**

3.1 Electrophysiological property reproduction 47

3.1.1 Bursting vs. Nonbursting behavior 47

3.1.2 AP backpropagation 49

3.1.3 Complex firing patterns in response to synaptic stimuli 52

3.2 Intracellular Ca^{2+} dynamics reproduction 55

3.2.1 Intracellular Ca^{2+} dynamics in response to single AP 55

3.2.2 Role of CICR 57

3.3 Intracellular Ca^{2+} dynamics in response to different firing patterns 61

3.3.1 L-type VSCCs distinguish different firing patterns 61

3.4 What properties of L-type VSCCs are important for firing pattern selection 67

3.5 Critical role of coupling between VSCCs and Ca^{2+} store 71

CHAPTER 4 DISCUSSION **73**

4.1 Significance of this study 73

4.2 Is the simple structure of our model enough to represent the complex properties of hippocampal CA1 neurons? 79

4.3 Shortcomings of the intracellular Ca^{2+} model 81

REFERENCES **84**

LIST OF TABLES

Table 1	Distribution of ionic channels	20
Table 2	Intracellular Ca^{2+} dynamics model parameters	39
Table 3	Intracellular Ca^{2+} dynamics in response to single AP – Comparison of experimental data and simulation results	57
Table 4	Group data: single AP leads to cytoplasmic and nuclear Ca^{2+} elevation that is sensitive to agents that deplete Ca^{2+} stores – CPA	59

LIST OF FIGURES

Figure 1 A model for the mechanism of L-type Ca^{2+} VSCC activation during synaptic stimulation. 13

Figure 2 Structure of NEUORN simulation environment. 17

Figure 3 Physical structure of hippocampal CA1 neuronal model. 19

Figure 4 Frequency dependent slow inactivation of sodium channels. 27

Figure 5 Properties of L-type VSCC model. 35

Figure 6 Intracellular Ca^{2+} dynamics model. 38

Figure 7 Simulated bursting vs. nonbursting behavior of hippocampal CA1 pyramidal neurons. 48

Figure 8 AP backpropagation. 51

Figure 9 Percentage of AP spike attenuation vs. distance from the soma with the indicated amounts of I_A for single or paired APs. 51

Figure 10 Complex firing patterns elicited by a 100 Hz synaptic tetanus in hippocampal pyramidal neurons. 54

Figure 11 Intracellular Ca^{2+} dynamics in response to single AP at 34°C. 56

Figure 12 Nuclear Ca^{2+} dynamics in response to AP trains with different frequencies, with and without CICR. 59

Figure 13 Role of CICR in intracellular Ca^{2+} dynamics in response to tetanic synaptic stimulation. 60

Figure 14 Ca^{2+} influx through L-type VSCCs in response to different firing patterns. 63

Figure 15 Ca^{2+} influx through P/Q-type VSCCs in response to

different firing patterns. 64

Figure 16 Nuclear Ca^{2+} dynamics in response to different firing patterns. 66

Figure 17 Impact of different half activation potentials on selective response of L-type VSCCs to different firing patterns. 68

Figure 18 10%-90% rise time of L-type Ca^{2+} current in response to different levels of step depolarization. 69

Figure 19 Impact of different opening rates on selective response of L-type VSCCs to different firing patterns. 70

Figure 20 Critical role of spatial coupling between VSCCs and Ca^{2+} stores. 72

Acknowledgement

I would like to express my sincere appreciation to my supervisor, Dr. Timothy Murphy, for his inspiration, patience and guidance during my studies in the Neuroscience program. He allowed me the freedom to choose a topic most interesting to me and at the same time most suitable for my background. Without his encouragement and always-valuable advice, it is impossible for me, as a layman with little knowledge in neuroscience two years ago, to conduct the research in this thesis today.

Also I would like to express my appreciation to Dr. Nicholas Swindale for his suggestions and help during the research and his time of reading my thesis and giving valuable suggestions.

Also I would like to thank other members in my supervisory committee: Dr. Terry Snutch and Dr. Robert Miura, as well as Dr. Lynn Raymond and Dr. Nansheng Chen for their suggestions and enlightening discussions during the research. I thank Tao Luo, Jessica Yu, Sabrina Wang for their technical support. Thanks go out to many of my fellows at UBC, but especially to those with whom I shared the lab, not only for their day-to-day help in the lab but also good times outside the lab.

Finally, I would like to thank my parents, Dehui Wu and Xuemei Ren, who have always offered encouragement regardless of my choices.

Chapter 1 Introduction

Over the last several decades, neuroscientists have made considerable efforts to understand basic mechanisms underlying learning and memory. At the cellular level, one common hypothesis is that neuronal information critical for memory may be encoded via synaptic plasticity, activity-dependent changes in synaptic structure and strength. A persistent increase in synaptic strength commonly known as long-term potentiation (LTP) can be rapidly induced by brief neuronal activity. It has received extensive study during the last few decades as an in vitro model of activity-dependent synaptic plasticity. How does neuronal activity lead to lasting adaptive changes? One hypothesis is that it is activity-dependent regulation of gene expression that mediates long-lasting changes in neuronal structure and function (Pittenger and Kandel, 1998). Evidence from animal models that are deficient for the immediate-early genes (IEGs) *c-fos* and FosB suggest an important role of gene expression in the long-lasting functional changes that underlie some adaptive responses induced by neuronal activity (Brown et al., 1996; Finkbeiner and Greenberg, 1998; Watanabe et al., 1996). Moreover, the role of activity-dependent gene expression in synaptic plasticity has been extensively studied in LTP. It was found that in the first few hours after LTP induction, there is increased gene expression activity. The early phase of LTP induced by brief tetanus appears resistant to inhibitors of protein synthesis and gene transcription (Sossin, 1997), whereas a longer lasting phase of LTP (> 3hr) is blocked (Frey et al., 1988; Frey and Morris, 1998; Nguyen et al., 1994). These inhibitor studies suggest a two-phase model of LTP, in which the early phase of LTP is likely mediated by modifications to existing proteins, such as phosphorylation, whereas

the later phase requires new gene expression and protein synthesis (reviewed in Finkbeiner and Greenberg (1998)).

How could various patterns of synaptic activity couple with the activation of nuclear transcription factors and thus regulate neuronal gene expression? There are a number of ways by which activated synapses might send signals to the nucleus (reviewed in Bito et al. (1997)). For example, microdomains of postsynaptic Ca^{2+} near the plasma membrane can activate type I adenylyl cyclase to produce cyclic AMP, which can either diffuse into the nucleus or can activate PKA, causing it to translocate into the nucleus (Bacskai et al., 1993). Moreover, Ca^{2+} can activate the ras/MAPK cascade (Bading and Greenberg, 1991; Kawasaki et al., 1997). (Martin et al., 1997) showed that MAP kinase translocates into the nucleus during the induction of LTP in Aplysia. Deisseroth et al. (1996) have suggested that Ca^{2+} influx through N-Methyl-D-aspartate (NMDA) receptors or L-type voltage-sensitive Ca^{2+} channels (VSCCs) might activate co-localized calmodulin (CaM) and that the activated CaM translocates into the nucleus, resulting in cAMP responsive element-binding protein (CREB) phosphorylation. In contrast to the studies of Deisseroth et al. (1996), Hardingham et al. (1997) have shown that, in order for CREB to induce transcription, it is necessary for Ca^{2+} to invade the nucleus. Meberg et al. (1996) showed that Ca^{2+}-sensitive transcriptional regulator NF-kappa B (NF-kB) mediated gene expression in the hippocampus is increased by augmented synaptic activity. NF-kB exists in cytoplasm as complex with the inhibitor I-kB. Cytoplasmic Ca^{2+} elevation may activate calcineurin which dephosphorylates the complex and induces its dissociation leading to translocation of the active subunits to the nucleus, resulting in gene expression (Meldolesi,

1998). Although this is an extensive network of interactions, it is clear that Ca^{2+} plays a critical role in neuronal gene transcription.

Besides alterations in gene expression, intracellular Ca^{2+} elevation can trigger various processes including neurotransmitter release, modulation of synaptic transmission and excitotoxic cell death (Ghosh and Greenberg, 1995). Although the physiological concentration of extracellular Ca^{2+} is in the mM range, the resting intracellular Ca^{2+} concentration is around 50 – 100 nM. This huge concentration gradient across the plasma membrane is maintained by the following mechanisms (reviewed in Berridge (1998)). **1)** Endogenous Ca^{2+} buffer in the form of Ca^{2+} binding proteins with various degrees of affinity, fixed or mobile. **2)** Various Ca^{2+} transporters, such as Ca^{2+} pumps and Na^{+}-Ca^{2+} exchangers, continuously extrude Ca^{2+} from the cytoplasm to extracellular space or into intracellular Ca^{2+} stores. The mechanisms described above lead to greatly restricted intracellular mobility of Ca^{2+} and make it an excellent local messenger (Llinas and Moreno, 1998). Intracellular Ca^{2+} concentration can be increased by Ca^{2+} influx through Ca^{2+} permeable ion channels, and by Ca^{2+} release from internal Ca^{2+} stores (Berridge, 1998). There are various types of Ca^{2+} channels with distinct electrophysiological and pharmacological properties and sub-cellular distribution (discussed below). The complex distribution profile of different types of Ca^{2+} channels, together with the restricted intracellular mobility of Ca^{2+}, achieves temporal and spatial compartmentalization of Ca^{2+} signaling during neuronal activity (Roberts, 1994).

Plasma membrane Ca^{2+} permeable ion channels consist of two groups: voltage (VSCCs) and ligand-gated. VSCCs include high voltage-activated (HVA) Ca^{2+} channels, such as P/Q, L, R-type Ca^{2+} channels, and low voltage-activated (LVA) Ca^{2+} channels,

such as T-type Ca^{2+} channels (Ertel et al., 2000). Ligand-gated Ca^{2+} channels include NMDA receptors, neuronal acetylcholine receptors (nAchRs), the type 3 serotonin receptors (5HT3Rs) and the Ca^{2+} permeable α-amino-3-hydroxy-5-methyl-4-isozazolepropionic acid (AMPA) and kainate glutamate receptors (Ghosh and Greenberg, 1995). Among these Ca^{2+} channels, evidence suggests an important role for both L-type VSCCs and NMDA receptors in activating IEGs (Bito et al., 1997; Murphy et al., 1991). IEGs are rapidly and transiently transcribed in response to a variety of extracellular signals. Several IEGs, including *c-fos*, encode transcription factors and control secondary programs of gene expression that may ultimately result in functional and structural changes to neurons (Bading et al., 1993). Bading et al. (1993) reported that treatment of hippocampal neurons with glutamate caused a rapid increase in *c-fos* transcription and this increase can be blocked by selective NMDA receptor antagonist D(-)-2-amino-5-phosphonovalerate (APV) or the addition of ethyleneglycol-bis-(β-amino-ethyl)-tetraacetic acid (EGTA) in bath solution, indicating important role of transmembrane Ca^{2+} through NMDA receptors. In addition, exposure to L-type VSCC antagonists or agonists rapidly suppresses or increases basal expression of several IEGs driven by spontaneous activity respectively (Murphy et al., 1991). Intuitively, it may be expected that the important role of L-type VSCCs in activity-dependent gene expression might be because they may be responsible for the intracellular Ca^{2+} elevation during synaptic or action potential (AP) stimuli. If so, the effect of L-type VSCC antagoinsts and agonists on basal expression of IEGs would be via suppressing and boosting intracellular Ca^{2+} elevation respectively. In contrast, most reports show a relatively small role for L-type VSCCs in mediating Ca^{2+} influx in response to synaptic or AP stimuli (Christie et al., 1995; Regehr and Tank, 1992).

Besides extracellular Ca^{2+}, there is an intracellular supply of Ca^{2+} stored within the endoplasmic reticulum (ER) of neurons. Inositol 1,4,5-tris-phosphate receptors (IP_3Rs) and ryanodine receptors (RyRs) are two types of Ca^{2+} channels distributed on the ER that are responsible for releasing Ca^{2+} from this intracellular Ca^{2+} store. Intracellular Ca^{2+} stores play an important role in controlling the intracellular Ca^{2+} concentration and shaping intracellular Ca^{2+} dynamics (Jacobs and Meyer, 1997; Usachev and Thayer, 1997). Recently, it was reported that blocking intracellular Ca^{2+} release from Ca^{2+} stores decreases synaptic activity induced gene transcription activity by ~50% (Hardingham et al., 1999).

The downstream events after activation of L-type VSCCs leading to gene expression are still a compelling question. Contradictory conclusions have been reached by different studies regarding the role of nuclear Ca^{2+} transients in triggering gene expression (Deisseroth et al., 1996; Hardingham et al., 1997). CREB has been suggested to play a central and highly conserved role in the production of protein synthesis-dependent long-term changes in synaptic strength and neuronal structure (Mayford et al., 1995; Stevens, 1994). The abrupt change in phosphorylation level of CREB serves as an early indicator of nuclear events that lead to gene expression. From the Deisseroth studies, it was suggested that Ca^{2+} influx through L-type VSCCs activates cytoplasmic Ca^{2+} targets such as CaM, the Ca^{2+}-CaM complex then translocates to the nucleus leading to CREB phosphorylation and gene expression. In contrast, studies by Hardingham suggested that activation of L-type VSCCs produces an elevation of nuclear Ca^{2+} concentration that triggers gene expression by interaction with nuclear CaM kinase IV. In the present work, we are interested in nuclear Ca^{2+} dynamics during synaptic stimuli. For the following

reasons we argue against models suggesting that cytoplasmic Ca^{2+} elevation is critical for activity-dependent gene expression. **1)** CaM is a large protein hence its translocation from cytoplasm to the nucleus is not a trivial issue for cell to manipulate. We believe that activated Ca^{2+} bound CaM would have a short half life preventing the intact complex from reaching the nucleus. **2)** CaM already exists in the nucleus and would therefore not need to translocate (Santella and Carafoli, 1997). **3)** Recently, it was reported by Hardingham et al 1999 that the presence of phosphorylated CREB is not sufficient for transcriptional activation since additional steps are required. They proposed that the additional step is targeted at CREB-binding protein (CBP), and CBP-dependent transcription is controlled by nuclear Ca^{2+} and Ca^{2+}/CaM dependent protein kinase IV. **4)** There are also some nuclear transcription factors such as DREAM which are themselves Ca^{2+} dependent (Carrion et al., 1999) which further supports the importance of nuclear Ca^{2+} flux in regulating gene expression. Therefore, in the present work, we are particularly interested in the role of L-type VSCCs as well as intracellular Ca^{2+} stores in nuclear Ca^{2+} dynamics during synaptic stimuli associated with plasticity.

1.1 Ca^{2+} channels

VSCCs are involved in the regulation of a variety of neuronal functions and neurotransmitter release (Sabria et al., 1995). Research in recent years has demonstrated numerous subtypes of VSCCs, which can be differentiated on the basis of their molecular, pharmacological and electrophysiological properties (Ertel et al., 2000). There are at least five types of high-threshold VSCCs (L, N, P, Q, and R) and one type of low-threshold VSCCs (T).

At the molecular level, they have the same configuration, composed of the main pore performing α_1 subunit, the accessory α_2 and β subunits, and some optional subunits such as γ, δ subunit in cardiac L-type VSCCs. Eight distinct α_1 subunits are expressed in the mammalian CNS (α_{1A}, α_{1B}, α_{1C}, α_{1D}, α_{1E}, α_{1G}, α_{1H} and α_{1I}) (Ertel et al., 2000). Functional expression and immunoprecipitation studies have demonstrated that α_{1C} and α_{1D} encode L-type VSCCs (Hell et al., 1993; Williams et al., 1992), whereas α_{1B} encodes N-type VSCCs (Stea et al., 1993; Westenbroek et al., 1992). It is generally accepted that differentially spliced forms of α_{1A} are components of P/Q-type VSCCs (Bourinet et al., 1999; Stea et al., 1994; Westenbroek et al., 1995). α_{1E} shows some features similar to R-type VSCCs (Westenbroek et al., 1998; Zhang et al., 1993). Channels containing α_{1G}, α_{1H}, and α_{1I} are believed to mediate T-type Ca^{2+} currents (Ertel et al., 2000).

In terms of pharmacological properties, N-type VSCCs are sensitive to ω-conotoxin GVIA (GVIA) (Tsien et al., 1988), whereas P/Q-type VSCCs are blocked by ω-conotoxin MVIIC (MVIIC) (Randall and Tsien, 1995). P/Q-type VSCCs have different sensitivity to ω-Aga-IVA (IC_{50}s of ~1 nM for P-type and ~0.1 μM for Q-type) (Randall and Tsien, 1995). L-type VSCCs preferentially bind 1,4-dihydropyridines (DHP) (Mori et al., 1991; Sabria et al., 1995; Tsien et al., 1988) and have unique electrophysiological properties. It was found that L-type VSCCs activate at more negative membrane potentials and more slowly than non-L-type HVA VSCCs (Mermelstein et al., 2000). L-type VSCCs show fairly little voltage-dependent inactivation which was shown by Ba^{2+} current experiments, but are profoundly sensitive to Ca^{2+} (Hofer et al., 1997). The Ca^{2+}-dependent inactivation of L-type VSCCs is suppressed if current carrier is Ba^{2+} instead of Ca^{2+} (Brehm and Eckert, 1978). For molecular mechanisms that initiate Ca^{2+}-dependent

inactivation, recent studies by (Peterson et al., 1999; Zuhlke et al., 1999) suggest that CaM acts as both Ca^{2+} concentration sensor and the mediator of the feedback effects of Ca^{2+} influx on L-type VSCC function. In contrast, P/Q-type VSCCs show voltage-dependent inactivation as well as Ca^{2+}-dependent inactivation (Forsythe et al., 1998; Lee et al., 1999). The Ca^{2+}-dependent inactivation of P/Q-type VSCCs is different from that of L-type VSCCs since it shows little selectivity between different divalent cations (Forsythe et al., 1998).

Besides kinetic properties of calcium channels, subcellular localization is another critical determinant of their physiological roles, such as whether they participate in regulation of gene expression, action potential generation, or neurotransmitter release. α_{1C} and α_{1D} which encode L-type VSCCs, have been shown to be localized predominantly in the soma and proximal dendrites of neurons throughout the brain (Hell et al., 1993; Williams et al., 1992) where they may participate in regulation of activity-dependent gene expression (Murphy et al., 1991). α_{1A} is distributed mainly in presynaptic terminals and dendritic shafts in brain neurons. This distribution profile is also consistent with the role of P/Q-type VSCCs in triggering neurotransmitter release and activating Ca^{2+} dependent messengers in dendrites (Jun et al., 1999). Immunochemical staining of α_{1A} extends along the entire length of the apical dendrites of CA1 pyramidal neurons (Westenbroek et al., 1998).

1.2 Ca^{2+} store

There is an elaborate endoplasmic reticulum that extends throughout the neuronal cell body. It appears to be a continuous membrane system, from outer nuclear membrane to axon terminal and dendrites (Martone et al., 1993). ER contains a relatively higher resting free Ca^{2+} concentration compared to the cytoplasm (Berridge, 1998; Verkhratsky and Petersen, 1998). The existence of this internal store of Ca^{2+} has a profound effect on shaping neuronal Ca^{2+} signals (Garaschuk et al., 1997). IP_3Rs and RyRs on this continuous network, responsible for Ca^{2+} release, are capable of regenerative Ca^{2+} release, which enables Ca^{2+} store to play an active role in neuronal Ca^{2+} signaling. They both are sensitive to Ca^{2+} and are capable of displaying the phenomenon of Ca^{2+} - induced Ca^{2+} release (CICR) (Berridge, 1998). IP_3Rs, although gated by IP_3, are also stimulated by Ca^{2+} (Bezprozvanny et al., 1991). IP_3 responses will thus in a crude way resemble that of RyRs. Thus, for simplicity, in the present work, only RyRs were taken into consideration.

The basic idea is that intracellular Ca^{2+} elevation mediated by plasma membrane Ca^{2+} channels, subsequently activates Ca^{2+} channels on internal stores, resulting in an amplification of an influx signal by release of Ca^{2+} from internal stores. This allows information to spread long distances in spite of the existence of strong Ca^{2+} buffers in cytoplasm (Berridge, 1998). Pharmacological studies suggested a role of Ca^{2+} stores in mediating synaptic plasticity. It was concluded that the induction of LTD by low frequency stimulation depends on a Ca^{2+} influx via VSCCs, which is then augmented by Ca^{2+} release from the internal stores through the RyRs (Wang et al., 1997). Inhibitors of the Ca^{2+} pump on Ca^{2+} stores, such as thapsigargin, were found to inhibit the onset of both LTP (Wang et al., 1997) and LTD (Reyes and Stanton, 1996). Hardingham et al. (1999)

found that blocking CICR reduced CREB phosphorylation by ~50%, which is possibly caused by reduction of nuclear Ca^{2+} elevation after blocking RyRs.

1.3 Co-localization of VSCCs with Ca^{2+} store

It is well documented that L-type channels are coupled to RyRs. In skeletal muscle, L-type VSCCs act as voltage sensors to control RyRs on sarcoplasmic reticulum (Nakai et al., 1996) and in turn RyRs generate a retrograde signal that modifies L-type VSCC activity (Grabner et al., 1999; Nakai et al., 1998). In cardiac cells, there is cross signaling between L-type VSCCs and RyRs (Sham et al., 1995). This kind of functional coupling is also found in neurons (Chavis et al., 1996).

Immunocytochemical and biochemical studies have demonstrated localization of RyRs in neuronal cell bodies, dendrites and axons (Padua et al., 1996). Although influx of extracellular Ca^{2+} triggers neurotransmitter release (Borst and Sakmann, 1996), several reports suggest intracellular Ca^{2+} release mediated by RyRs may play a major role in modulating neurotransmitter release (Peng, 1996; Smith and Cunnane, 1996) and the induction of both LTP and LTD (Wang et al., 1997; Wang et al., 1996). The localization of RyRs on terminal as well as VSCCs (N-type and P/Q type) and their important role in transmitter release implicate that there probably exists some kind of coupling between them. Recently, Sutton et al. (1999) have shown that selective influx of Ca^{2+} through P/Q-type VSCCs is responsible for activating expression of syntaxin-1A, a presynaptic protein that mediates vesicle docking, fusion and neurotransmitter release. Blocking Ca^{2+} release from intracellular Ca^{2+} store, blocks expression of syntaxin by P/Q –type VSCCs (Sutton

et al., 1999). Their data indicates that there may be a privileged close association between P/Q-type channels and Ca^{2+} stores.

1.4 Research Hypothesis

Classical experimental methods of inducing long-term potentiation are high frequency trains of activity, while low frequency stimulation results in depression. This indicates that plastic stimuli that might trigger gene expression are inherently different from normal synaptic transmission. For example, Deisseroth et al. (1996) reported that LTP-inducing synaptic stimuli (high frequency synaptic input) but not action potential firing, produces nuclear CREB phosphorylation. Interestingly, they found that the two types of input both resulted in comparable global increases in Ca^{2+}. Recent studies show that the contribution from L-type VSCCs to intracellular Ca^{2+} transient induced by EPSPs-like sustained depolarization is larger than that of APs (Mermelstein et al., 1999; Nakazawa and Murphy, 1999). It is possible that stimulus paradigms, such as high frequency synaptic stimuli might result in synchronized activation of multiple neuronal inputs and thus bring neurons to a sustained depolarizing membrane potentials. Fig. 1 illustrates a model for signal transduction from the synapse to the nucleus. High frequency synaptic input causes synchronized activation of synaptic AMPA receptors causing depolarization and a reduction of NMDA receptor Mg^{2+} block. The slow decay kinetics of NMDA receptor cause sustained depolarization of dendrite. This strong and sustained depolarization in dendrites propagates to soma and provides sustained changes of membrane potential preferred by L-type VSCC activation. Ca^{2+} influx through L-type VSCCs efficiently causes Ca^{2+} release from Ca^{2+} store, resulting in large cytoplasmic Ca^{2+}

transient. Free Ca^{2+} in cytoplasm diffuses to the nucleus and causes nuclear Ca^{2+} elevation and nuclear CaMK IV activation leading to CREB phosphorylation and gene expression. According to above model, in the present work, we sought to investigate the following hypotheses:

1) LTP-inducing stimulus patterns could result in sustained depolarization of the soma.

2) The specific kinetic properties of L-type VSCCs distinguish different firing patterns.

3) The coupling between Ca^{2+} channels and Ca^{2+} stores plays an important role in regulating nuclear Ca^{2+} concentration.

To test these hypotheses, a hippocampal CA1 neuron model was built with a detailed representation of intracellular Ca^{2+} dynamics. Key electrophysiological features of hippocampal CA1 neurons and intracellular Ca^{2+} dynamics were reproduced. By doing so, we were able to investigate the activation of L-type VSCCs and the resulting intracellular Ca^{2+} transients during plasticity inducing synaptic stimuli. Since we included Ca^{2+} stores in the intracellular Ca^{2+} dynamics model, we were able to study the role of physical coupling between Ca^{2+} channels and Ca^{2+} stores in regulating nuclear Ca^{2+} concentration.

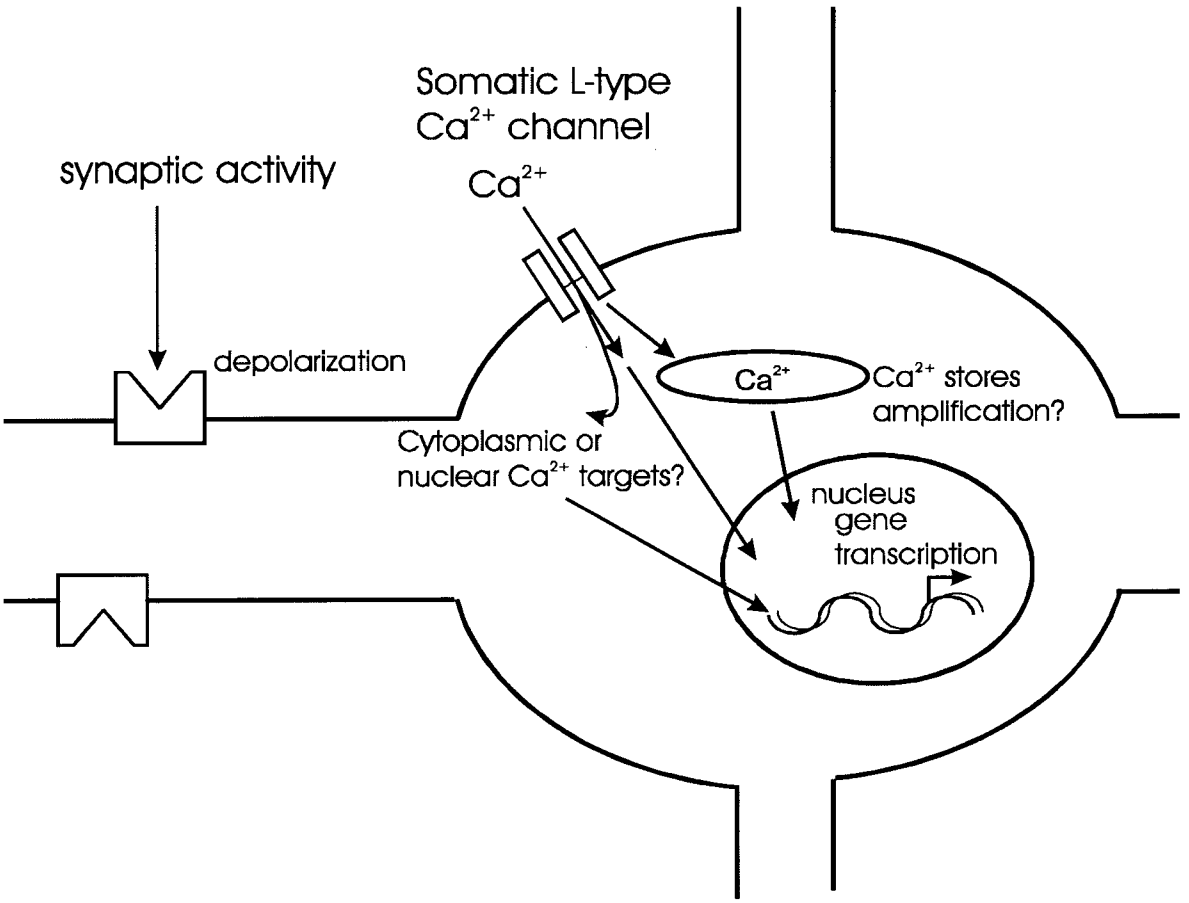

Figure 1 A model for the mechanism of L-type Ca^{2+} VSCC activation during synaptic stimulation. Synaptic activity causes depolarization of dendrites which propagates to the soma, resulting in somatic membrane potential changes. Depolarization of the soma activates L-type Ca^{2+} VSCCs and causes Ca^{2+} influx into the cytoplasm. There may be three ways through which Ca^{2+} influx via L-type Ca^{2+} VSCCs may alternate gene expression activities in the nucleus. **1)** Ca^{2+} activates some cytoplasmic Ca^{2+} targets such as CaM and activated Ca^{2+} targets tanslocate to the nucleus. **2)** Ca^{2+} diffuses to nucleus directly and activates nuclear targets. **3)** Ca^{2+} causes Ca^{2+} release from intracellular Ca^{2+} stores, resulting in mobilization of intracellular Ca^{2+} which finally causes Ca^{2+} elevation in the nucleus and activates nuclear targets.

Chapter 2 Methods

2.1 Experimental procedure

Embryonic cortical neurons and glial cells (from day 18 rat fetuses) were grown 3-4 weeks *in vitro* on polylysine coated glass coverslips before use in imaging experiments (as in Nakazawa and Murphy, 1999). Confocal imaging with a Bio Rad MRC 600 system attached to a Zeiss upright (Axioskop) microscope was used for all experiments. Two objectives were used, either a 0.9 N.A. Zeiss 63X water immersion or an Olympus 0.9 N.A. 60X water immersion. The laser intensity was attenuated to 1% and the confocal pinhole was set to 3.5 (Bio Rad units). Images were acquired using the linescan mode (3.9 ms/line) in which a 1 pixel line across the soma and the nucleus is scanned repeatedly. For imaging of $[Ca^{2+}]_i$ neurons were loaded with 11 μM fluo-3 AM (MINTA ET AL., 1989) for 50 min. To determine the position of the neuronal nucleus, images were also taken by scanning in both X and Y dimensions. The nucleus was readily identifiable since it accumulated more fluo-3 Ca^{2+} probe than the cytoplasm (Nakazawa and Murphy, 1999; O'Malley, 1994). Using X, Y scanning the approximate center of the nucleus was identified and linescan images were taken across the cytoplasm and nucleus. Synaptic stimuli were delivered using pclamp6 software and constant current stimulation using platinum bath electrodes (1 ms duration (Ryan and Smith, 1995)). The intensity (stimulus current) of field stimulation was adjusted over a 30-90 mA range to produce APs, normally around 1.5 times the firing threshold. Three μM APV and 60 μM CNQX were added in bath solutions to reduce synaptic activity. To examine the role of Ca^{2+} store in intracellular Ca^{2+} dynamics, 30 μM cyclopiazonic acid (CPA), a Ca^{2+} pump inhibitor

which empties intracellular Ca^{2+} store by blocking its refilling, was included in the bath solution in some experiments. To synchronize delivery of field pulses with confocal image acquisition, a TTL signal from the confocal was used to trigger a second computer running pclamp6 software to produce synaptic stimuli. Confocal images were exported as byte arrays by removal of data headers and analyzed using routines written in IDL programming language (Research Systems Inc., Boulder, CO) on a Pentium computer. Linescan data were analyzed by breaking the cytoplasmic and nuclear compartments of the cell into discrete regions by averaging the value of 5 adjacent pixels (1.1 μm). Off line averaging was done using floating point arrays to obtain additional precision over byte data (256 levels). Multiple 1.1 μm regions corresponding to cytoplasm and nucleus were averaged to improve the signal to noise ratio. The means of these adjacent pixels were plotted over time. In all of our experiments, Ca^{2+} levels were reported as raw fluo-3 fluorescence intensity. Experiments performed on vehicle treated neurons indicated best stability of Ca^{2+} transients (over time) if Ca^{2+} transients were quantitated in this way (Nakazawa and Murphy, 1999).

2.2 Modeling hippocampal CA1 neuron

The hippocampal CA1 neuron model was built using NEURON simulator (Version 4.1.1) (Hines, 1999) on a PII-450 PC, using a 25-μs time step.

2.2.1 Introduction to NEURON simulator

NEURON provides a powerful and flexible environment for implementing biologically realistic models of electrical and chemical signaling in neurons and networks of neurons. It is designed to address these problems by enabling both the convenient creation of biologically realistic quantitative models of brain mechanisms and the efficient simulation of the operation of these mechanisms.

The structure of NEURON simulator written by Hines group is illustrated in Fig. 2. NEURON incorporates a programming language based on `hoc`, a floating point calculator with C-like syntax. With `hoc` one can quickly write short programs in terms that are familiar to neurophysiologists. The interpreter is used to define the morphology and membrane properties of neurons, establish graphical user interface, execute simulations, optimize parameters and analyze experimental data. It is suitable for biologists since it provides efficient mathematical tools and users can focus on biological mechanism instead of mathematical methods. It provides many ionic mechanisms, such as HH model for fast sodium channels and fast potassium channels that are responsible for AP firing. Moreover, it is especially convenient for investigating new kinds of membrane channels since they are described in a high level language (NMODL) which allows the expression of models in terms of kinetic schemes or sets of simultaneous differential and algebraic equations (explained in detail later) (Hines and Carnevale, 2000). All user-defined mechanisms in NMODL have .mod extension. To maintain efficiency, user defined mechanisms in NMODL are automatically translated into C, compiled, and linked into the rest of NEURON. The mechanisms described below, including various kinds of ionic channels,

Ca^{2+} buffer and Ca^{2+} stores, were described with NMODL and then compiled, linked to NEURON as a dynamic link library (Hines and Carnevale, 1997).

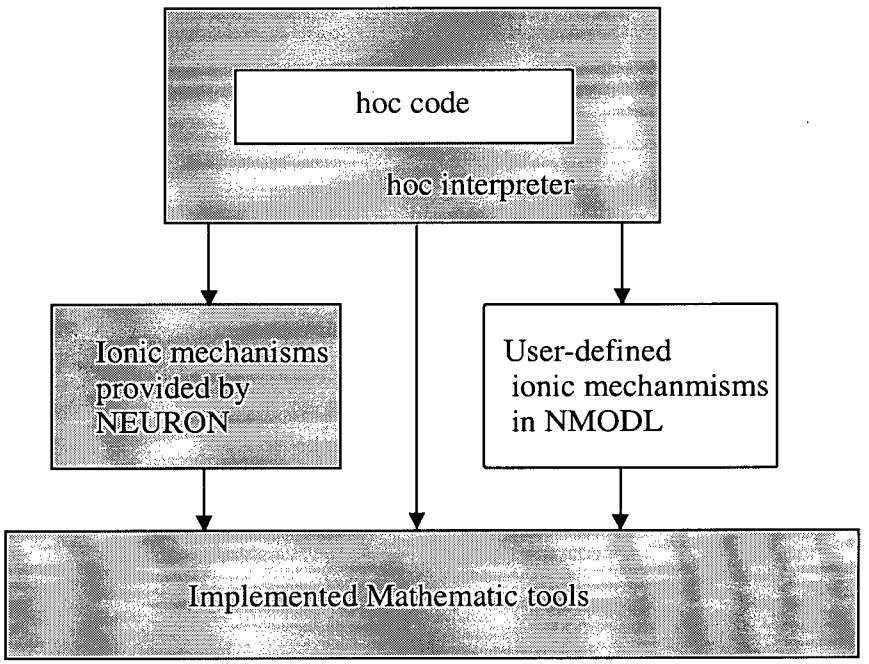

Figure 2 Structure of NEURON simulation environment. All gray boxes are provided by NEURON. Morphological and ionic properties of neurons are described with hoc (file extension is .hoc also). Specific ionic mechanisms such as Ca^{2+} channel model are described in NMODL, with file extension mod.

2.2.2 Modeling hippocampal CA1 neuron eletrophysiology

2.2.2.1 Structure of model cell and electrotonic parameters

Studies by Mainen and Sejnowski (1996) and Pinsky and Rinzel (1994) indicate that the complex spiking behavior of pyramidal neurons can be modeled using relatively few compartments. For this hippocampal CA1 neuron model, we have used four compartments that include a central soma as well as two dendrites and an axon (see Fig.

3). The dendrites and axon are each represented by a cylinder with different diameter (see Fig. 3). The model cell has the following passive membrane parameters: axial resistance R_i = 200 Ω-cm (for dendrites and soma, 50 Ω-cm for axon), membrane resistance R_m = 50,000 Ω-cm^2, membrane capacitance C_m = 1 μF/cm^2 (Spruston et al., 1994). In NEURON, a continuous length of unbranched cable is denoted as a section. Thus, the above four compartments (2 dendrites, 1 soma and 1 axon) are four sections. To satisfy requirements for numerical accuracy, NEURON represents each section by one or more segments of equal length. The discretization method employed by NEURON makes the location of the second-order correct voltage at the center of a segment (Hines and Carnevale, 1997). The choice of segment size affects the accuracy of a compartmental simulation. There is a tradeoff between the computational complexity and accuracy. As long as the segment size is smaller than 5%λ, where λ is the electrotonic length, the numerical error in simulation is tolerable (Mainen and Sejnowski, 1998). In physical terms, λ is the distance along an infinite cylinder (with same radius r, membrane resistance R_m and axial resistance R_i) over which a steady-state voltage decays e-fold. Since the cable is finite, the actual voltage decay is less than e-fold per λ. The value of λ is determined by the cable properties: $\lambda = \sqrt{\frac{rR_m}{2R_i}}$ (Spruston et al., 1994; Traub et al., 1991). The passive membrane parameters described above together with structural parameters (diameter of each compartment), result in different λ values for different sections. Among them, basal dendrite has the smallest λ (0.196 cm). Thus, 50 μm, which is smaller than 5%*0.196 cm = 98 μm, was chosen for dendrites and axon (λ = 0.223 cm). The soma has

a very large λ (50 cm). 5%λ (2.5 cm) is still much larger than its length (30 μm). Thus, it is represented by single segment.

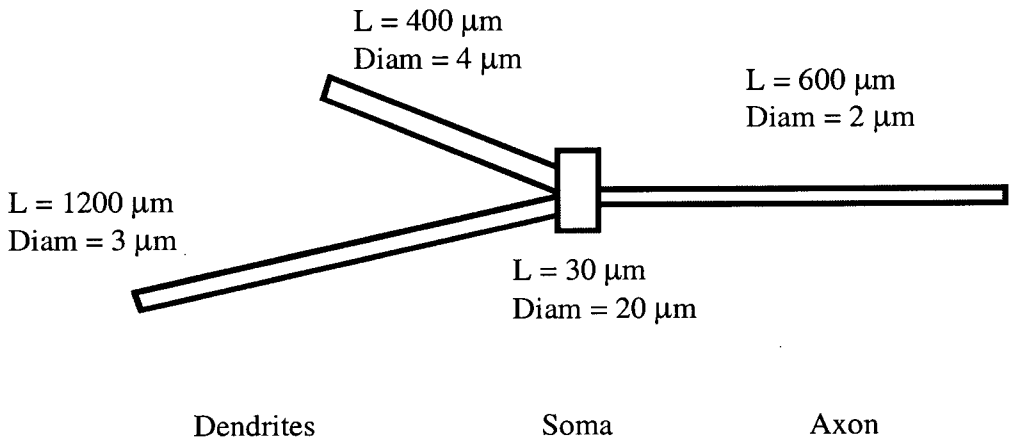

Figure 3 Physical structure of hippocampal CA1 neuronal model. The model cell contains 4 compartments with structural parameters shown in the figure. Each compartment is represented by a cylinder. An axon hillock (not shown) is also included and placed between the soma and the axon. The axon hillock is 50 μm long and has the same diameter as the axon.

2.2.2.2 Ionic channel kinetics

Twelve intrinsic membrane conductances g_{Na}, g_{NaP}, g_{KA}, g_{KDR}, g_{KM}, g_{BK}, g_{Ksk}, g_{sIAHP}, g_{CaP}, g_{CaL}, NMDA and AMPA receptors are incorporated in the compartmental model in order to reproduce hippocampal CA1 neuron electrophysiological properties as closely as possible. The distribution of these conductances is illustrated in Table 1.

Table 1 Distribution of ionic channels

	Dendrite (distal)	*Dendrite (proximal)* mS/cm^2	Soma mS/cm^2	Hillock mS/cm^2	Axon mS/cm^2	**Comments**
Na	15 mS/cm^2	15	15	300	15	Maximum conductance was from Destexhe 1994 and Mainen et al. 1998. Na conductance at hillock was adjusted to obtain AP backpropagation and AP spike amplitude at the soma ~100 mV.
NaP	0.02 mS/cm^2	0.05	0.1	0.1	--	From Lipowsky et al 1996. Maximum conductance on the dendrites was adjusted to obtain proper excitability of the model cell.
K_{dr}	3 mS/cm^2	3	3	60	3	From Mainen et al. 1998
K_A	7+11*(distance from soma in μm/100) (mS/cm^2)	7	7	--	--	From Hoffman et al 1997
K_M	0.2 mS/cm^2	0.2	0.2	0.4	--	Adjusted to balance NaP at resting membrane potential (Mainen et al. 1998).
K_{BK}	--	0.2	0.2	0.1	0.8	From Lipowsky et al 1996
sI_{AHP}	--	0.2	0.2	0.2	--	Adjusted from Sah et al. 1996.
K_{SK}	--	0.1	0.1	0.1	0.3	Lipowsky et al 1996
Ca_P	--	2.5	--	--	2.5	Maximum conductance was from Destexhe et al 1994. Distribution was based on Westenbroek et al. 1995.
Ca_L	--	--	2.5	2.5		Maximum conductance was from Destexhe et al 1994. L-type VSCCs are distributed on the neuronal soma (Hell et al. 1993). VSCCs were put on the hillock in order to activate Ca^{2+} activated potassium channels.
NMDA	0.002 mS (at synapse)	--	--	--	--	Adjusted during simulation to give different levels of synaptic stimulation.
AMPA	0.01 mS (at synapse)	--	--	--	--	Adjusted during simulation to give different levels of synaptic stimulation.

Note: 1) In most simulations, there are three synapses, two on distal dendrite, one on proximal dendrite. The synaptic conductances (NMDA and AMPA) are adjusted in simulations according to need.

2) Above distribution of ionic channels is for nonbursting cells. For bursting cell, there is more NaP (0.1 mS/cm^2 on proximal dendrites, 0.05 mS/cm^2 on distal dendrites).

Most ionic channel models used are based on a Hodgkin-Huxley (HH) type formalism. In HH type formalism, an ionic channel is described with one or more gating particles. If x is a membrane state variable, corresponding to the probability of a gating particle in open state, then

$$\frac{dx}{dt} = \alpha(1-x) - \beta x$$

where α and β are functions of voltage or ion concentration. The steady-state value of x, $x_\infty = \alpha/(\alpha+\beta)$, and the time constant for relaxation to x_∞, $\tau = 1/(\alpha+\beta)$. Sometimes, x_∞ and τ are given directly as functions of voltage or ion concentration.

The macroscopic current I is the product of the maximum conductance g_{max}, probability of gating particles in open state $x_1 \cdot x_2 \cdots x_n$, and the driving force across the membrane (the difference between membrane potential and the reversal potential of the ionic channel).

$$I = g_{\max} \cdot x_1 \cdot x_2 \cdots x_n \cdot (v - E_{ion})$$

Besides the above HH-type channel model, in the present work some channels such as NMDA receptors and g_{sAHP} are described with a Markov kinetic scheme. A Markov kinetic scheme describes the movement between different conformational states of a protein. A simple Markov scheme containing only two states, an open state and a closing state, is shown below.

$$C \underset{\beta}{\overset{\alpha}{\Leftrightarrow}} O$$

α and β are the forward and reverse reaction rates respectively. For a voltage-dependent channel, the reaction rates normally depend on the membrane potential. For a ligand-gated channel, normally at least the forward reaction rate depends on the ligand concentration.

As described in the section "Introduction to NEURON simulator", it is quite convenient using NEURON to describe new ionic mechanisms in terms of sets of differential and algebraic equations or kinetic schemes. The following is an example of a user-defined membrane channel model used in the present work.

```
************************ IM.mod ************************
: Potassium IM current.
:HH-type formalism, with only one activation state variable m.

INDEPENDENT {t FROM 0 TO 1 WITH 1 (ms)}

NEURON {
SUFFIX IM                       :Specify a density mechanism with name IM.
USEION k READ ek WRITE ik       :By USEION statement, NEURON will keep track
                                :the total outward current that is carried by an ion,
                                :in this case, potassium.
RANGE gkmbar, ik, gk            :gkmbar is the maximum macroscopic
                                :conductance while gk is the product of gkmbar
                                :and the fraction of channels that are open at any
                                :moment. ik is the current that passes through gk.
}

UNITS {                         :Define new names for units in terms of existing
        (mA) = (milliamp)       :names in the database.
        (mV) = (millivolt)
        (S)  = (siemens)
}

PARAMETER {
        gkmbar  = 0.005  (S/cm2)
        ek      = -90    (mV)
        dt              (ms)
        v               (mV)
        celsius    (degC)       :Simulation temperature, normally 36°C.
```

```
        temp = 25 (degC)            :Original temperature at which experiments were
                                    :conducted.
        q10 = 3                     :Temperature sensitivity
}

STATE {                             :Declare state variables which are variables
        m                           :depending on differential equations or kinetic
                                    :reaction schemes.
}

ASSIGNED {                          :Variables whose values are calculated
        ik    (mA/cm2)
        tadj
}

BREAKPOINT {                        :Main computation block of the mechanism.
        SOLVE states                :BREAKPOINT block is usually called twice per
        gk  = gkmbar * m * m        :time step. By the end of this block, all variables
        ik  = gk * (v - ek)         :are consistent with the new time.
}

DERIVATIVE states {                 :Exact HH equations
        m' = (1-m)*alpha(v) – m*beta(v)
}

INITIAL {                           :Initialize state variables at time 0.
        m = alpha(v)/(alpha(v) + beta(v))
}

FUNCTION alpha(v(mV)) (/ms) {
        ... Calculate alpha according to membrane potential v(mV).
}

FUNCTION belta(v(mV)) (/ms) {
        ... Calculate beta according to membrane potential v(mV).
}
```

********** IM.mod **********

For Markov processes, NMODL provides extremely convenient tool – kinetic scheme (Hines and Carnevale, 2000). For the simple two-state Markov model described above, the following KINETIC block can be used to substitute the DERIVATIVE block in IM.mod.

```
KINETIC state {
        Rates(v)                        :Rates(v) function calculates the reaction rates
                                        :alpha and belta based on membrane potential
                                        :v(mV) (or ligand concentration in the case of
                                        :ligand-gated channel), which needs to be defined
                                        :later as a FUNCTION block (similar to alpha(v)
                                        :and belta(v) block in IM.mod).
        ~ C <-> O       (alpha, belta)  :Kinetic scheme used to describe transitions
                                        :between closing and open states. C and O
                                        :denote fraction of channels in closing and open
                                        :state, respectively.
        conserve C + O = 1              :total channel amount is conserved.
}
```

All user-defined channel models used in the present work were similarly implemented with NMODL. Before illustrating those channel models, it is important to discuss the temperature dependence of channels and how it is treated in NEURON, since many physiological studies are performed at room temperature (22°C to 25°C) whereas we are trying to model neuronal behavior at physiological temperature (36°C). Temperature has been found to affect the kinetics of channels (Schwarz and Eikhof, 1987) and may also affect the channel conductance (Acerbo and Nobile, 1994). Although the effect of temperature on channel properties is significant, experimental data at physiological experiments and data on temperature dependence are still insufficient to construct accurate kinetic models of ionic channels at physiological temperature. In modeling studies, it is

normally assumed that steady state parameters are insensitive to temperature, which was implicated experimentally (Schwarz and Eikhof, 1987). Usually, to compensate for the effect of temperature, the temperature coefficient Q_{10} (fractional rate increase per 10°C temperature increase) is used to scale rate constants (Mainen and Sejnowski, 1996). For example, in the case of the relaxation time constant τ of the activation variable x, after compensation for temperature dependence,

$$\tau = 1/(\alpha + \beta)/Q_{10}^{(36-temp)/10°C}$$

where *temp* is the temperature at which experiments were performed. In the present work, Q_{10} was assumed to be 3 for most channels, otherwise indicated (Destexhe et al., 1994).

1) Fast sodium channels

It is well known that fast sodium channels are responsible for AP firing. Fast sodium channels have fast activation and inactivation kinetics. The classic HH-type sodium channel model describes its fast kinetics fairly well. Recently, it was found that in many kinds of neurons, including neocortical pyramidal neurons and hippocampal pyramidal neurons, there is slow cumulative sodium channel inactivation that is much slower than the fast, HH-type inactivation mentioned above (Fleidervish et al., 1996; Mickus et al., 1999; Mickus et al., 1999). This slow cumulative inactivation of sodium channel was found to contribute to the following phenomena: **1)** Slow cumulative adaptation of spike firing which persists even after Co^{2+} replaced Ca^{2+} in the bathing medium to block Ca^{2+}-activated potassium channels (Fleidervish et al., 1996). This slow cumulative adaptation of spiking firing is associated with a gradual decrease in maximal rates of rise of action potentials, a slowing in the post-spike depolarization towards

threshold, and a positive shift in the threshold voltage for the next spike in the train. **2)** Regulation of back-propagating AP amplitude and therefore dendritic excitation (Mickus et al., 1999).

Here, the slow inactivation of sodium channels is taken into account by adding a slow variable into the classic HH-type model as the following. Parameter values for slow inactivation were adjusted according to experiments conducted by Mickus et al. (1999). Parameters for fast activation and inactivation were from Destexhe et al. (1994).

$$I_{Na} = g_{\max} \cdot m^3 \cdot h \cdot s \cdot (v - E_{Na})$$

with

$$\alpha_m = 0.32 \cdot (13 - v_2)/(e^{(13-v_2)/4} - 1)$$

$$\beta_m = 0.28 \cdot (v_2 - 40)/(e^{(v_2-40)/5} - 1)$$

$$\alpha_h = 0.128e^{(17-v_2)/18}$$

$$\beta_h = 4/(1 + e^{(40-v_2)/5})$$

where $v_2 = V_m - V_{traub}$ and V_{traub} is the parameter controlling the AP firing threshold.

$$\alpha_s = 0.005e^{(-95-v)/35} \qquad \alpha_{\tau s} = 0.0015e^{(-85-v)/65}$$

$$\beta_s = 0.017/(e^{(-17-v)/7} + 1) \qquad \beta_{\tau s} = 0.034/(e^{(-14-v)/9} + 1)$$

$$s_{\inf} = \alpha_s/(\alpha_s + \beta_s) \qquad \tau_s = 1/(\alpha_{\tau s} + \beta_{\tau s})$$

Fig. 4A shows an example of simulated sodium current in response to 50 Hz square pulses. The slow cumulative inactivation is apparent and the percentage of inactivation at different frequencies is similar to experimental data reported by Mickus et al. (1999) (see Fig. 4B).

A.

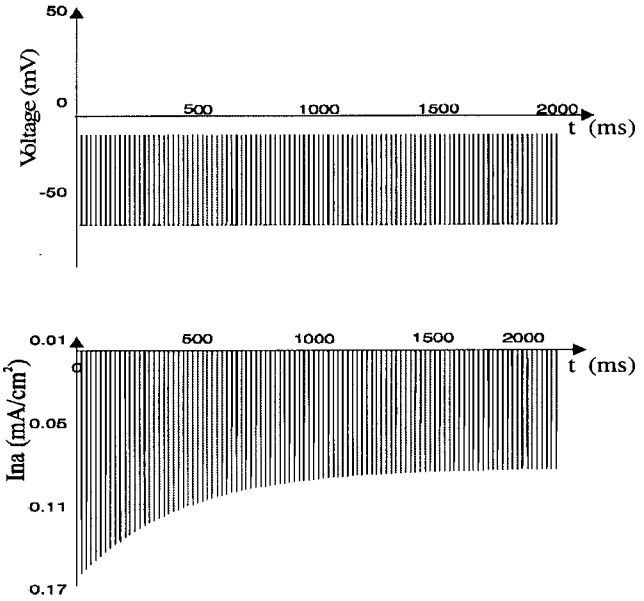

B.

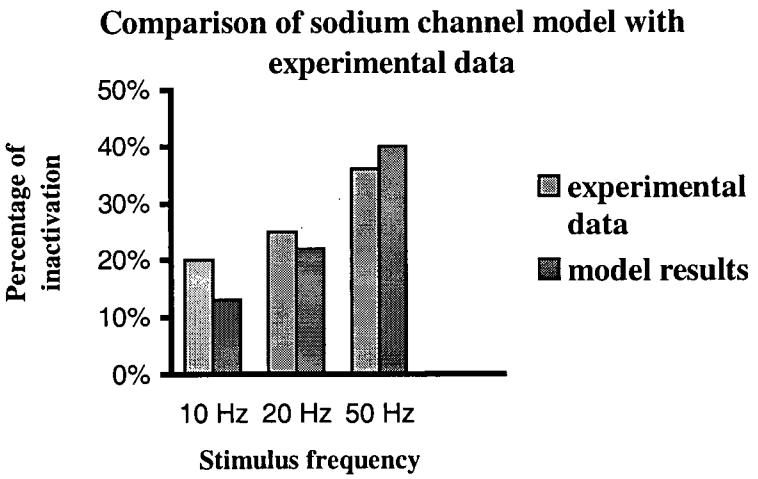

Figure 4 Frequency dependent slow inactivation of sodium channels. (a) Simulated sodium current in response to 2 ms 50 mV square pulses of 50 Hz. (b) Percentage of inactivation (steady state) caused by 2 ms 50mV-step depolarization of different frequencies, compared with experimental data from (Mickus et al., 1999).

2) Persistent sodium channels

Persistent sodium current has been found in various neurons including hippocampal CA1 neurons (French et al., 1990; Mainen and Sejnowski, 1998). It activates below threshold and maybe boost the propagation of EPSP from dendrites to the soma. Since it has been suggested that the magnitude of persistent sodium currents I_{NaP} is approximately 1% of the fast sodium current (Crill, 1996; Mainen and Sejnowski, 1998), we set the maximum conductance of the persistent sodium channels as ~1% of the fast sodium conductance (see Table 1). The kinetic model of I_{NaP} is from Lipowsky et al. (1996), which was based on experimental data on hippocampal neurons from French et al. (1990).

$$I_{NaP} = g_{NaP} \cdot m \cdot (V_m - E_{Na})$$

with

$$\alpha_m = -1.74 \cdot (V_m - 11)/(e^{(V_m - 11)/(-12.94)} - 1)$$

$$\beta_m = 0.06 \cdot (V_m - 5.9)/(e^{(V_m + 49)/(-5)} + 1)$$

$$m_{\inf} = 1/(e^{(V_m + 49)/(-5)} + 1)$$

3) Delayed rectifier Potassium channels

Model for delayed rectifier potassium channels, which are responsible for AP repolarization, is from Destexhe et al. (1994), described by the following HH-type equations.

$$I_K = g_K \cdot n^4 \cdot (V_m - E_K)$$

with

$$\alpha_n = 0.032 \cdot (15 - v_2)/(e^{(15-v_2)/5} - 1)$$

$$\beta_n = 0.5 \cdot e^{(10-v_2)/40}$$

$$v_2 = V_m - V_{traub}$$

where V_{traub} is the parameter controlling the AP firing threshold.

4) A-type potassium channels

Studies of Hoffman et al. (1997) on hippocampal CA1 neuron revealed a very high density of transient A-type potassium channels and the density increases with distance from the soma. Their study suggested a very important role of this channel in limiting the excitability of CA1 neuron dendrites. We have used their kinetic models for proximal and distal A-type potassium channels.

$$I_A = g_{K_A} m^4 \cdot h \cdot (V_m - E_K)$$

with

$$\alpha_m = -0.01(V_m + 21.3)/(e^{(V_m+21.3)/-35} - 1)$$

$$\beta_m = 0.01(V_m + 21.3)/(e^{(V_m+21.3)/35} - 1) \qquad \text{for proximal channels}$$

$$\alpha_m = -0.01(V_m + 34.4)/(e^{(V_m+34.4)/-21} - 1)$$

$$\beta_m = 0.01(V_m + 34.4)/(e^{(V_m+34.4)/21} - 1) \qquad \text{for distal channels}$$

$$\alpha_h = -0.01(V_m + 58)/(e^{(V_m+58)/-8.2} - 1)$$

$$\beta_h = 0.01(V_m + 58)/(e^{(V_m+58)/8.2} - 1) \qquad \text{for all channels}$$

$\tau_m = 0.2ms$

$\tau_h = 5 + (2.6ms/mV)(V_m + 20)/10$ for $V_m > -20$ mV

$\tau_h = 5ms$ for $V_m < -20$ mV

5) M current

I_M is a slow, muscarine-sensitive, voltage-dependent potassium current. It partially activates at resting membrane potential. Together with persistent sodium currents, it gives rise to sub-threshold membrane potential oscillations (Gutfreund et al., 1995). Together with Ca^{2+}-dependent potassium channels, it is responsible for frequency accommodation in hippocampal neurons (Mainen and Sejnowski, 1998; Sah and Bekkers, 1996). The channels underlying this current have not yet been isolated and cloned. A model describing the kinetics of this current in hippocampal CA1 neuron is given by Warman et al. (1994) which is based on the work of Halliwell and Adams (1982) on guinea pig CA1 neurons.

$$I_M = g_M n^2 (V_m - E_K)$$

with

$\alpha_n = 0.016/e^{(V_m+52.7)/-23}$

$\beta_n = 0.016/e^{(V_m+52.7)/18.8}$

6) Ca^{2+}-dependent potassium channels (BK, SK, sI_{AHP})

In hippocampal CA1 pyramidal neurons, actually in many neurons of the central nervous system, APs are followed by a prolonged afterhyperpolarization (AHP) which is

caused by a rise in intracellular Ca^{2+} concentration. There are several groups of AHP according to their kinetic and pharmacological properties:

I) fI_{AHP} is voltage-dependent and also Ca^{2+} dependent. It activates very rapidly and is presumably mediated by big conductance Ca^{2+}-activated potassium channels (BK) (Davies et al., 1996; Storm, 1990; Yoshida et al., 1991). This current, designated I_C, contributes to AP repolarization (Poolos and Johnston, 1999; Shao et al., 1999). The following equations from Lipowsky et al. (1996) were used to describe the kinetics of this current. The difference between the Lipowsky I_C model and the model we used is the internal Ca^{2+} dynamics. In our model, we incorporated a detailed intracellular Ca^{2+} dynamics model. $[Ca^{2+}]_i$ at the outermost sub-membrane shell (within 100 μm from the plasma membrane, see section 2.2.3), together with membrane potential, was used to activate this channel. There is evidence showing that Ca^{2+} dynamics rather than channel kinetics itself determine the kinetics of this current, as well as I_{AHP} described later (Mainen and Sejnowski, 1998).

$$I_C = g_{BK} \cdot m^2 h \cdot (V_m - E_K)$$

with

$$V_{shift} = -3.78 \log_{10}[Ca]_i - 11.8$$

$$\tau_m = 1.1 \text{ ms}$$

$$m_{\inf} = 1/(e^{(-0.095V_m + V_{shift})} + 1)$$

$$\alpha_h = 1/e^{(V_m+79)/10}$$

$$\beta_h = 4/(e^{(V_m-82)/-27} + 1)$$

II) I_{AHP} activates fast (<5 ms) after Ca^{2+} influx and decays with a time constant of hundred ms similar to that of the intracellular Ca^{2+} transient, and is apamin-sensitive and voltage independent (Kirkpatrick and Bourque, 1996; Mainen and Sejnowski, 1998; Neely and Lingle, 1992; Sacchi et al., 1995). The underlying channels are suggested to be SK-type Ca^{2+}-activated potassium channels (Engel et al., 1999; Stocker et al., 1999; Xia et al., 1998). Together with I_M, it is responsible for the medium-duration AHP and affects the instantaneous firing rate, contributing to the interval between APs within a train (Storm, 1989). It is activated by submicromolar concentration of intracellular Ca^{2+} (EC_{50} = 0.4-0.7 μM) in cultured rat hippocampal neurons (Hirschberg et al., 1998; Sah and Clements, 1999; Stocker et al., 1999). This current was modeled by the following equations modified from Destexhe et al. (1994), with the midpoint of the activation state variable m at 0.7 μM instead of 25 μM according to above experimental data in hippocampal neurons.

$$I_{sk} = g_{sk} \cdot m^2 \cdot (v - E_k)$$

with

$$m_{\inf} = ([Ca^{2+}]_i / 0.0007)^2 / (1 + ([Ca^{2+}]_i / 0.0007)^2)$$

$$\tau_m = 3 \text{ ms}$$

III) sI_{AHP} has much slower kinetics and is activated by intracellular Ca^{2+} with a time constant larger than 100 ms (Mainen and Sejnowski, 1998). It is voltage independent and apamin insensitive (Sah and Bekkers, 1996). Unlike I_{AHP}, its kinetics is independent of the intracellular Ca^{2+} dynamics. It persists for seconds even after intracellular Ca^{2+} back to resting level (Sah and Clements, 1999). The underlying channel has not been identified but is suggested to have intrinsic slow kinetics and be gated by Ca^{2+} directly (Sah and

Clements, 1999). It is a key determinant of the repetitive firing properties of CA1 pyramidal neurons and is modulated by second messenger systems (Pedarzani et al., 1998). It affects long-term changes of firing rate such as slow adaptation in CA1 pyramidal neurons (Stocker et al., 1999). A modified version of the markov model of sI_{AHP} given by Sah et al. (1999) was used.

$$C_1 \underset{r_u}{\overset{4r_b[Ca]_i}{\Leftrightarrow}} C_2 \underset{2r_u}{\overset{3r_b[Ca]_i}{\Leftrightarrow}} C_3 \underset{3r_u}{\overset{2r_b[Ca]_i}{\Leftrightarrow}} C_4 \underset{4r_u}{\overset{r_b[Ca]_i}{\Leftrightarrow}} C_5 \underset{r_c}{\overset{r_o}{\Leftrightarrow}} O$$

where $r_b = 10\ /\mu M{\cdot}s$, $r_u = 0.5/s$, $r_o = 600/s$, and $r_c = 400/s$.

7) L-type VSCCs

L-type Ca^{2+} channels are modeled based on experimental data from Imredy and Yue (1994) and Mermelstein et al. (2000). A simple 3-state markov process, in which reaction rates are either voltage-dependent or Ca^{2+}-dependent, was used.

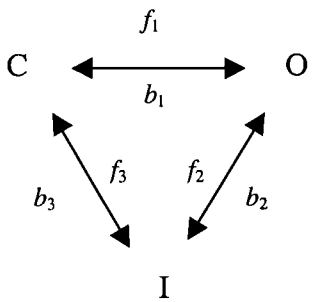

$$f_1 = 0.4/(1+e^{-(v+14.6)/7})$$

$$b_1 = 0.6/(1+e^{(v+14.6)/7})$$

$$f_2 = 1.5*[Ca^{2+}]_i$$

$$b_2 = 0.0045$$

$$f_3 = [Ca^{2+}]_i$$

$$b_3 = 0.05/(1+e^{(v+7.5)/2.5})$$

Among those rates, f_1 and b_1 is voltage-dependent, f_2 and f_3 are Ca^{2+} dependent. Initial parameter values for the voltage-dependent rates were from McDonald et al. (1994) in which experiments were conducted at 35°C on cardiac tissue, and were adjusted to give a rise time of approximately 8 ms at room temperature to match experimental results from Mermelstein et al. (2000). Initial parameter values for Ca^{2+} dependent rates were from Imredy and Yue (1994). f_2 and b_2 were adjusted to get a good match to fast inactivation time constant ~40 ms at 0-10 mV. Recovery from the inactivation state was found to be voltage dependent. It was reported that the recovery rate is smaller than 0.005 ms at –5 ~ 10 mV and increases steeply with hyperpolarization negative to –10 mV (Imredy and Yue, 1994). So the slope of the voltage-dependence of recovery rate b_3 was chosen to be 2.5 mV.

A simpler L-type VSCC model using HH-type formalism was also developed based on experimental data from Mermelstein et al. (2000). This L-type VSCC model has almost the same properties, such as the IV curve, as the one above. Most simulation results reported here were obtained with this L-type model, unless indicated otherwise. The Ca^{2+}-dependent inactivation time course was roughly chosen according to our own experimental data. The rise time of this model at 24°C is closer to what was reported (Mermelstein et al., 2000), and its rise time curve (rise time vs. voltage) is easier to change without changing the IV curve.

$$I_{Ca} = g_{\max} \cdot m \cdot f \cdot (v - E_{Ca})$$

with

$$\tau_m = (1 - e^{((v+14.6)/9.24)}) / (0.03(-v - 14.6) \cdot (1 + e^{((v+14.6)/9.24)})) \qquad (2.1)$$

$$m_\infty = 1/(1 + e^{(-(v - v_{half})/3.24)}) \qquad (2.2)$$

$$\tau_f = 75 \text{ ms}$$

$$f_\infty = 1/(1+[Ca^{2+}]_i/0.001)$$

where V_{half} = -18.6 mV for most simulations. The rise time of this model closely resembled what was reported by Mermelstein et al. (2000) at 24°C. The temperature dependence coefficient Q_{10} was assumed to be 2.5 (Acerbo and Nobile, 1994). 10-90% rise time of L-type Ca^{2+} current in response to different levels of voltage steps before and after temperature compensation is plotted in Fig. 5.

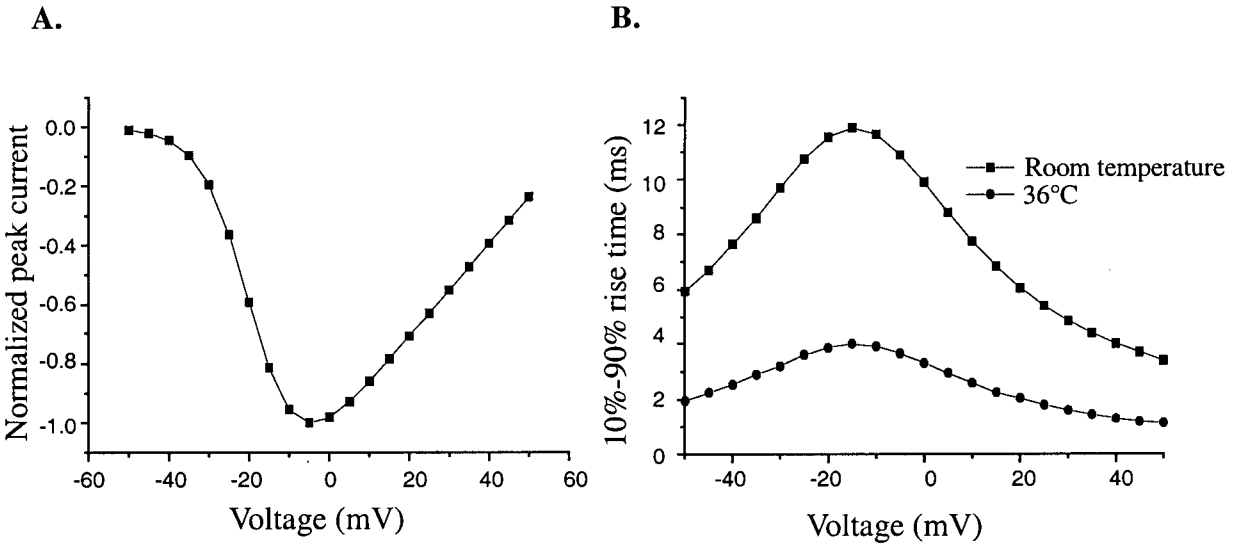

Figure 5 Properties of L-type VSCC model using HH-type formalism with V_{half} = -18.6 mV (see eq. 2.1, 2.2). Parameters for L-type VSCC model were adjusted based on experiments by Mermelstein et al. (2000), which were conducted at room temperature. **A.** IV curve, **B.** 10%-90% rise time of L-type Ca^{2+} current in response to different levels of step depolarization. Square indicates the rise time curve before temperature correction. Circle indicates the rise time curve at 36°C.

8) P/Q-type VSCCs

The P/Q-type Ca^{2+} channel was modeled using HH-type of formalism, based on experimental data from Dove et al. (1998) on Purkinjie cells. In this model, voltage-dependent inactivation and Ca^{2+}-dependent inactivation were taken in consideration. The middle point of Ca^{2+}-dependent inactivation was set to 4 μM (Dove et al., 1998).

$$I_{Ca} = g_{\max} \cdot m \cdot h \cdot f \cdot (v - E_{Ca})$$

with

$$\tau_m = (1 - e^{(-(v+15.3)/6.24)}) / (0.035 \cdot (v + 15.3) \cdot (1 + e^{(-(v+15.3)/6.24)}))$$

$$m_{\inf} = 1/(1 + e^{(-(v+15.3)/3.5)})$$

$$\tau_h = 9/(0.0197 \cdot e^{(-0.0337 \cdot 0.0337 \cdot (v+18.3)^2)} + 0.02)$$

$$h_{\inf} = 1/(1 + e^{((v+21.8)/13.3)})$$

$$\tau_f = 10 \text{ ms}$$

$$f_{\inf} = 1/(1 + [Ca]_i / 0.004)$$

9) Synaptic conductances (NMDA receptor and AMPA receptor)

A very simple model that approximates the kinetics of AMPA and NMDA receptors is used, which was provided in Destexhe (1997). The kinetics of AMPA and NMDA currents is modeled by the same scheme, except that there is a magnesium block of NMDA receptors, which is dependent on membrane potential. The following equations are used,

$$I_r = G_r f B(V_m)(V_m - E_r)$$

where r denotes NMDA or AMPA, f denotes the fraction of receptors in open state. For AMPA receptors, the term $B(V_m)$ equals 1. In this model, the kinetics of these receptors are simply represented by a two-state markov process:

$$C+T \underset{\beta}{\overset{\alpha}{\Leftrightarrow}} O$$

where α and β are voltage-dependent on- and off-binding rate. The values for these parameters are also from Destexhe et al. (1998). This is a simplification of the multi-state model in (Clements et al., 1992; Destexhe et al., 1994; Hessler et al., 1993), which contains two glutamate-binding sites and a desensitization state. Although the multi-state model more accurately represents the behavior of NMDA and AMPA receptors, the simplified model captured their basic properties, such as the time course of rise and decay, and their summation behavior (Destexhe et al., 1998). Since what we are interested in is somatic potential changes and nuclear Ca^{2+} dynamics, great details of synaptic activity are not very important. Moreover, this simplified model is more computationally efficient (Destexhe et al., 1998). Thus, in the present work, we used the simplified model of NMDA and AMPA receptors instead of the multi-state model.

10) Presynaptic cell and transmitter release

The presynaptic cell contains fast sodium channels and delayed rectifier potassium channels that are responsible for AP firing and repolarization. A current injection mechanism was incorporated into the presynaptic cell to elicit APs. Different levels of current injection give different AP firing frequencies. The presynaptic glutamate release is simply modeled by brief pulse with a duration of 1 ms. Once there is an AP, there will be a

1 ms, 1mM pulse of glutamate present at the postsynaptic side (Clements et al., 1992; Destexhe et al., 1994).

2.2.3 Modeling intracellular Ca^{2+} dynamics

The intracellular Ca^{2+} dynamics representation was placed in the soma and dendrites. Since what we are interested in is nuclear Ca^{2+} dynamics, somatic Ca^{2+} dynamics was described in great detail (see below). Dendritic Ca^{2+} dynamics was modeled much more simply with only Ca^{2+} diffusion and Ca^{2+} buffering mechanism, merely for activating Ca^{2+}-activated potassium channels on dendrites.

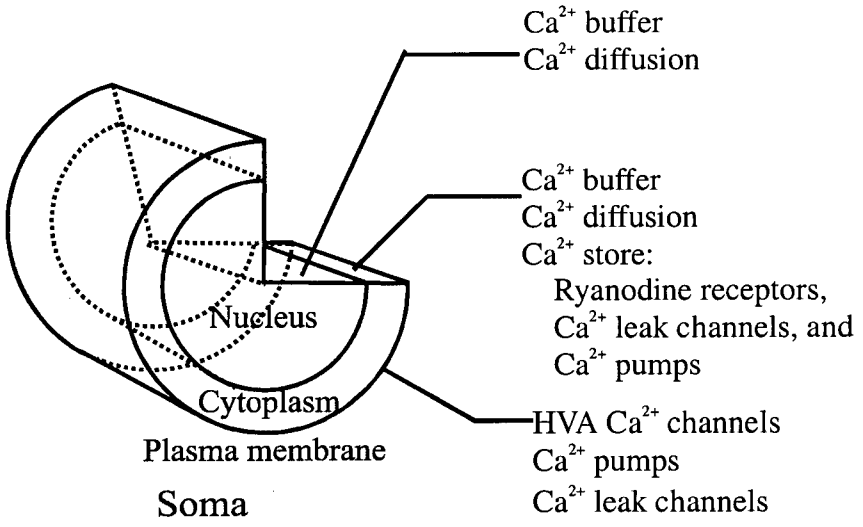

Figure 6 Intracellular Ca^{2+} dynamics model. In the compartmental model, the soma is represented by a cylinder with diameter of 30 μm and length of 20 μm (see Fig. 3). It is divided into 50 concentric shells. The inner 35 shells are nucleus and outer 15 shells are cytoplasm. Mechanisms such as Ca^{2+} diffusion, Ca^{2+} stores, Ca^{2+} buffers and Ca^{2+} channels are placed in the nucleus, cytoplasm and plasma membrane according to literature.

Table 2 Intracellular Ca^{2+} dynamics model parameters

Kinetic models	Parameter values	Comments
Ca^{2+} Buffer	K_{on} = 0.3 /mM·ms (Cyto) 0.05 /mM·ms (Nuclear) K_d = 400 nM Totalbuffer = 146 μM	Totalbuffer concentration was derived from K_d (Sinha et al. 1997) and Ca^{2+} binding ratio from Helmchen et al. 1996. K_{on} of Ca^{2+} buffer in cytoplasm was from Sala et al. 1992. K_{on} of Ca^{2+} buffer in nucleus was adjusted in order to obtain proper delay time between cytoplasmic Ca^{2+} transient and nuclear Ca^{2+} transient.
Ca^{2+} Diffusion	D_{ca} = 0.3 μm^2/ms (Cyto) 0.05 μm^2/ms (Nuclear)	D_{Ca} in cytoplasm is from De Schutter 1998 and Kargacin 1994. D_{Ca} in nucleus was adjusted to obtain proper delay time between cytoplasmic Ca^{2+} transient and nuclear Ca^{2+} transient and proper decay time constant of Ca^{2+} transient.
Ryanodine Receptor	K_o = 0.0001 τ_{on} = 1.2 ms τ_{off} = 40 ms	τ_{off} was adjusted to match the decay time constant of the simulated cytoplasmic calcium transient to experimental data. τ_{on} was set according to experimental data from Gyorke and Fill 1993. K_o was adjusted to make cytoplasmic calcium transient peak value ~300 nM (Helmchen et al. 1996).
Ca^{2+} pumps	V_{max} = 4.9e-13 mol/cm^2·s (for Ca^{2+} pumps on Ca^{2+} store) 9e-13 mol/cm^2·s (for Ca^{2+} pumps on plasma membrane) n = 2 K = 0.001 mM	Parameters were from De Schutter 1998 and kargacin 1994.
Ca^{2+} leak channels		K_{leak} was chosen to balance calcium pump at the resting state. Ca^{2+} leak channels on plasma membrane were the same as those on ER (Girard et al. 1992; Goldbeter et al. 1990).

The soma is divided into 50 concentric shells around a cylindrical core (see Fig. 6). The thickness of the outermost shell is half of the others (200 nm). Concentration is second-order correct midway through the thickness of those shells and at the center of the core. These shells are divided into two compartments, cytoplasm and nucleus. The inner 35 shells are the nucleus (diameter = 14 μm). The remaining shells are the cytoplasm (thickness = 6 μm). Based on values found in the literature we have placed appropriate levels of Ca^{2+} handling mechanisms, such as Ca^{2+} buffer and Ca^{2+} stores, within the cytoplasm and the nucleus (See Fig. 6). Ca^{2+} buffering and Ca^{2+} diffusion were taken into consideration throughout the soma. It is well known that in cytoplasm, there is an elaborate ER system that can function as a Ca^{2+} store (reviewed in Verkhratsky and Petersen, 1998). IP_3Rs and RyRs distributed on ER are capable of releasing Ca^{2+} from this intracellular Ca^{2+} store (Berridge, 1998). Since they both are sensitive to Ca^{2+} and able to elicit CICR (see Chapter 1), for simplicity, only RyRs are taken into account in present work. Ca^{2+} pumps on ER which are responsible for refilling this intracellular Ca^{2+} reservior, and also Ca^{2+} leak channels which balance Ca^{2+} pumps at resting Ca^{2+} level are also placed on the Ca^{2+} store. Unlike in cytoplasm, so far, no Ca^{2+} uptake or release mechanisms have been found in nuclear interior (Fox et al., 1997; Verkhratsky and Petersen, 1998). Ca^{2+} release only occurs at the nuclear envelope which is an extension of ER and contains several kinds of calcium release machinery (Lanini et al., 1992; Petersen et al., 1998; Verkhratsky and Petersen, 1998). In this model, all properties of the nuclear envelope, such as the distribution of RyRs and Ca^{2+} pumps, are the same as the cytoplasmic Ca^{2+} store. For simplicity, the barrier effect of the ER to Ca^{2+} diffusion is not taken into consideration. This effect could be compensated by the adjustment of diffusion

constant of Ca^{2+}. Moreover, the effect of the nuclear envelope on Ca^{2+} diffusion is still a compelling question. The nuclear envelope is normally very permeable to Ca^{2+} because of the existence of large nuclear pores (Petersen et al., 1998), although it seems that the permeability might be modulated (Badminton et al., 1998).

2.2.3.1 Ca^{2+} buffering

There is an elaborate Ca^{2+} buffering system within the cell, which contributes to achieve the temporal and spatial functional compartmentalization of Ca^{2+} signaling. A number of potential buffering systems for intracellular Ca^{2+} have been proposed (Kargacin, 1994; Naraghi and Neher, 1997; Neher and Augustine, 1992). Here, a non-mobile Ca^{2+} buffer is incorporated into the model. The following rate equation is used to describe the non-mobile Ca^{2+} buffer system.

$$\frac{\partial Ca}{\partial t} = -K_{on}([Buffer]_{free})(Ca) + K_{off}(Totalbuffer - [Buffer]_{free})$$

The coefficient K_{on} and K_{off} are on and off-binding rate respectively, Totalbuffer is the total intracellular Ca^{2+} buffer concentration.

The dissociation constant for Ca^{2+} binding to the intracellular Ca^{2+} buffer, K_d, which equals K_{on}/K_{off} was set as 400 nM (Kargacin, 1994; Sinha et al., 1997). Total Ca^{2+} buffer concentration is 146 μM which is estimated from K_d and Ca^{2+} binding ratio by the following equation (Helmchen et al., 1996).

$$K_B = \frac{Totalbuffer \cdot K_d}{([Ca]_{rest} + K_d)([Ca]_{peak} + K_d)}$$

K_B (200) is the Ca^{2+}-binding ratio of intracellular Ca^{2+} buffer (Helmchen et al., 1996). Since peak Ca^{2+} concentration in response to single AP was suggested to be 150 ~ 300

nM (Helmchen et al., 1996). The total Ca^{2+} buffer concentration was deduced from the resting Ca^{2+} level (50 nM) and peak Ca^{2+} concentration (250 nM).

The on-binding rate K_{on} used in the simulation was 0.3 /mM·ms for the cytoplasmic Ca^{2+} buffer and 0.05 /mM·ms for the nuclear Ca^{2+} buffer (see Table 2), which was adjusted to match the cytoplasmic and nuclear Ca^{2+} kinetics to experimental data (see Table 3).

2.2.3.2 Diffusion of Ca^{2+}

A one-dimensional equation derived from Fick's law was used to describe Ca^{2+} diffusion in the radial direction within the cylindrical compartments (Crank, 1975).

$$\frac{\partial Ca}{\partial t} = \frac{1}{r}\frac{\partial}{\partial r}(rD\frac{\partial Ca}{\partial r})$$

D is the diffusion coefficient for Ca^{2+} within the cell and r is the radial distance variable. The diffusion coefficient used in the simulation was 0.3 μm^2/ms for the cytoplasm (De Schutter, 1998) and 0.05 μm^2/ms for the nucleus which was adjusted to match the simulated nuclear Ca^{2+} kinetics to experimental data (see Table 2).

The explicit finite difference method (Crank, 1975) was used to solve the above equation. The cylindrical soma is divided into 50 shells. The index of the outmost shell is 49 and the index of the core is 0. The outermost shell and the inner core are half as thick as the others. The intervening 48 shells each have a thickness Δr which equals diam/(2*49) = 20/(2*49) = 0.204 μm, where diam is the diameter of the segment. Ca^{2+} diffusion within dendrites and the axon was treated similarly. The only difference is the

number of shells because of the different diameters of these compartments. The cylindrical dendrites and axon were divided into 5 shells.

$$\frac{Ca[i,t+\Delta t]-Ca[i,t]}{\Delta t}=\frac{D}{2\Delta r^2 i}((2i+1)Ca[i+1,t]-4iCa[i]+(2i-1)Ca[i-1,t]) \quad i\neq 0$$

$$\frac{Ca[0,t+\Delta t]-Ca[0,t]}{\Delta t}=\frac{4D}{\Delta r^2}(Ca[1,t]-Ca[0,t]) \quad i=0$$

The diffusion coefficient D was set according to the location of the shell i (if it is in the nucleus, D is 0.05 μm^2/ms otherwise D is 0.3 μm^2/ms).

Since the cytoplasmic and nuclear Ca^{2+} diffusion coefficients are different, diffusion between the nuclear envelope shell and the adjacent cytoplasmic shell was solved using a composite media approach described in Crank 1975. The diffusion problem in composite media was solved through the following steps. Imagining the nuclear boundary N to be extended one step (Δr) to the cytoplasm area, we can obtain:

$$\frac{Ca[N,t+\Delta t]-Ca[N,t]}{\Delta t}=\frac{Dn}{2\Delta r^2 N}((2N+1)Ca[N+1,t]-4NCa[N,t]+(2N-1)Ca[N-1,t])$$

where D_n is the nuclear Ca^{2+} diffusion coefficient, N is the index of the shell where nuclear boundary is. Also, imagining the cytoplasm boundary N to be extended one step to the nucleus area, we can obtain:

$$\frac{Ca[N,t+\Delta t]-Ca[N,t]}{\Delta t}=\frac{Dc}{2\Delta r^2 N}((2N+1)Ca[N+1,t]-4NCa[N,t]+(2N-1)Ca[N-1,t])$$

D_c is the cytoplasmic Ca^{2+} diffusion coefficient. Let $F(Ca_N,t)$ denote the flux across the interface. Since the diffusant enters one medium at the same rate as it leaves the other, the following condition should be satisfied.

$$D_n\frac{\partial Ca_N}{\partial r}=D_C\frac{\partial Ca_N}{\partial r}=F(Ca_N,t)$$

Eliminating F term from the first and the second equation, we can get the final diffusion equation:

$$\frac{Ca[N,t+\Delta t]-Ca[N,t]}{\Delta t}=\frac{(2N-1)^2}{8N^2}\frac{Dn}{\Delta r^2}(Ca[N-1,t]-Ca[N,t])+\frac{(2N+1)^2}{8N^2}\frac{Dc}{\Delta r^2}(Ca[N+1,t]-Ca[N,t])$$

N represents where the nuclear envelope is. In all simulations, N is equal to 34.

2.2.3.3 Ca^{2+} Store

Ca^{2+} stores were assumed as long tubes with diameter of 0.05 μm, occupying 20% of the volume of each cytoplasmic diffusion shell (De Schutter, 1998). The effect of stores on Ca^{2+} diffusion was not taken into consideration in this model. 100 mM of a non-mobile low-affinity (K_d 1 mM) Ca^{2+} buffer was placed in Ca^{2+} stores based on studies of De Schutter (1998). The resting level of free Ca^{2+} concentration in the stores was assumed to be 200 μM (Verkhratsky and Petersen, 1998). RyRs, Ca^{2+} pumps and Ca^{2+} leak channels were assumed to be evenly distributed on the surface of Ca^{2+} stores.

1) Ryanodine receptors

The kinetics of Ca^{2+} release through RyRs is modeled by a permeability change of the Ca^{2+} store with an exponential increase process combined with a slower exponential decay (Backx et al., 1989; Kargacin, 1994).

$$\frac{\partial Ca}{\partial t}=K_o(1-e^{-t/\tau_{on}})(e^{-t/\tau_{off}})(Ca_s-Ca)$$

The activation time constant τ_{on} (1.2 ms) was set according to activation rate of RyRs (Gyorke and Fill, 1993). The inactivation time constant τ_{off}(40 ms) was adjusted to match the decay time constant of the simulated cytoplasmic Ca^{2+} transient to

experimental data (Helmchen et al., 1996). K_o was adjusted to make cytoplasmic Ca^{2+} transient peak value ~300 nM (Helmchen et al., 1996).

In neurons, all-or-none CICR and a discrete threshold for CICR activation that was subject to modulation has been reported (Usachev and Thayer, 1997). Then, the release kinetics responding to single Ca^{2+} influx was modeled by assuming above release kinetics combined with a fixed threshold. The threshold was set to 150nM for all simulations.

Experiments conducted by Gyorke and Fill (1993) revealed a mechanism of Ca^{2+}-dependent adaptation of RyRs that is distinct from conventional desensitization in that the channels adapt to a Ca^{2+} stimulus, but are still able to respond to new Ca^{2+} influx. In the present study, the adaptation only to maintained Ca^{2+} stimulus is taken into account and implemented by detecting the sign of the first derivative of Ca^{2+} transient. If the sign of the first derivative of Ca^{2+} transient is changed from minus to positive and the Ca^{2+} concentration level is above release threshold, a new Ca^{2+} release event is switched on.

2.2.3.4 Ca^{2+} pumps and leak channels

Ca^{2+}-ATPase pumps on Ca^{2+} stores continuously extrude cytoplasmic Ca^{2+} into Ca^{2+} stores. The pumps were modeled using Hill's equation based on those of Goldbeter et al. (1990) and De Schutter (1998).

$$\frac{\partial Ca}{\partial t} = \frac{V_{max}(Ca)^n}{K^n + Ca^n}$$

The maximum pump velocity V_{max} = 4.9e-14 mol/cm$^2 \cdot$ s), Hill's coefficient n = 2, K_d = 0.001 mM.

An inward Ca^{2+} leakage was described by the equation

$$\frac{\partial Ca}{\partial t} = K_{leak}(Ca_s - Ca)$$

in which K_{leak} was adjusted to balance the pump efflux at the resting state.

Chapter 3 Results

In the present work, a realistic model of a hippocampal CA1 neuron with a detailed representation of intracellular Ca^{2+} dynamics, was built. Twelve kinds of ion channels found in hippocampal CA1 neurons experimentally were included (see Chapter 2.1). When tested, this model reproduced many important features of hippocampal CA1 neurons, including bursting vs. nonbursting behavior, AP backpropagation and AP frequency accommodation (Azouz et al., 1996; Cohen et al., 1999; Hoffman et al., 1997; Jensen et al., 1996; Johnston et al., 1999; Sah and Bekkers, 1996). Different firing patterns were obtained by adjusting ionic conductances and presynaptic firing frequencies. The intracellular Ca^{2+} dynamics model reproduces important features of Ca^{2+} transient kinetics in response to a single AP. Using the model we have predicted the cytoplasmic and nuclear Ca^{2+} transient in response to different firing patterns.

3.1 Electrophysiological property reproduction

3.1.1 Bursting vs. Nonbursting behavior

Hippocampal CA1 neurons although relatively homogenous do have different properties. For example, recordings by Jensen et al. (1996) have indicated that some hippocampal neurons exhibit burst-firing patterns in response to short depolarizing injections of current, while other CA1 neurons exhibit a regular spiking pattern. The difference between these two types is thought to be due to the relative abundance of the persistent sodium current (I_{NaP}) (Lipowsky et al., 1996). By only varying the amount of

I_{NaP} on dendrites (see Table 1), we were able to model this essential feature of hippocampal CA1 neurons. Fig. 7 shows different firing patterns, bursting and nonbursting, elicited by same amount of synaptic depolarization with two different parameter sets - one contains more I_{NaP} along dendrites than the other (0.1 mS/cm^2 vs. 0.05 mS/cm^2 on proximal dendrites, 0.05 mS/cm^2 vs. 0.02 mS/cm^2 on distal dendrites). An increase in the I_{NaP} was found to be associated with bursting behavior. Less synaptic conductance was needed to bring the cell to its firing threshold, with larger amount of I_{NaP}. In other words, I_{NaP} boosts synaptic currents in dendrites and contributes to bursting, which is consistent with what was suggested by experimental studies (Franceschetti et al., 1995; Lipowsky et al., 1996; Stuart and Sakmann, 1995).

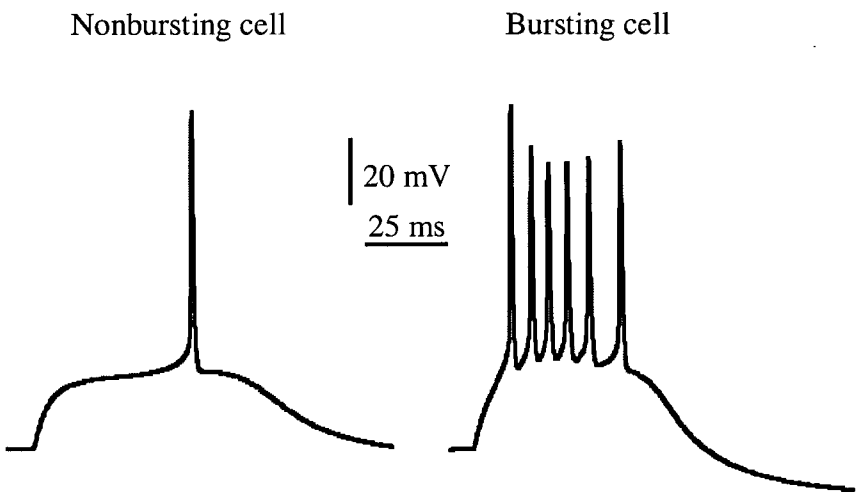

Figure 7 Simulated bursting vs. nonbursting behavior of hippocampal CA1 pyramidal neurons, by varying the amount of persistent sodium current (I_{NaP}) (see Table 1). Both waveforms are postsynaptic potential recorded at the soma resulting from single presynaptic AP and same amount of synaptic conductances. Bursting cell contains more I_{NaP} along dendrites than nonbursting cell (0.1 mS/cm^2 vs. 0.05 mS/cm^2 on proximal dendrites, 0.05 mS/cm^2 vs. 0.02 mS/cm^2 on distal dendrites).

3.1.2 AP backpropagation

A notable feature of hippocampal CA1 pyramidal neurons is the presence of backpropagating APs (Johnston et al., 1999; Spruston et al., 1995; Stuart et al., 1997). The fact that APs are initiated in the axon suggests that this site has the lowest threshold for AP initiation. Both theoretical and experimental evidence suggests the axon contains a high sodium channel density (reviewed in Stuart and Sakmann, 1994)). To model this, we included a higher concentration of voltage-gated sodium conductance within the axon hillock region (Mainen and Sejnowski, 1998) (see Table 1). Recent data suggests that the dendritic A-type potassium current plays an important role in attenuating dendritic backpropagating APs in hippocampal CA1 neurons (Hoffman et al., 1997). Along first three-fourths of apical dendrites, the density of A-type potassium channels increases five-fold (Hoffman et al., 1997). To model this we used a gradient of I_A expression as in Hoffman et al (1997). Both these factors were critical for reproducing AP backpropagation features of hippocampal CA1 pyramidal neurons. In Fig. 8 it is apparent that synaptically triggered APs are elicited in the somatic compartment before the dendrite, whereas with the same amount of voltage-gated sodium conductance within the axon hillock region as in other compartments, APs are elicited in dendrites following synaptic stimulation. The amount of AP spike attenuation at the dendrite 400 μm from soma is ~60% (see Fig. 9) which is quite similar to what was reported for hippocampal CA1 neurons in Stuart and Sakmann (1994). Interestingly, the amount of AP spike attenuation along the dendrite for the first AP is different from the successive APs (see Fig. 9). In Fig. 9 the diamond indicates the first AP in control condition (with the same amount I_A as reported by Hoffman et al. 1997). The square indicates the amplitude of a

second AP in control condition. It is apparent that the amount of attenuation is smaller for the second AP, especially at the middle part of the dendrite (400 μm – 800 μm). This result is consistent with what was proposed by Hoffman et al. 1997 and is likely due to the inactivation of distal dendritic A-type potassium channels by depolarizing voltage, resulting in a smaller shunting current. This also could be verified by decreasing the amount of A-type potassium conductance to 10% of the original amount (see Table 1), which mimics pharmacological experiment condition. This results in a much smaller AP amplitude attenuation along the dendrite, and also a smaller difference between the first AP and the second one. The increasing density of A-type potassium channels is suggested to decrease the peak amplitude of backpropagating APs, to suppress the amplitude of EPSPs, and to limit the occurrence of dendritically initiated APs (Johnston et al., 1999). The braking effect of A-type potassium channels for dendritic signal propagation can be modulated in a number of ways, including through voltage-dependent inactivation, and phosphorylation by protein kinases (Johnston et al., 1999).

Experimental evidence shows that APs propagate actively into the dendrites in hippocampal pyramidal cells due to the existence of dendritic sodium channels (Stuart and Sakmann, 1994). The boosting effect of dendritic sodium channels on backpropagating APs is demonstrated clearly by comparing backpropagation under the condition of a passive dendrite (star curve) with that of an active dendrite containing almost only sodium channels by reducing A-type potassium current to 10% of the original (triangle curve). The simulation result (Fig. 9) shows that the amplitude of a backpropagating AP is greatly reduced when dendritic sodium channels are not included (the passive dendrite case).

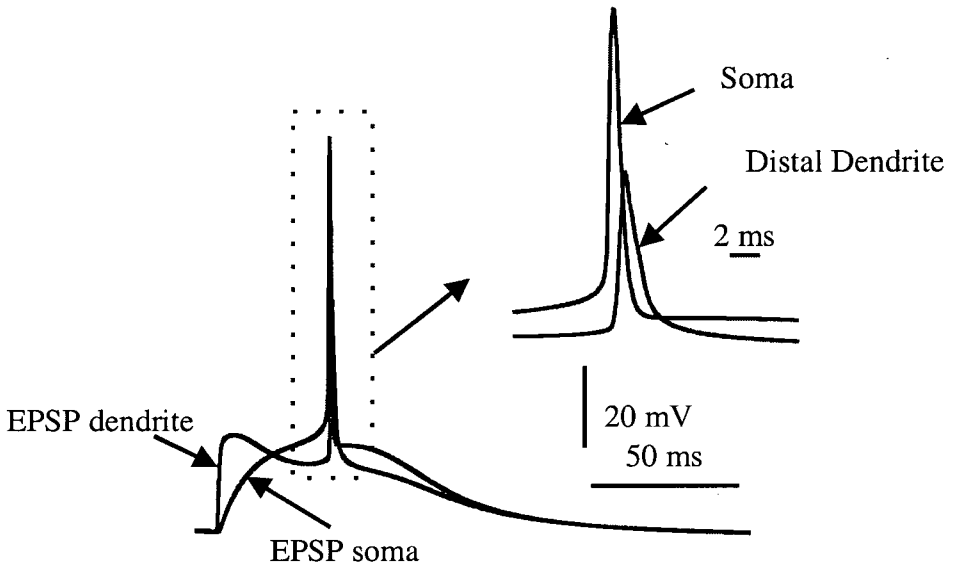

Figure 8 AP backpropagation. Dendritic membrane potential was recorded at 300 μm from the soma. The AP occurs within the soma before the dendrite. This suggests that suprathreshold synaptic stimulation leads to AP generation near the soma and subsequent propagation to the dendrites.

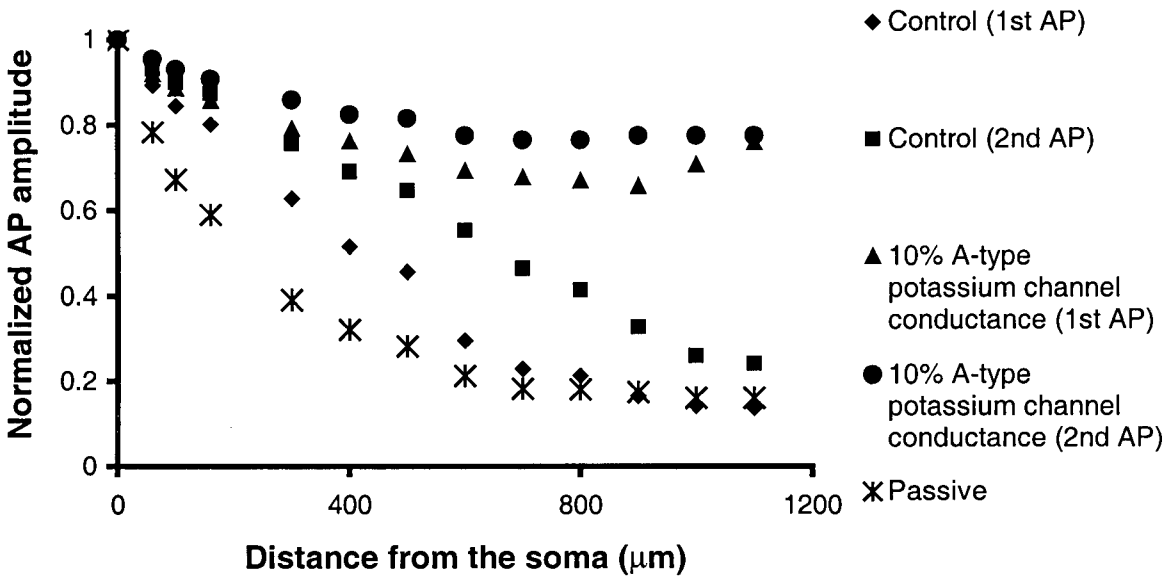

Figure 9 Percentage of AP spike attenuation vs. distance from the soma with the indicated amounts of I_A for single or paired APs.

3.1.3 Complex firing patterns in response to synaptic stimuli

To study the activation of VSCCs during stimuli that are relevant to synaptic plasticity, we modeled high frequency presynaptic stimulation and its effect on the postsynaptic membrane potential and somatic cytoplasmic and nuclear Ca^{2+} dynamics. Notably, analysis of the literature and our own experimental data suggest that hippocampal CA1 neurons exhibit a complex firing behavior in response to high frequency tetanic stimulation. The most notable features are AP frequency accommodation (Azouz et al., 1997; Storm, 1990; Yoshida et al., 1991) and AP spike adaptation (Fleidervish et al., 1996; Mickus et al., 1999). These two phenomena lead to a slowing of AP frequency during the burst as well as a reduction in amplitude (Mickus et al., 1999).

It has been reported that in hippocampal CA1 neurons, one type of voltage-activated potassium channel and three types of Ca^{2+}-activated potassium channels are responsible for spike frequency accommodation (Hirschberg et al., 1998; Sah and Bekkers, 1996; Sah and Clements, 1999; Stocker et al., 1999; Storm, 1990; Yoshida et al., 1991). Voltage-activated potassium channels include I_M and the Ca^{2+}-activated potassium channels include BK, sI_{AHP}, and SK. Among them, BK is voltage and Ca^{2+} activated, responsible for fI_{AHP} and contributing to AP repolarization (Velumian and Carlen, 1999). SK together with I_M, determines the interval between APs (Hirschberg et al., 1998; Stocker et al., 1999). Intracellular Ca^{2+} dynamics instead of intrinsic channel kinetics determines the SK current as well as the BK current (Mainen and Sejnowski, 1998). sI_{AHP} has very slow kinetics (slow onset and slow closing), responsible for late phase of I_{AHP} which lasts for seconds even after intracellular Ca^{2+} concentration returns

back to resting level (Sah and Clements, 1999). The kinetics of these potassium channels was modeled according to reported experimental data (see Chapter 2). To produce the voltage-dependent slow cumulative inactivation of sodium channels we added a slow variable *s* into the classical HH-type sodium channel model (see Chapter 2) and were able to obtain a frequency and voltage dependent inactivation of sodium channels during AP trains (see Fig. 4).

By reproducing the above features of hippocampal CA1 neurons, we were able to obtain a complex firing behavior in response to high frequency tetanic stimulation, which qualitatively resembled that recorded experimentally (Fig. 10). The left panel of Fig. 10 shows some typical firing patterns recorded from rat hippocampal neurons in response to 100 Hz synaptic tetanus stimulation. Fig. 10Aa is AP bursting behavior superimposed on a big membrane potential oscillation. Instead of bursting, the second cell (Fig. 10A b) fires repetitive APs with decreasing frequency during the tetanic stimulation. The right panel shows simulation results obtained with different stimulus strength and parameter sets. Fig. 10Ba was obtained with the parameter set for bursting cells (see Table 1), and 0.008 μS synaptic conductance and 100 Hz presynaptic APs. This record is similar to the experimental result shown in Fig. 10Aa. Fig. 10Bb was obtained with the parameter set for nonbursting cells (see Table 1), and 0.008 μS synaptic conductance and 100 Hz presynaptic APs. This cell fires repetitive APs with decreasing frequency similar to the one on the left. Moreover, if we increase the synaptic conductance to 0.3 μS, we can obtain a plateau waveform (a few APs followed by a high depolarized plateau), similar to what was recorded by Yeckel et al. (1995) on hippocampal neurons with tetanic stimulation. Comparison of simulated 100 Hz synaptic stimulus trains to experimental

data from Yeckel et al. (1999) as well as our own experiments indicated good qualitative correspondence (see Fig. 10).

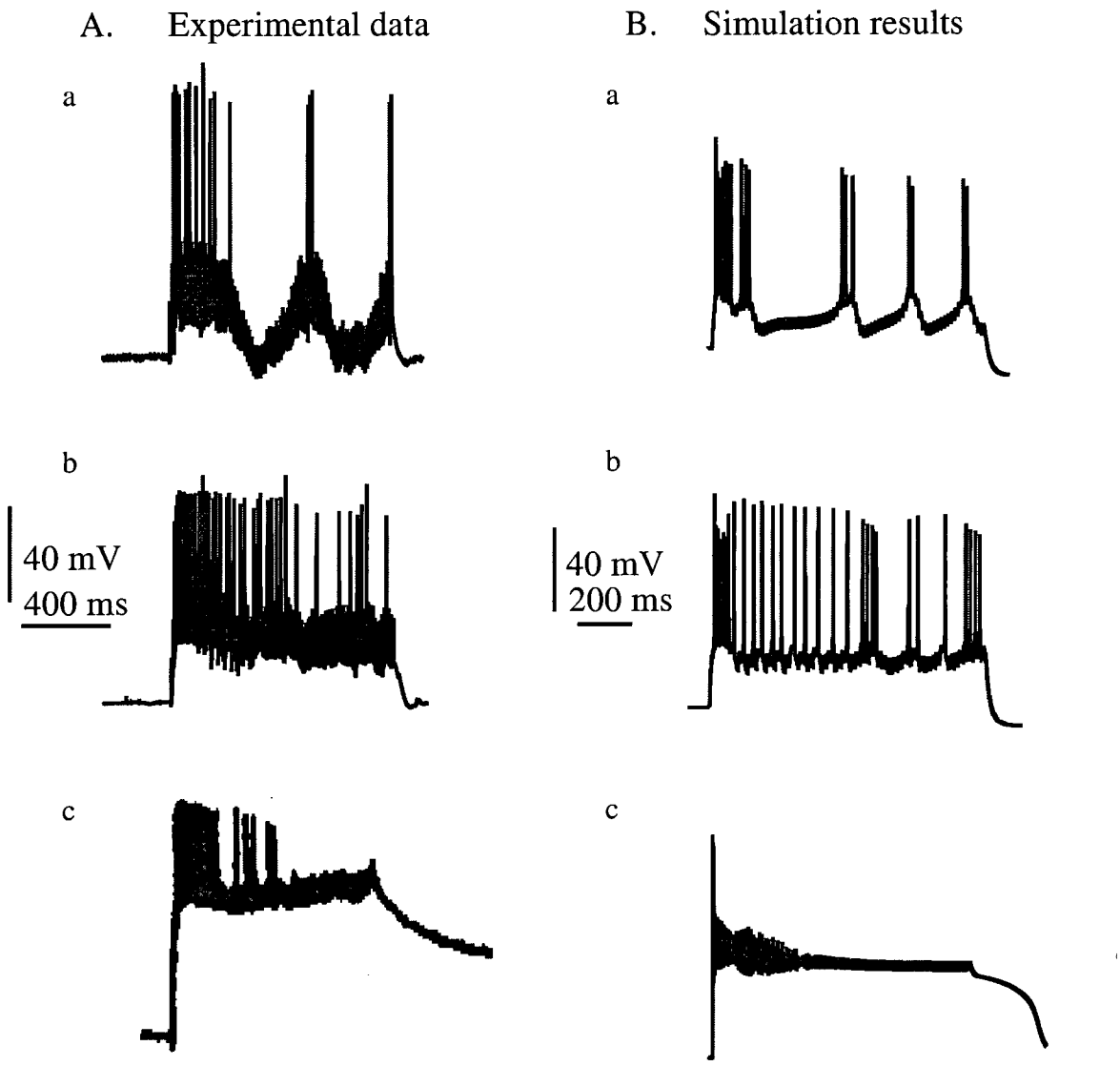

Figure 10 Complex firing patterns elicited by a 100 Hz synaptic tetanus in hippocampal pyramidal neurons, experimental data and simulation results. Left panel is experimental data. The first two were obtained in collaboration with Dr. S. Wang from rat hippocampal slices at ~32 degrees in the presence of picrotoxin. They were two different cells. The data on the lower left is experimental data from Yeckel et al. 1995. Right panel is the simulation result obtained with different stimulus strength and parameter sets (see text for details).

3.2 Intracellular Ca^{2+} dynamics reproduction

3.2.1 Intracellular Ca^{2+} dynamics in response to single AP

Analysis of experimental data indicated that somatic Ca^{2+} elevation attributed to VSCCs results in a delayed increase in intracellular Ca^{2+} levels within the nucleus (Nakazawa and Murphy, 1999). To better understand how synaptic stimuli might lead to nuclear elevations in Ca^{2+} we attempted to model this phenomenon. Several features are notable about the synaptically induced rise in nuclear Ca^{2+} levels. For example, there is a well-defined delay between the rise in cytoplasmic Ca^{2+} and nuclear Ca^{2+} of about 60 ms (Nakazawa and Murphy, 1999; O'Malley, 1994). In order to model this delay in nuclear Ca^{2+} elevation, we needed to reduce the Ca^{2+} diffusion constant within the nucleus to 0.05 $\mu m^2/s$ (0.3 $\mu m^2/s$ is the cytoplasmic value) (see Table 2). This also results in a slower decay time constant for the nuclear Ca^{2+} transient similar to what was obtained experimentally (Fig. 11; Table 3). The nuclear decay time constant obtained experimentally (Nakazawa and Murphy, 1999) is still larger than the simulation result (500 ms vs. 250.9 ms). This is probably because there was additional exogenous buffer (Ca^{2+} indicator fluo-3) in the cell, especially there was a higher concentration of fluo-3 in nucleus (Nakazawa and Murphy, 1999). Fluo-3 binds to free Ca^{2+} when Ca^{2+} concentration goes high and release Ca^{2+} when Ca^{2+} concentration goes low, thus it influences intracellular Ca^{2+} kinetics by slowing down Ca^{2+} signal.

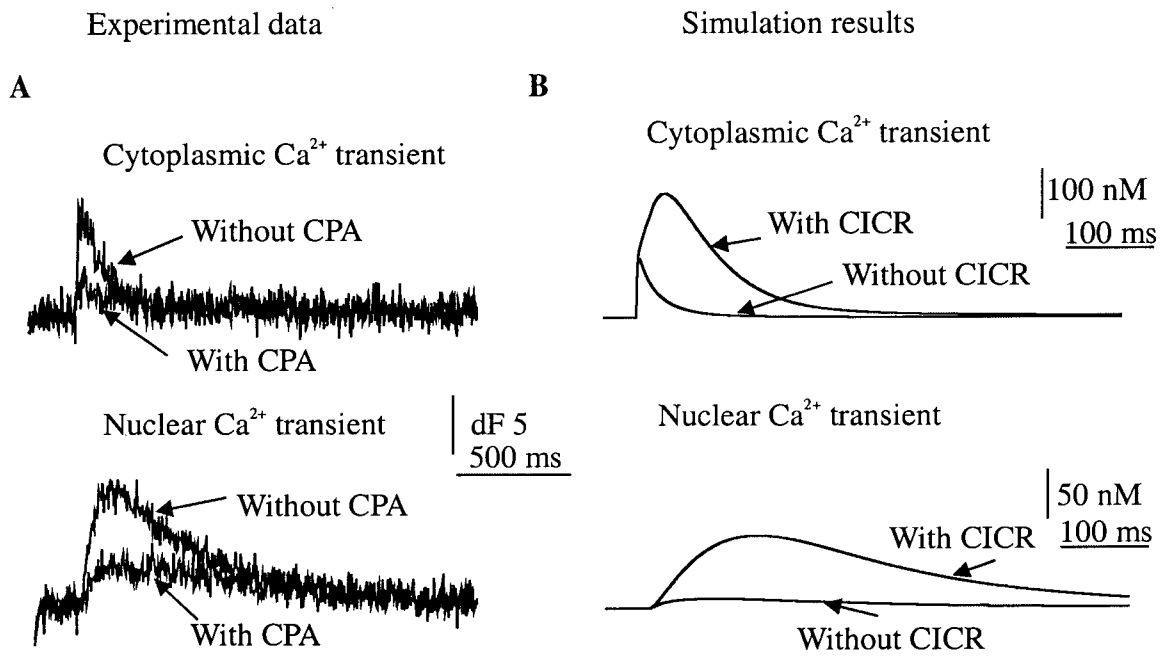

Figure 11 Intracellular Ca^{2+} dynamics in response to single AP at 34°C. **A.** Cytoplasmic and nuclear Ca^{2+} transients recorded from cortical neuron primary culture. CPA was used to block Ca^{2+} store refilling, and thus empty Ca^{2+} stores and block Ca^{2+} release mechanisms. To improve signal to noise ratio, all regions of the neuronal cytoplasm and the nucleus were averaged from the linescan data. Data were obtained with and without CPA perfusion. **B.** Simulated cytoplasmic and nuclear Ca^{2+} transients with and without CICR mechanism in the cytoplasm. In order to be able to compare with experimental data, all regions of the neuronal cytoplasm and the nucleus were also averaged.

Another important feature we produced in our model was the decay constant for cytoplasmic Ca^{2+} transient in response to a single AP stimulus (see Table 3). For determination of this value we could not rely on our previous experimental data since we did not correct for the presence of a Ca^{2+} indicator and its expected buffering. Therefore, we used data from Helmchen et al. (1996) that includes Ca^{2+} transient decay values extrapolated for conditions in which exogenous calcium buffers were absent. Adjustment of our model parameters (see Chapter 2.2) yielded a decay time constant for a single AP

stimulus that closely resembled that found in the Helmchen paper (Table 3). Furthermore, the peak value of the simulated cytoplasmic calcium transient in response to a single AP was around 300 nM, similar to what was reported for hippocampal CA1 neuron (Helmchen et al., 1996).

	Model	**Data**
Latency to peak nucleus versus cytoplasm	50 ms	60 ms
Role of Ca^{2+} stores for nuclear elevation	Almost complete	partial
Kinetics of nuclear Ca^{2+} transient decay (single AP)	250.9 ms	506.4 ms (with exogenous Ca^{2+} buffer)
Kinetics of cytoplasmic Ca^{2+} transient decay (single AP)	84.2 ms	92 ms (without exogenous Ca^{2+} buffer) (Helmchen et al. 1996) 141.9 ms (with exogenous Ca2+ buffer)

Table 3 Intracellular Ca^{2+} dynamics in response to single AP – Comparison of experimental data and simulation results.

3.2.2 Role of CICR

Garaschuk et al. (1997) investigated the properties of ryanodine-sensitive Ca^{2+} stores in rat hippocampal CA1 pyramidal neurons. Their study suggested an important role of Ca^{2+} stores in controlling the kinetics of Ca^{2+} signals in hippocampal CA1 pyramidal neurons. Recently, it was reported that blocking CICR decreases synaptic activity induced gene transcription activity by ~50% (Hardingham et al., 1999). Thus, we sought to investigate the role of Ca^{2+} stores in nuclear Ca^{2+} elevation. Our

pharmacological experiments on cultured cortical neurons suggested an important role of Ca^{2+} stores in nuclear Ca^{2+} elevation (Fig. 11 A). Using CPA, a Ca^{2+} pump inhibitor (Garaschuk et al., 1997), we were able to empty Ca^{2+} stores by blocking Ca^{2+} store refilling. In Fig. 11 A, a single AP caused cytoplasmic and nuclear Ca^{2+} elevation, which is sensitive to CPA application. Table 4 shows the group data of the pharmacological experiments. Data are expressed in percent increase of raw fluorescence signal over basal fluorescence level. With CPA application, the cytoplasmic Ca^{2+} peak decreased by 32% and the nuclear Ca^{2+} peak decreased by 30.5%. Consistent with this, inclusion of cytoplasmic Ca^{2+} stores readily allowed Ca^{2+} levels to be elevated within the nuclear compartment, whereas removal of a Ca^{2+} store mechanism from the cytoplasm (Fig. 11 B), greatly diminished the nuclear Ca^{2+} transient. This result suggested that propagation of Ca^{2+} signals to the nucleus was likely dependent on a store mechanism. Interestingly, simulation data suggested a much stronger role for Ca^{2+} stores than actual experiment (Table 3). This discrepancy may be caused by the fact that in the experimental conditions, there were several kinds of Ca^{2+} channels that mediate Ca^{2+} influx during an AP. It has been suggested that L-type VSCCs only mediate a small portion of total Ca^{2+} influx during an AP (Mermelstein et al., 2000), whereas in the simulation, only Ca^{2+} influx through L-type VSCCs was taken into consideration. Thus, under our experimental condition, Ca^{2+} influx itself resulted in significant intracellular Ca^{2+} elevation, while in the simulation, Ca^{2+} influx itself only resulted in a small intracellular Ca^{2+} elevation. Moreover, there may exist CPA-insensitive Ca^{2+} stores, that may further contribute to the discrepancy.

After establishing the role of CICR in nuclear Ca^{2+} transients in response to single APs (see Fig. 11), we examined its role in response to AP trains with different frequencies. Simulation results suggested that the existence of a Ca^{2+} store greatly differentiates high frequency stimuli from low frequency stimuli in terms of nuclear Ca^{2+} level (Fig. 12). Whereas, without the Ca^{2+} store, the relationship between nuclear Ca^{2+} peak value and AP frequency is linear.

Ca^{2+} *transient*	*Control* ($\Delta F/F_0$)	*CPA* ($\Delta F/F_0$)	*P value*
Nuclear	28.1%±0.1%	19.0%±0.4%	0.012783
Cytoplasmic	33.6%±1.1%	23.4%±1.0%	0.016994

Table 4 Group data: single AP leads to cytoplasmic and nuclear Ca^{2+} elevation that is sensitive to agents that deplete Ca^{2+} stores – CPA.

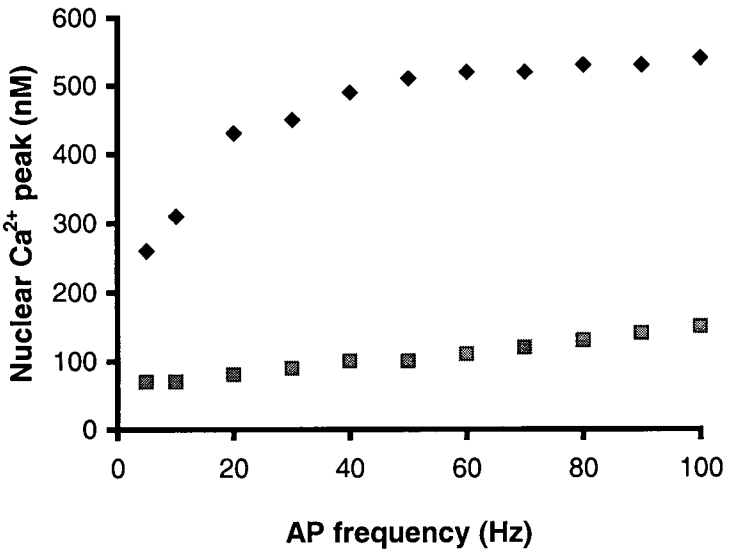

Figure 12 Nuclear Ca^{2+} dynamics in response to AP trains with different frequencies, with and without CICR. Diamonds denote the nuclear Ca^{2+} peak in response to AP trains with the presence of CICR. Squares denote that without the presence of CICR.

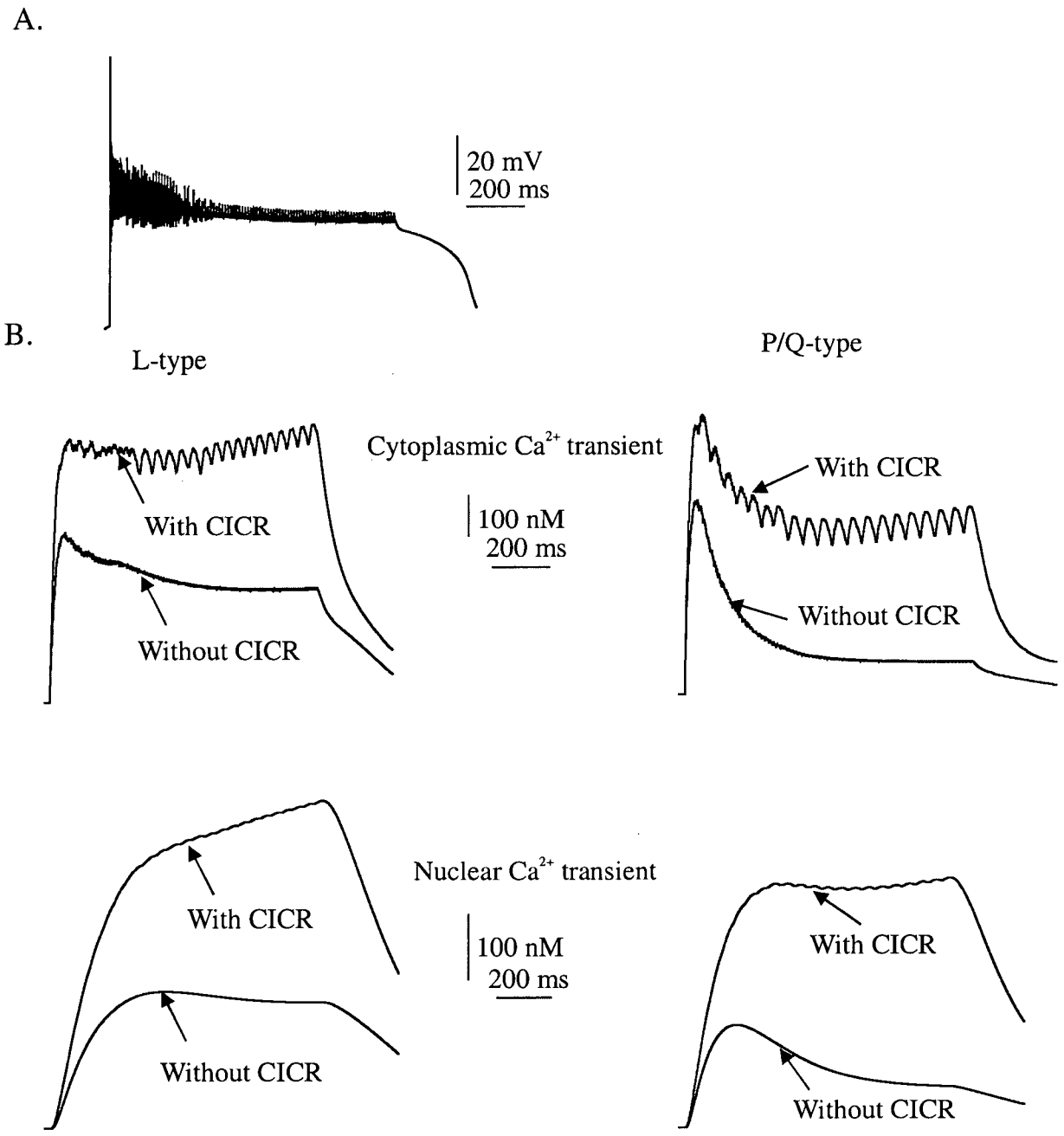

Figure 13 Role of CICR in intracellular Ca^{2+} dynamics in response to tetanic synaptic stimulation. **A.** Postsynaptic membrane potential at the soma obtained with 100 HZ presynaptic APs and $g_{max(NMDA,\ AMPA)}$ = 0.3 μS. **B.** Resulting intracellular Ca^{2+} transients with and without CICR. Left panel is simulation results obtained with L-type VSCCs on the soma, while right panel shows simulation results with P/Q-type VSCCs on the soma.

Since previous modeling and experimental data suggested a critical role for Ca^{2+} stores in nuclear Ca^{2+} elevation we also sought to examine their role in synaptic stimuli in tetanic synaptic stimulation. For both L-type and P/Q-type calcium channels we observed in the model that the Ca^{2+} stores had a substantial influence on the amplitude of the nuclear Ca^{2+} transient (Fig. 13). In contrast to that observed with the single AP stimulation (Fig. 11), in the absence of Ca^{2+} stores there was still a significant elevation of nuclear Ca^{2+} concentration, which was caused by the large amount of Ca^{2+} influx via VSCCs during the tetanic synaptic stimulation.

3.3 Intracellular Ca^{2+} dynamics in response to different firing patterns

3.3.1 L-type VSCCs distinguish different firing patterns

After establishing a model of nuclear Ca^{2+} elevation that was in part dependent on calcium stores, we applied different synaptic membrane potential waveforms that might be associated with forms of plasticity (Deisseroth et al., 1996). Four classes of stimuli were chosen. The first was a subthreshold EPSP (Fig. 16A a). With larger synaptic conductances and the parameter set for bursting cells (increased I_{NaP}), we could produce a bursting waveform (Fig. 16A b). With the parameter set for a nonbursting cell and strong synaptic inputs, we could produce a repetitive firing waveform (Fig. 16A c). A very high level of synaptic stimulation (synaptic conductance is twenty times higher than above condition) produces a depolarized plateau (Fig. 16A d). We then examined the effects of these different stimuli on Ca^{2+} influx through L-type VSCCs. As recent experiments

suggest that the neuronal L-type calcium channels might have unique properties that allow them to distinguish between EPSPs and action potentials, we adjusted L-type current activation parameters to match that observed (Mermelstein et al., 2000) (see Chapter 2). The simulated Ca^{2+} currents in response to different firing patterns are shown in Fig. 14 A. The amount of Ca^{2+} influx in response to a firing pattern is represented by the integral of Ca^{2+} current over 1 s, designated as $I_{\text{firing pattern}}$. $I_{\text{Repetitive APs 2}}$ is only 47% of the I_{Plateau}, although the repetitive AP pattern contains a large number of APs (see Fig. 14 B). This result is consistent with what was speculated in Mermelstein et al. (2000). In order to see whether this phenomenon is L-type VSCCs specific, P/Q-type VSCCs were put on the soma instead of L-type VSCCs. P/Q-type VSCCs and L-type VSCCs have different kinetics. Compared with L-type VSCCs, P/Q-type VSCCs activate at higher membrane potential and have faster kinetics (Mermelstein et al., 1999). Simulated Ca^{2+} currents are shown in Fig. 15 A and the integral of Ca^{2+} current in response to different firing patterns is compared in Fig. 15 B. The results show that in the case of P/Q-type VSCCs, there is little advantage of one waveform over another. Comparison of the Ca^{2+} current via L-type VSCCs with that of P/Q-type VSCCs in response to plateau waveform indicates that L-type VSCCs activate substantially during steady-state depolarization (~ -30 mV) whereas P/Q-type VSCCs mainly respond to the AP, which agrees with what was suggested by Mermelstein et al. (2000).

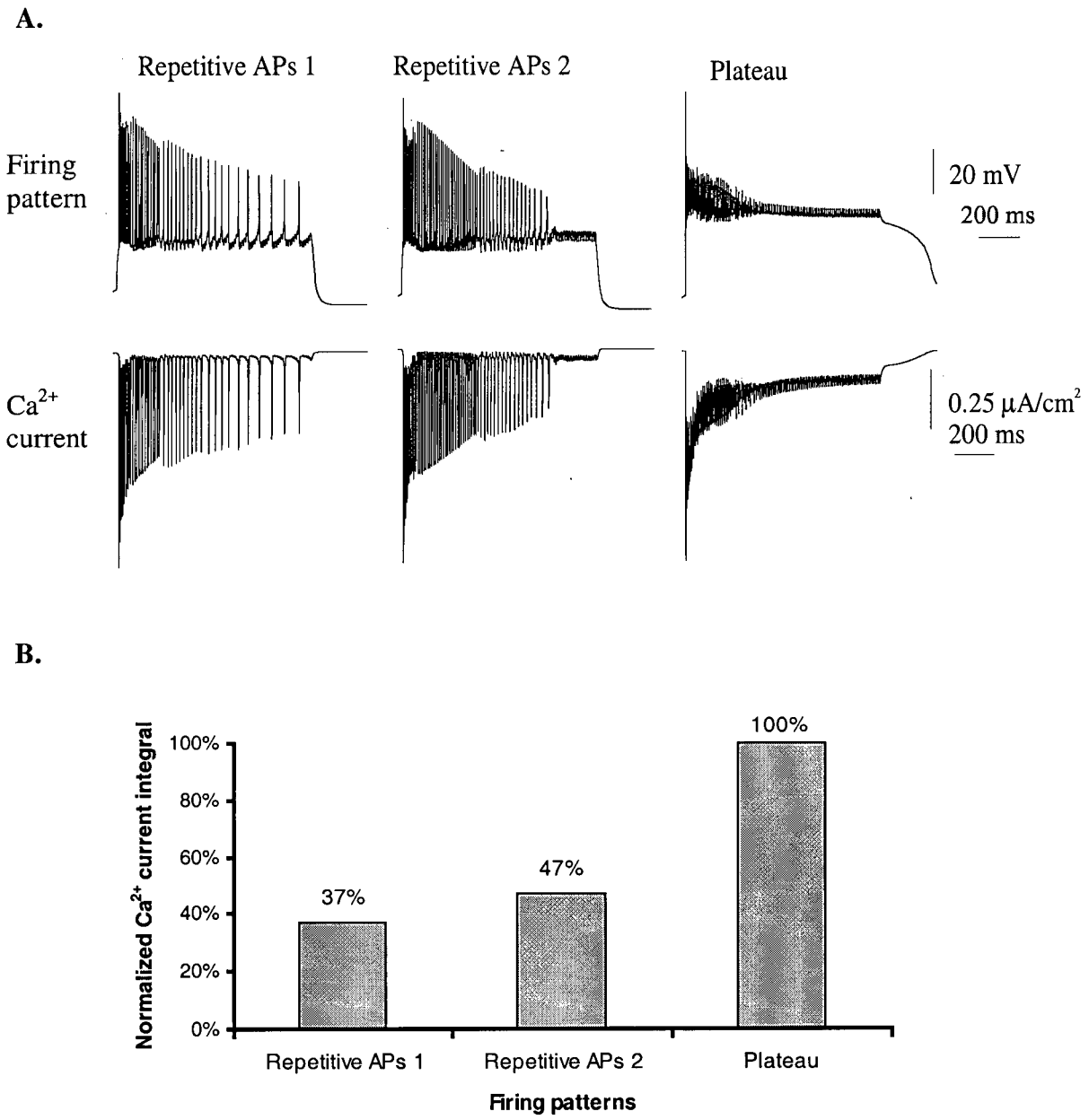

Figure 14 Ca^{2+} influx through L-type VSCCs in response to different firing patterns. **A.** Ca^{2+} current in response to different firing patterns. Repetitive APs 1 is obtained with 100 Hz presynaptic APs and $g_{max(NMDA,AMPA)}$ = 0.01 μS, whereas, repetitive APs 2 is obtained with $g_{max(NMDA,AMPA)}$ = 0.015 μS. The synaptic conductance was set as 0.3 μS for the plateau. **B.** Comparison of Ca^{2+} current integral over 1 s, normalized to the Ca^{2+} current integral in response to plateau waveform.

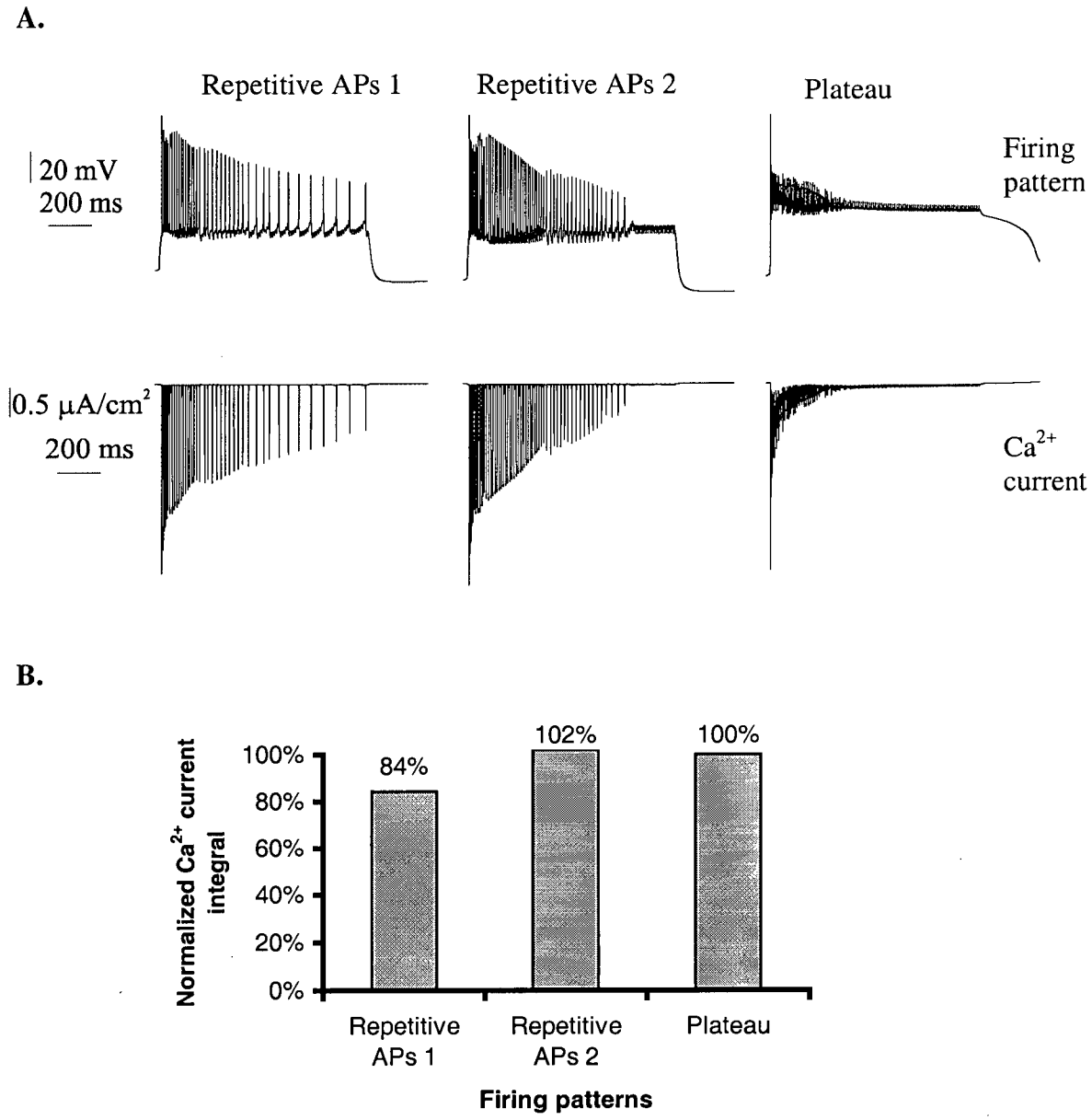

Figure 15 Ca^{2+} influx through P/Q-type VSCCs in response to different firing patterns. **A.** Ca^{2+} current in response to different postsynaptic firing patterns. Repetitive APs 1 is obtained with 100 Hz presynaptic APs and $g_{max(NMDA,AMPA)}$ = 0.01 μS, whereas, repetitive APs 2 is obtained with $g_{max(NMDA, AMPA)}$ = 0.015 μS. The synaptic conductance was set as 0.3 μS for the plateau. **B.** Comparison of Ca^{2+} current integral over 1s, normalized to the Ca^{2+} current integral in response to plateau waveform.

We then examined the effects of these different stimuli on nuclear Ca^{2+} transients produced by L-type VSCCs expressed on the neuronal soma. Simulated Ca^{2+} transients in response to different synaptic stimuli are shown in Fig. 16. Sub threshold EPSPs of ~16 mV did not result in any detectable increase in Ca^{2+} in the soma or the nucleus. In contrast, bursting waveforms resulted in Ca^{2+} transients that were largely associated with the presence of APs. For repetitive firing waveforms we observed robust nuclear and cytoplasmic Ca^{2+} transients that seem to become attenuated with repetitive stimulation and associated voltage-dependent inactivation of the AP. Whereas the high depolarization plateau causes a sustained higher level of cytoplasmic and nuclear Ca^{2+} transient. The differential response to these firing patterns agrees with what was suggested by experimental data (Mermelstein et al., 2000; Nakazawa and Murphy, 1999). In order to know whether these results are L-type specific, we also examined the effects of these different stimuli on nuclear Ca^{2+} transient produced by P/Q-type VSCCs expressed on the neuronal soma (see Fig. 16 C). The simulation results suggest that with P/Q-type VSCCs on the soma, Ca^{2+} transients in response to high depolarization plateau and repetitive APs are similar. The results suggest that L-type VSCCs have specific kinetic properties, together with their somatic distribution, making them be able to distinguish different types of synaptic stimuli in terms of nuclear Ca^{2+} transient. This may account for how normal synaptic activity is discriminated from activity that leads to gene expression.

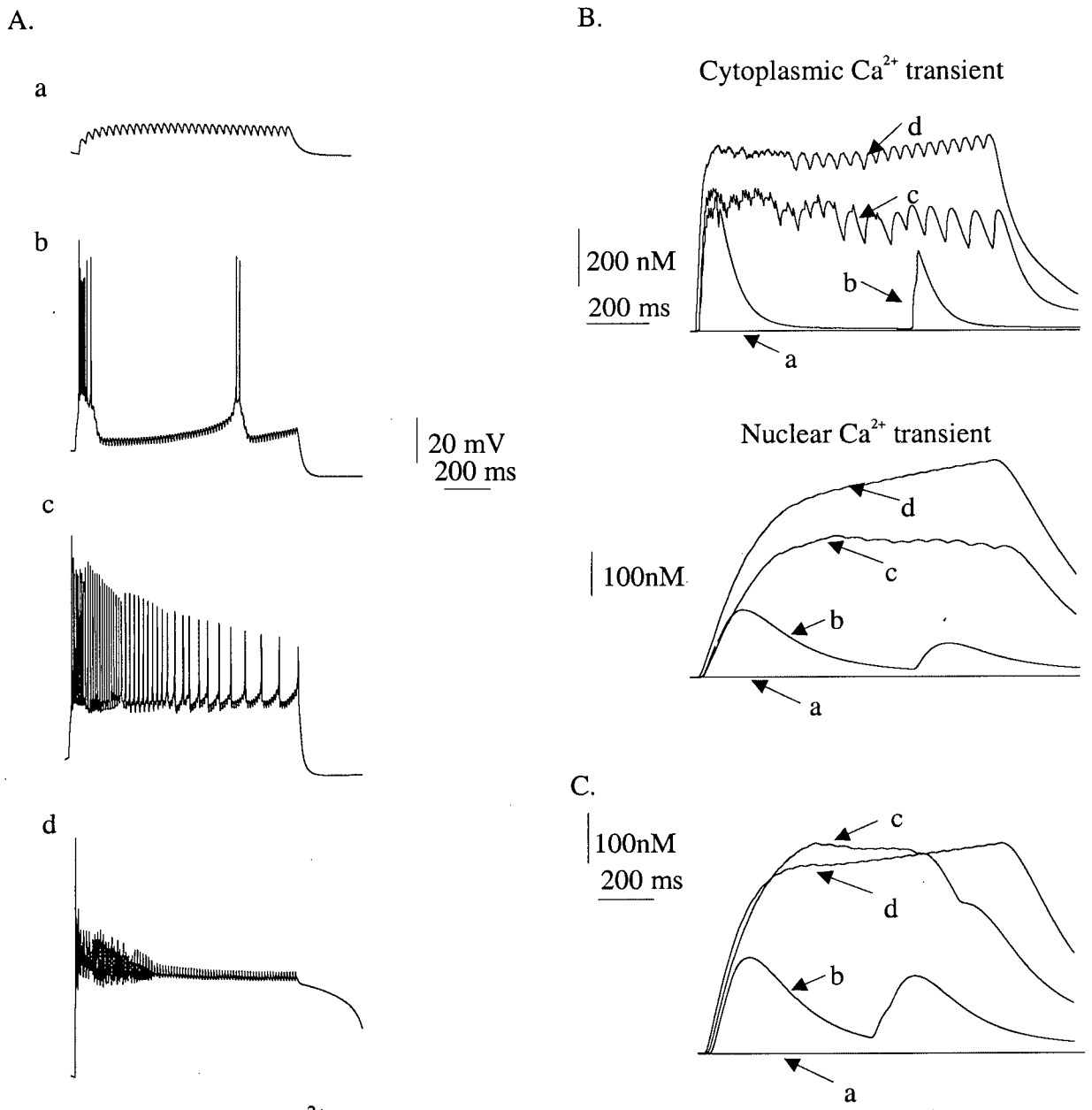

Figure 16 Nuclear Ca^{2+} dynamics in response to different firing patterns. **A.** Firing patterns obtained with different parameter sets. **a.** subthreshold EPSP, obtained with nonbursting cell parameter set (see table 2.1), 30 Hz synaptic stimulus and $g_{max(NMDA,AMPA)}$ = 0.005 μS. **b.** Bursting APs, obtained with bursting cell parameter set (see table 2.1), 100 Hz synaptic stimulus and $g_{max(NMDA,AMPA)}$ = 0.008 μS. **c.** Repetitive APs, obtained with nonbursting cell parameter set (see table 2.1), 100 Hz presynaptic stimulus and $g_{max(NMDA,AMPA)}$ = 0.01 μS. **d.** Plateau, obtained with nonbursting cell parameter set (see table 2.1), 100 Hz synaptic stimulus and $g_{max(NMDA,\ AMPA)}$ = 0.3 μS. **B.** Cytoplasmic and nuclear Ca^{2+} dynamics with L-type VSCCs on the soma in response to firing patterns shown on the left. **C.** Nuclear Ca^{2+} dynamics with P/Q-type VSCCs on the soma in response to firing patterns shown on the left.

3.4 What properties of L-type VSCCs are important for firing pattern selection

After the observation that L-type VSCCs distinguish different firing patterns, we sought to investigate that what properties of L-type VSCCs are important for this selective response to different firing patterns.

Half activation membrane potential (V_{half})

Since it was reported by Mermelstein et al. (2000) that L-type VSCCs respond to more negative potentials than non L-type VSCCs, we first investigated L-type VSCC models with different V_{half}. Fig. 17 A shows IV curves with different V_{half}. Integral of Ca^{2+} current in response to different waveforms (repetitive firing and plateau) is compared in Fig. 17 B. When V_{half} is –18.6 mV (default), $I_{Repetitive\ APs}/I_{Plateau}$ = 47%, whereas, when V_{half} is –12 mV, $I_{Repetitive\ APs}/I_{Plateau}$ = 65%. It is clear that V_{half} is very important to the selective response in terms of the amount of Ca^{2+} influx.

Opening rate of L-type VSCCs

Since Mermelstein et al. (2000) suggested that the slower opening rate of L-type VSCCs (as compared with non L-type VSCCs) may contribute to distinguishing EPSPs over APs, we sought to change the opening rate of L-type VSCCs and see its influence on the amount of Ca^{2+} influx in response to different firing patterns ($I_{firing\ pattern}$). In order to change the opening rate independently, we changed the dependence of the L-type VSCC activation time constant on voltage from eq. 2.1 to eq. 3.1:

$$\tau_m = (1 - e^{((v+14.6)/9.24)})/(0.03(-v-14.6)\cdot(1+e^{((v+14.6)/9.24)})) \qquad (2.1)$$

$$\tau_m = (1 - e^{(v+14.6)/15.24)})/(0.01\cdot(-v-14.6)\cdot(1+e^{(v+14.6)/7.24)})) \qquad (3.1)$$

A.

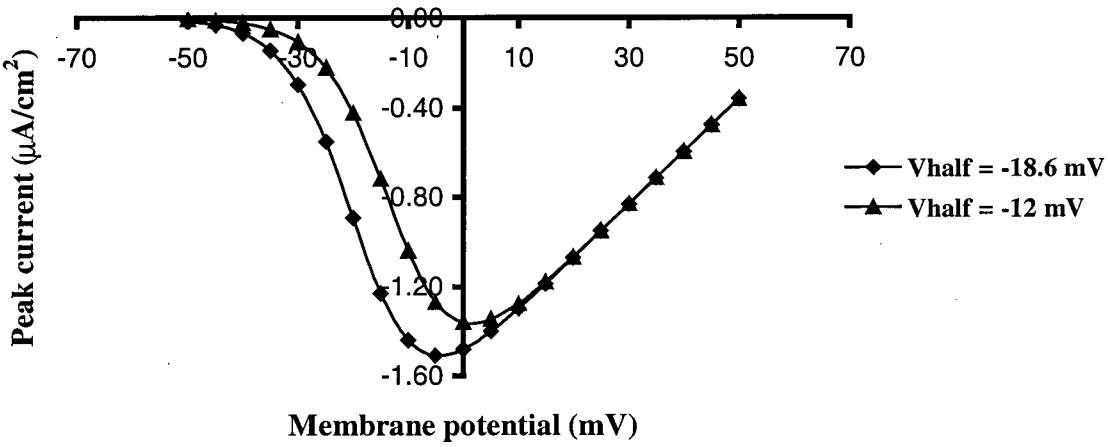

B.

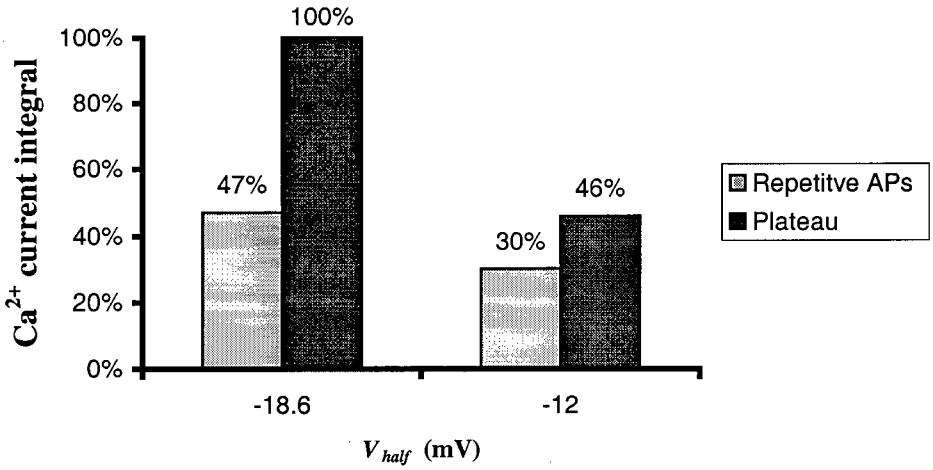

Figure 17 Impact of different half activation potentials on selective response of L-type VSCCs to different firing patterns. **A.** IV curves of L-type VSCC model with different V_{half}, **B.** Comparison of Ca^{2+} current integral in response to repetitive APs and plateau, with different V_{half} of L-type VSCCs. Repetitive APs and plateau were obtained with $g_{max(NMDA,AMPA)}$ = 0.015 μS and 0.3 μS respectively, and both with 100 Hz synaptic stimulus.

The resulting rise time vs. voltage curve is shown in Fig. 18. By doing this, we changed the opening rate of L-type VSCCs while keeping the closing rate almost the same, and did not influence the IV curve. Simulated Ca^{2+} currents in response to different levels of synaptic stimuli are shown in Fig. 19 A. The upper panel shows simulated Ca^{2+} currents with eq. 2.1 (slower opening rate), while the lower panel is that with eq. 3.1 (faster opening rate). It is clear that the opening rate will influence the amount of Ca^{2+} influx during each AP (peak current almost 2 times larger in faster opening rate case than the other). $I_{\text{firing pattern}}$ for each case is shown in Fig. 19 B. The faster opening rate results in a significant increase of Ca^{2+} influx during repetitive firing, whereas it has little influence on Ca^{2+} influx during plateau. $I_{\text{Repetitive Aps}}/I_{\text{Plateau}}$ increases from 47% with the slower opening rate (default) to 62% with the fast opening rate. From the above simulation results, it is clear that the slow opening rate of L-type VSCCs does contribute to distinguishing different firing patterns.

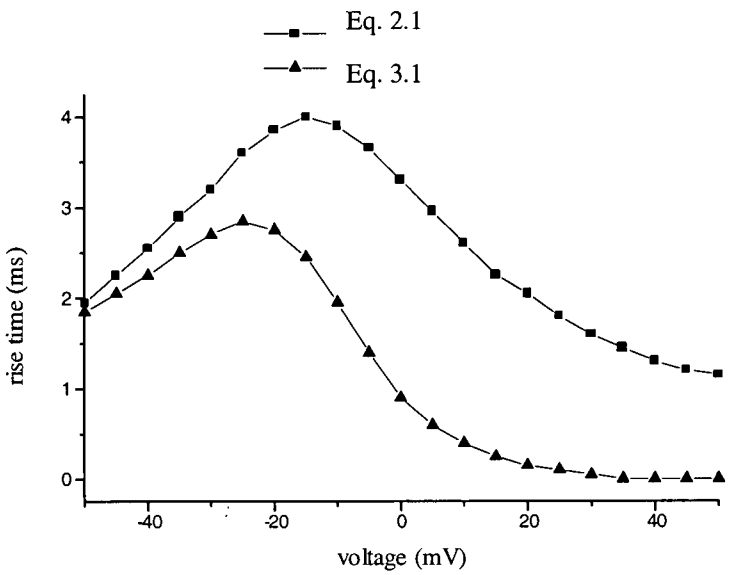

Figure 18 10%-90% rise time of L-type Ca^{2+} current in response to different levels of step depolarization. Different rise time curves are achieved by changing the dependence of activation time constant (τ_m) of L-type VSCC model on membrane potential (eq. 2.1 (default) vs. eq. 3.1 (faster opening rate case)).

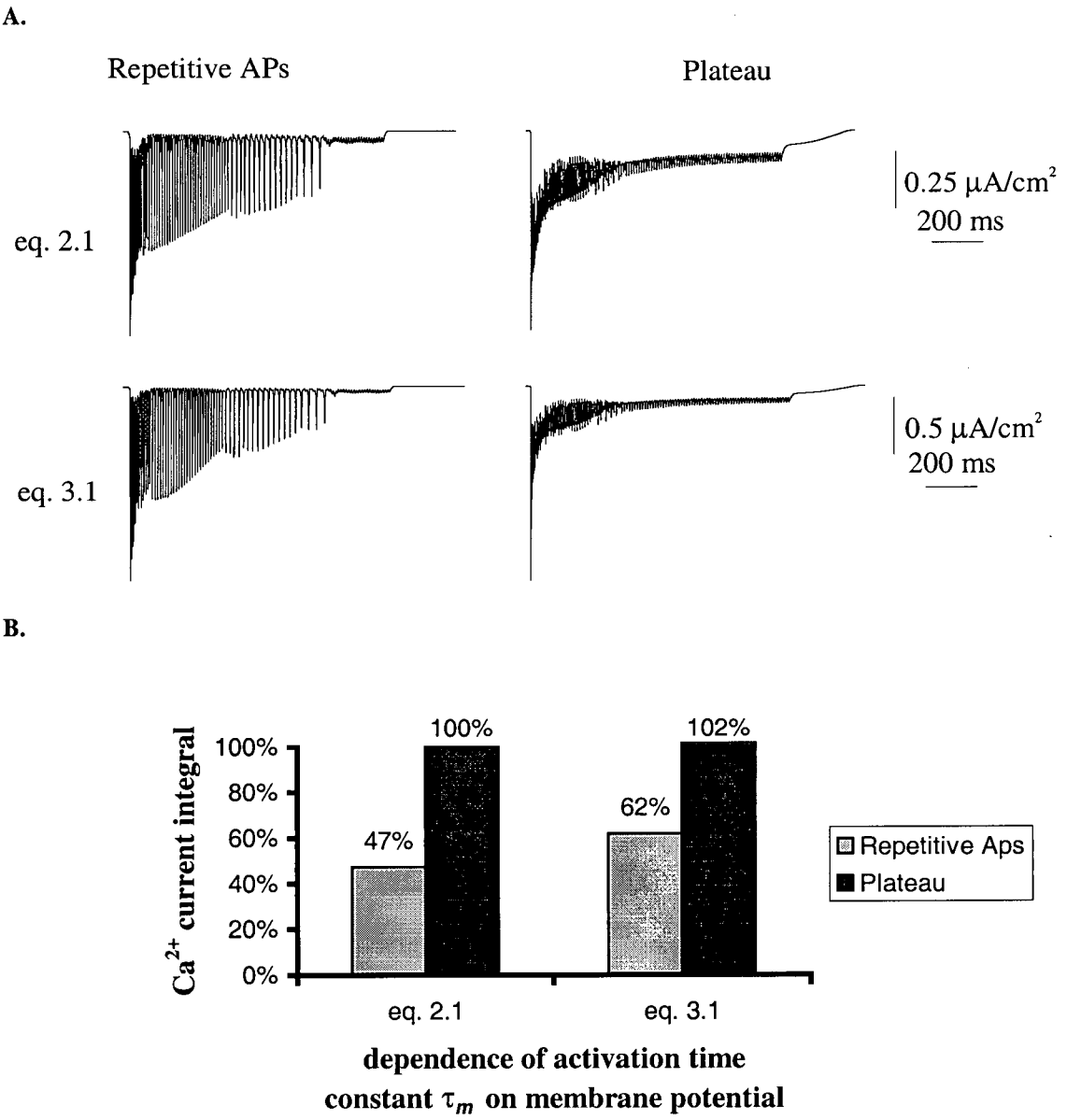

Figure 19 Impact of different opening rates on selective response of L-type VSCCs to different firing patterns. Opening rate of L-type VSCCs is determined by the activation time constant τ_m, which is set by eq. 2.1 in the default case. To achieve faster opening rate, eq. 3.1 is used. **A.** Simulated Ca^{2+} currents with different opening rate in response to different firing patterns. Repetitive APs and plateau were obtained with $g_{max(NMDA,AMPA)}$ = 0.015 μS and 0.3 μS respectively, and both with 100 Hz synaptic stimulus. **B.** Comparison of Ca^{2+} current integral in response to different firing patterns.

3.5 Critical role of coupling between VSCCs and Ca^{2+} store

Previous studies in muscle suggest a highly specific spatial relationship between the L-type VSCCs and the RyRs (Nakai et al., 1996). In neurons, it has been suggested that there is functional coupling between RyRs and L-type VSCCs (Chavis et al., 1996). The functional coupling between them was so tight that it even persisted in inside-out membrane patches (Chavis et al., 1996), which suggested a possibility that the co-localization between Ca^{2+} stores and L-type VSCCs may also happen in neurons. Besides the coupling between L-type VSCCs and Ca^{2+} stores, the distribution of Ca^{2+} stores on axon terminals as well as P/Q-type VSCCs, and their important role in transmitter release, implicate that there probably also exists similar coupling between them. Sutton et al. (1999) show that selective influx of Ca^{2+} through P/Q-type channels is responsible for activating expression of syntaxin-1A, while blockade Ca^{2+} release from intracellular Ca^{2+} store reduces syntaxin expression stimulated by P/Q-type VSCCs.

Therefore, we sought to determine whether a similar coupling between VSCCs and stores would facilitate CICR action. In Fig. 20 we located the Ca^{2+} stores at varying distances from VSCCs. When the stores were within 50 nm of the Ca^{2+} channels we observed a robust store-dependent intracellular Ca^{2+} increase. Whereas, moving the Ca^{2+} stores 2 μm from Ca^{2+} channels resulted in a large reduction in the elevation of Ca^{2+} concentration.

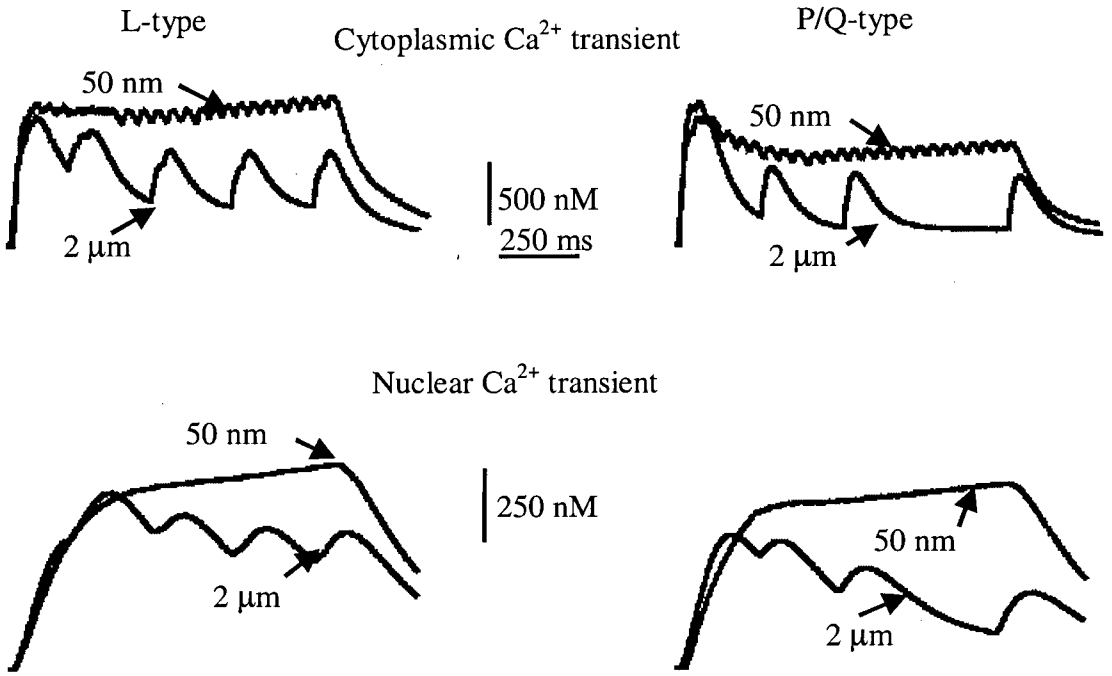

Figure 20 Critical role of spatial coupling between VSCCs and Ca^{2+} stores. To examine the role of spatial coupling between VSCCs and Ca^{2+} stores on intracellular Ca^{2+} dynamics, cytoplasmic and nuclear Ca^{2+} transients were obtained with Ca^{2+} stores placed 50 nm and 2 μm away from the plasma membrane respectively. Left panel shows intracellular Ca^{2+} transients with L-type VSCCs on the soma. Right panel shows simulation results with P/Q-type VSCCs on the soma.

Chapter 4 Discussion

4.1 Significance of this study

This compartmental cell model, built with NEURON, contains 4 compartments, including one soma, one axon and two dendrites. It includes 12 kinds of ion channels that were found in hippocampal CA1 neurons experimentally, and reproduces many electrophysiological properties of hippocampal CA1 neurons. By adjusting the amount of persistent sodium current along dendrites, the model cell exhibits nonbursting or bursting behavior, which resembles properties of two types of hippocampal CA1 neurons respectively (Jensen et al., 1996). By including a complex array of active conductances in dendrites based on experimental data and other modeling studies, we reproduced another key feature of hippocampal CA1 neurons, AP backpropagation. We were able to closely model most features of AP backpropagation in hippocampal CA1 neurons, such as the amount of amplitude attenuation along dendrites (see Fig. 9) and the propagation time course (the delay between somatic AP and dendritic AP at 200 μm from the soma is approximately 1.5 ms, similar to what was reported in Stuart et al. (1997). The literature suggests that hippocampal CA1 neurons exhibit a complex firing behavior, such as AP frequency accommodation and AP spike adaptation. Many studies have been carried out to investigate the mechanisms underlying these behaviors in hippocampal CA1 neurons. It has been suggested that four types of potassium currents (I_M, BK, SK and sI_{AHP}) are responsible for the induction of AP frequency accommodation (Azouz et al., 1997; Storm, 1990; Yoshida et al., 1991), whereas the slow-inactivation of sodium current is responsible for AP spike adaptation (Fleidervish et al., 1996; Mickus et al., 1999). By

including the above mechanisms, the model cell exhibits complex firing behavior similar to what was recorded from hippocampal neurons (see Fig. 10).

Being able to reproduce several key features of hippocampal CA1 neuron electrophysiology, we sought to examine the role of L-type VSCCs in differentiating synaptic activity that leads to gene expression from normal synaptic activity. In order to study the activation of VSCCs by stimuli that are relevant to synaptic plasticity, we have modeled high frequency presynaptic stimulation and its effect on postsynaptic membrane potential. The L-type VSCC model was based on experimental data from Mermelstein et al. (2000) in which experiments were conducted at room temperature. A Q_{10} equal to 2.5 was used to predict the behavior of L-type VSCCs at physiological temperature (Acerbo and Nobile, 1994). Simulation results suggest that a plateau waveform with steady-state depolarization to ~–30 mV is preferred by L-type VSCCs over repetitive APs. The integral of the Ca^{2+} current mediated by L-type VSCCs in response to repetitive APs ($g_{max(NMDA,\ AMPA)}$ = 0.015 μS) is only 47% of that of plateau, although the repetitive AP firing pattern contains a larger number of APs (see Fig. 14). This phenomenon is L-type VSCC specific, since with P/Q-type VSCCs on the soma instead of L-type VSCCs, the integral of Ca^{2+} current in response to above two waveforms is similar ($I_{repetitive\ APs\ 2}/I_{plateau}$ = 102% (see Fig. 15)). We also examined the properties of the L-type VSCC that contribute to differentiating different firing patterns. It was found that the relatively low activation membrane potential together with slow activation rate contribute to this property of L-type VSCCs.

Since it has been suggested that nuclear Ca^{2+} elevation plays a critical role in triggering activity-dependent gene expression, we sought to determine whether L-type

mediated – nuclear Ca^{2+} transient also discriminates different firing patterns. Thus, a detailed intracellular Ca^{2+} dynamics model was placed in the soma. Various mechanisms, including Ca^{2+} buffering, Ca^{2+} diffusion, Ca^{2+} release and Ca^{2+} pumps, were placed in cytoplasmic and nuclear compartments respectively according to the literature (See Chapter 2). By adjusting parameter values (such as the diffusion constant of Ca^{2+} in nucleus), we were able to reproduce most features of cytoplasmic and nuclear Ca^{2+} dynamics in response to a single AP, such as the latencies and decay time constants (see Table 3). After reproducing Ca^{2+} dynamics in response to a single AP, we predicted intracellular Ca^{2+} dynamics in response to different firing patterns. Consistent with experimental data, it was found that intracellular Ca^{2+} stores play an important role in nuclear Ca^{2+} elevation in response to either a single AP or tetanic synaptic stimulation. Most interestingly, simulated nuclear Ca^{2+} dynamics mediated by L-type VSCCs can differentiate different firing patterns (see Fig. 16). The results suggest that L-type VSCCs have specific kinetic properties, which together with their somatic distribution, makes them able to distinguish different types of synaptic stimuli in terms of nuclear Ca^{2+} transients.

The simulation results described above support the model for signal transduction from the synapse to the nucleus illustrated in Fig. 1.1. Synaptic activity causes depolarization of dendrites which propagates to the soma, resulting in somatic membrane potential changes. At the soma, L-type VSCCs, acting as filters, prefer synaptic stimuli and conditions that result in a high depolarization plateau over other types of waveforms including repetitive APs, subthreshold EPSPs, or burst firing. Ca^{2+} influx through L-type VSCCs efficiently causes Ca^{2+} release from Ca^{2+} stores, resulting in enhanced nuclear

Ca^{2+} elevation. Firing patterns are differentiated in terms of the amount of Ca^{2+} influx and the resulting nuclear Ca^{2+} elevation. This may account for how normal synaptic activity is discriminated from activity that leads to gene expression.

To understand how differences in nuclear Ca^{2+} transients may lead to specific programs of gene expression, it is necessary to understand: 1) encoding and decoding strategies that may be used by Ca^{2+}; 2) the characteristics of the intracellular Ca^{2+} transient and Ca^{2+} - sensitive transcriptional factors. It is well known that abundant information is encoded in Ca^{2+} signals (Berridge, 1998). Studies suggest that information might be encoded by the *amplitude, duration, frequency* and *spatial localization* of intracellular Ca^{2+} transients (Bading et al., 1997; Bito et al., 1997; Dolmetsch et al., 1998; Finkbeiner and Greenberg, 1998). Some transcription factors, such as c-Jun N-terminal kinase (JNK), have been reported to be sensitive to the amplitude and duration of Ca^{2+} signals (Dolmetsch et al., 1997). With regard to frequency, Dolmetsch et al. (1998) reported that rapid oscillations activate NF-AT, Oct/OAP and NF-kB, whereas infrequent oscillations activate only NF-kB. Moreover, direct in vitro experiments and computer simulation studies suggest that CaMKII could act as a frequency decoder for intracellular Ca^{2+} signaling (De Koninck and Schulman, 1998; Hanson et al., 1994). Recent studies show that cytoplasmic and nuclear Ca^{2+} signals activate distinct mechanisms of transcriptional control (reviewed in Bading et al., 1997). The SRF-linked pathway that is triggered by cytoplasmic Ca^{2+} elevation mediates SRE-dependent transcriptional activation in AtT20 cells and in primary hippocampal neurons, whereas nuclear Ca^{2+} elevation is required for CRE-dependent transcription.

Interestingly, activators of gene expression, such as NF-kB, NF-AT (Dolmetsch et al., 1998) and CaMKII (De Koninck and Schulman, 1998), that have been reported to be sensitive to the intracellular Ca^{2+} oscillation frequency, have one common feature: their ability to be autonomous of Ca^{2+} after activation. How long they could remain active after intracellular Ca^{2+} concentration decreases determines the threshold frequency they decode. Activation of NF-kB, NF-AT, and Oct/OAP is mediated by a Ca^{2+}-dependent phosphatase called calcineurin. After dephosphorylation by calcineurin, active subunits dissociate from these transcription factors and migrate to the nucleus. Gene expression keeps on going as long as active subunits remain in the nucleus. NF-AT returns to the cytoplasm rapidly (~ one min) after rephosphorylation, whereas NF-kB returns much more slowly (>16 min after a single spike). So NF-AT needs higher frequency oscillation to be activated, whereas infrequent Ca^{2+} oscillation is enough to induce persistent activity of NF-kB (Dolmetsch et al., 1998). With regard to CaMKII, once Ca^{2+}/CaM binds CaMKII, the kinase not only phosphorylates its target substrates but also autophosphorylates its own auto-inhibitory domain. Autophosphorylation increases its CaM affinity from 45 nM to 60 pM, and thus prolongs the binding of CaM to over 3 s even when free Ca^{2+} is reduced to basal level. Moreover, autophosphorylation disrupts the function of the auto-inhibitory domain so that the kinase remains partially active (autonomous of Ca^{2+}) even after Ca^{2+}/CaM dissociates and until the site is dephosphorylated (reviewed in Heist et al. 1998).

Interestingly, these Ca^{2+} frequency-sensitive activators of gene expression are all localized in the cytoplasm (Dolmetsch et al., 1998; Heist et al., 1998; Meberg et al., 1996). Whereas, till now, there is no report about the frequency sensitivity of CaM kinase

IV, which is predominantly localized in the nucleus (Nakamura et al., 1995; Jensen et al., 1991) and has been suggested to be the nuclear mediator of Ca^{2+}-regulated transcription (Hardingham et al., 1999; Chawla et al., 1998). In contrast to activation of CaMKII which only needs Ca^{2+} and CaM, regulation of CaMKIV involves several phosphorylation steps that require not only Ca^{2+}/CaM but also other activated CaMK kinase (reviewed in (Heist and Schulman, 1998)). Ca^{2+}/CaM directly activate CaMK kinase, which in turn phosphorylates and upregulates CaMKIV. Ca^{2+}/CaM must be bound to CaMKIV when it is phosphorylated by activated CaMK kinase. This requirement for the phosphorylation of CaMKIV may make activation steeply dependent on the concentration of Ca^{2+}/CaM, which may make CaMKIV more sensitive to duration and amplitude of nuclear Ca^{2+} elevation, instead of frequency.

Experimental data and simulation results show that cytoplasmic Ca^{2+} and nuclear Ca^{2+} transients have different kinetics (see Table 3). The cytoplasmic Ca^{2+} transient has relatively fast kinetics (see Table 3), which makes it tend to oscillate in response to a repetitive stimulus. On the other hand, the nuclear Ca^{2+} transient has a much slower decay time constant (see Table 3) and would be a better integrator. Interestingly, consistent with the kinetics of the cytoplasmic Ca^{2+} transient, its downstream effectors, those cytoplasmic distributed Ca^{2+}-sensitive activators of gene expression described above are reported to be sensitive to the frequency of Ca^{2+} oscillation. While consistent with the slow kinetics of the nuclear Ca^{2+} transient, properties of CaMK IV, which is localized in nucleus, make it more sensitive to the amplitude and duration instead of frequency.

4.2 Is the simple structure of our model enough to represent the complex properties of hippocampal CA1 neurons?

Neurons have a very complex array of axonal and dendritic processes. In contrast, our cell model only contains 2 primary dendrites, one soma and one axon. Can such simple structure represent most features of a real neuron, especially when firing patterns induced by synaptic activity are concerned? Many recent studies have addressed this important question and suggest that compartmental models, first developed by Rall in 1960s, provide a practical approach and a sound basis for representing dendritic function (Cook and Johnston, 1997; Cook and Johnston, 1999; Jaffe and Carnevale, 1999; Mainen and Sejnowski, 1996; Shepherd, 1999). The influence of a synaptic current on the soma could be represented by the transfer impedance, which reflects how a current applied at one location affects membrane potential at other locations. Simulation studies by (Jaffe and Carnevale, 1999) in 4 reconstructed CA1 pyramidal cell models suggest that the transfer impedance decreases with distance from the soma but second- or higher order dendritic branches produce very little further decline. Their results suggest that a synaptic current that enters anywhere along a terminal branch will produce almost the same PSP at the soma regardless of its exact location on that branch. So moving all synaptic inputs to the primary dendrites and using two cylinders instead of reconstructed dendritic processes to represent the complex dendritic structure of hippocampal CA1 neurons should not have much effect on postsynaptic membrane potential at the soma. Moreover, studies by Mainen and Sejnowski (1996) and Pinsky and Rinzel (1994) show that the full range of regular spiking responses, adaptation, after-depolarization, and repetitive

bursting observed in recordings and in models of reconstructed pyramidal cells could be reproduced in a model with only two compartments.

To simplify our model we have used very few synapses with strong synaptic conductances, in contrast to the situation in vivo where many relatively weak synapses are present. Therefore, a second major question is whether a few synapses with adjustable synaptic conductances on the apical dendrites can represent thousands of synapses distributed on dendritic processes? The passive electrotonic structure of dendrites makes synaptic inputs from distal dendritic locations suffer considerable attenuation on the way to the soma (Mainen and Sejnowski, 1996). Or in other words, with only passive dendrites, the effect of a synaptic input on the soma depends on its dendritic location. Hence, besides synapse strength, with passive dendrites, synapse location is an important component of the synaptic signal. Experimental evidence established that the dendrites of central neurons contain a complex array of voltage-gated channels (Hoffman et al., 1997; Johnston et al., 1999). Experimental and modeling studies suggest that sodium current boosts the amplitude of distal synaptic EPSPs measured at the soma (Lipowsky et al., 1996; Stuart and Sakmann, 1995). Furthermore, studies by (Cook and Johnston, 1997; Cook and Johnston, 1999) suggest that the active property of dendrites minimizes the location-dependent variability of the synaptic inputs. Thus, a few synapses on the main branch of apical dendrites should still be able to reproduce most features of synaptic activity.

4.3 Shortcomings of the intracellular Ca^{2+} model

Although the current intracellular Ca^{2+} model reproduces important kinetic properties of cytoplasmic and nuclear Ca^{2+} dynamics in response to single AP, there are some shortcomings that could be compensated in the future.

One-dimensional model without longitudinal diffusion

Because of the limitation of the current NEURON version, the intracellular Ca^{2+} model is a one-dimensional cylindrical model without longitudinal diffusion of Ca^{2+} from one compartment to another. Without longitudinal diffusion, it is not possible to examine the contribution of dendritic P/Q-type VSCCs to the nuclear Ca^{2+} transient since the endogenous P/Q-type VSCCs are distributed on dendrites and axonal terminals instead of soma. Although NEURON has tools to deal with longitudinal diffusion, they are currently not stable and could not reflect the real situation (personal communication with Dr. Carnevale). Moreover, because of time limitation and what we are most interested in is L-type VSCCs which are distributed on the neuronal soma, longitudinal diffusion was not implemented.

IP_3 receptors

It has been suggested that intracellular Ca^{2+} stores play an important role in intracellular Ca^{2+} dynamics (Berridge, 1998; Garaschuk et al., 1997). There are two types of Ca^{2+}-sensitive Ca^{2+} channels, IP_3Rs and RyRs, distributed on Ca^{2+} stores in many kinds of brain neurons including hippocampal CA1 neurons (Verkhratsky and Petersen, 1998). As has been discussed in Chapter 1 and Chapter 2, for simplicity, only RyRs were taken into consideration in the intracellular Ca^{2+} dynamics model. IP_3Rs are sensitive to

both IP_3 and Ca^{2+} (Bezprozvanny et al., 1991). To include IP_3Rs, the dynamic change of IP_3 within cytoplasm after synaptic stimulation has to be considered, which makes the story even more complicated since we would also need to model the characteristics and distribution of metabotropic receptors that are coupled to phospholipase C activity. Currently, considerably less is known about the kinetic behavior of metabotropic receptors and their localization as compared with ionotropic receptors. Since IP_3Rs are sensitive to Ca^{2+} and similar to RyRs they also exhibit the CICR phenomenon, it is reasonable to combine IP_3Rs into RyRs, by assuming that the intracellular IP_3 level does not change dramatically following neuronal electrical activity.

Exogenous Ca^{2+} *buffer (fluo-3)*

In the Ca^{2+} imaging experiments, Ca^{2+} indicator fluo-3 was loaded into the cell. The low capacity, affinity and mobility of the endogenous Ca^{2+} buffer makes it possible for relatively small amounts of exogenous Ca^{2+} buffers, such as fluo-3, to exert a significant influence on the characteristics of the Ca^{2+} concentration signal (Neher and Augustine, 1992). In our model, exogenous Ca^{2+} buffer was not included. Including Ca^{2+} indicator could give us a better understanding of experimental data and the effect of Ca^{2+} indicator on intracellular Ca^{2+} dynamics. The following method could be used to add Ca^{2+} indicator fluo-3 into the model in the future.

To model the effect of Ca^{2+} indicator Fluo-3, the following assumptions were made. a) Since the on-binding rate of fluo-3 (1000 /mM-ms) is more than 1000 times faster than other processes, we can assume that it is always in equilibrium at each time step. b) We assume that the diffusion constant for free fluo-3 and Ca-bound fluo-3 are the

same, so the total amount of fluo-3 remain constant in each shell. So the Ca^{2+}-bound fluo-3 concentration at each shell can be calculated by the following equilibrium equation:

$$Ca_{fluo} = Totalfluo - fluo = Totalfluo/(1 + \frac{1}{K_d Ca})$$

K_d = 800 nM is the dissociation constant of fluo-3 to Ca^{2+} (Minta et al., 1989). In each shell the Ca^{2+}-bound fluo-3 concentration Ca_{fluo} equals total calcium concentration (including free Ca^{2+} and bound Ca^{2+}) minus free Ca^{2+} and Ca^{2+} which binds endogenous buffer, i.e.

$$Ca_{fluo} = TotalCa - Cabuffer - Ca$$

Combining above two equations, we can easily get *Ca* and *Cafluo* if *TotalCa* concentration in each shell at any moment is known.

$$a = K_d$$
$$b = K_d Ca_{buffer} - K_d TotalCa + 1 + TotalfluoK_d$$
$$c = Ca_{buffer} - TotalCa$$

$$Ca = \frac{-b + \sqrt{b^2 - 4ac}}{2a}$$

The new *TotalCa* at any moment is first calculated by the following equation.

$$TotalCa_{t+\Delta t} = TotalCa_t + (diffusion_{ca} + diffusion_{Cafluo} + buffer) \cdot \Delta t$$

References

Acerbo, P., and Nobile, M. (1994). Temperature dependence of multiple high voltage activated Ca^{2+} channels in chick sensory neurones. Eur Biophys J *23*, 189-95.

Azouz, R., Alroy, G., and Yaari, Y. (1997). Modulation of endogenous firing patterns by osmolarity in rat hippocampal neurones. J Physiol (Lond) *502*, 175-87.

Azouz, R., Jensen, M. S., and Yaari, Y. (1996). Ionic basis of spike after-depolarization and burst generation in adult rat hippocampal CA1 pyramidal cells. J Physiol (Lond) *492*, 211-23.

Backx, P. H., de Tombe, P. P., Van Deen, J. H., Mulder, B. J., and ter Keurs, H. E. (1989). A model of propagating calcium-induced calcium release mediated by calcium diffusion. J Gen Physiol *93*, 963-77.

Bacskai, B. J., Hochner, B., Mahaut-Smith, M., Adams, S. R., Kaang, B. K., Kandel, E. R., and Tsien, R. Y. (1993). Spatially resolved dynamics of cAMP and protein kinase A subunits in Aplysia sensory neurons. Science *260*, 222-6.

Bading, H., Ginty, D. D., and Greenberg, M. E. (1993). Regulation of gene expression in hippocampal neurons by distinct calcium signaling pathways. Science *260*, 181-6.

Bading, H., and Greenberg, M. E. (1991). Stimulation of protein tyrosine phosphorylation by NMDA receptor activation. Science *253*, 912-4.

Bading, H., Hardingham, G. E., Johnson, C. M., and Chawla, S. (1997). Gene regulation by nuclear and cytoplasmic calcium signals. Biochem Biophys Res Commun *236*, 541-3.

Badminton, M. N., Kendall, J. M., Rembold, C. M., and Campbell, A. K. (1998). Current evidence suggests independent regulation of nuclear calcium. Cell Calcium *23*, 79-86.

Berridge, M. J. (1998). Neuronal calcium signaling. Neuron *21*, 13-26.

Bezprozvanny, I., Watras, J., and Ehrlich, B. E. (1991). Bell-shaped calcium-response curves of Ins(1,4,5)P3- and calcium-gated channels from endoplasmic reticulum of cerebellum. Nature *351*, 751-4.

Bito, H., Deisseroth, K., and Tsien, R. W. (1997). Ca^{2+}-dependent regulation in neuronal gene expression. Curr Opin Neurobiol *7*, 419-29.

Borst, J. G., and Sakmann, B. (1996). Calcium influx and transmitter release in a fast CNS synapse [see comments]. Nature *383*, 431-4.

Bourinet, E., Soong, T. W., Sutton, K., Slaymaker, S., Mathews, E., Monteil, A., Zamponi, G. W., Nargeot, J., and Snutch, T. P. (1999). Splicing of alpha 1A subunit gene generates phenotypic variants of P- and Q-type calcium channels. Nat Neurosci *2*, 407-15.

Brehm, P., and Eckert, R. (1978). Calcium entry leads to inactivation of calcium channel in Paramecium. Science *202*, 1203-6.

Brown, J. R., Ye, H., Bronson, R. T., Dikkes, P., and Greenberg, M. E. (1996). A defect in nurturing in mice lacking the immediate early gene fosB. Cell *86*, 297-309.

Carrion, A. M., Link, W. A., Ledo, F., Mellstrom, B., and Naranjo, J. R. (1999). DREAM is a Ca^{2+}-regulated transcriptional repressor [see comments]. Nature *398*, 80-4.

Chavis, P., Fagni, L., Lansman, J. B., and Bockaert, J. (1996). Functional coupling between ryanodine receptors and L-type calcium channels in neurons. Nature *382*, 719-22.

Christie, B. R., Stellwagen, D., and Abraham, W. C. (1995). Reduction of the threshold for long-term potentiation by prior theta- frequency synaptic activity. Hippocampus *5*, 52-9.

Clements, J. D., Lester, R. A., Tong, G., Jahr, C. E., and Westbrook, G. L. (1992). The time course of glutamate in the synaptic cleft. Science *258*, 1498-501.

Cohen, A. S., Coussens, C. M., Raymond, C. R., and Abraham, W. C. (1999). Long-lasting increase in cellular excitability associated with the priming of LTP induction in rat hippocampus. J Neurophysiol *82*, 3139-48.

Cook, E. P., and Johnston, D. (1997). Active dendrites reduce location-dependent variability of synaptic input trains. J Neurophysiol *78*, 2116-28.

Cook, E. P., and Johnston, D. (1999). Voltage-dependent properties of dendrites that eliminate location- dependent variability of synaptic input. J Neurophysiol *81*, 535-43.

Crank, J. (1975). The mathematics of diffusion. Oxford, [Eng] : Clarendon Press, 1975. Edition: 2d ed.

Crill, W. E. (1996). Persistent sodium current in mammalian central neurons. Annu Rev Physiol *58*, 349-62.

Davies, P. J., Ireland, D. R., and McLachlan, E. M. (1996). Sources of Ca^{2+} for different Ca(2+)-activated K+ conductances in neurones of the rat superior cervical ganglion. J Physiol (Lond) *495*, 353-66.

De Koninck, P., and Schulman, H. (1998). Sensitivity of CaM kinase II to the frequency of Ca^{2+} oscillations [see comments]. Science *279*, 227-30.

De Schutter, E. (1998). Detailed model of ryanodine receptor-mediatedcalcium release in Purkinje cells. In Computational Neuroscience:Trends in research, J. M. Bower, ed. (New York: Plenum Publishing Corporation), pp. 161-166.

Deisseroth, K., Bito, H., and Tsien, R. W. (1996). Signaling from synapse to nucleus: postsynaptic CREB phosphorylation during multiple forms of hippocampal synaptic plasticity. Neuron *16*, 89-101.

Destexhe, A. (1997). Conductance-based integrate-and-fire models. Neural Comput *9*, 503-14.

Destexhe, A., Mainen, Z. F., and Sejnowski, T. J. (1998). Kinetic Models of Synaptic Transmission. In Methods in Neuronal Modeling, C. Koch and I. Segev, eds. (Cambridge, MA: MIT Press), pp. P. 1-25.

Destexhe, A., Mainen, Z. F., and Sejnowski, T. J. (1994). Synthesis of models for excitable membranes, synaptic transmission and neuromodulation using a common kinetic formalism. J Comput Neurosci *1*, 195-230.

Dolmetsch, R. E., Lewis, R. S., Goodnow, C. C., and Healy, J. I. (1997). Differential activation of transcription factors induced by Ca^{2+} response amplitude and duration [see comments] [published erratum appears in Nature 1997 Jul 17;388(6639):308]. Nature *386*, 855-8.

Dolmetsch, R. E., Xu, K., and Lewis, R. S. (1998). Calcium oscillations increase the efficiency and specificity of gene expression [see comments]. Nature *392*, 933-6.

Dove, L. S., Abbott, L. C., and Griffith, W. H. (1998). Whole-cell and single-channel analysis of P-type calcium currents in cerebellar Purkinje cells of leaner mutant mice. J Neurosci *18*, 7687-99.

Engel, J., Schultens, H. A., and Schild, D. (1999). Small conductance potassium channels cause an activity-dependent spike frequency adaptation and make the transfer function of neurons logarithmic. Biophys J *76*, 1310-9.

Ertel, E. A., Campbell, K. P., Harpold, M. M., Hofmann, F., Mori, Y., Perez-Reyes, E., Schwartz, A., Snutch, T. P., Tanabe, T., Birnbaumer, L., Tsien, R. W., and Catterall, W. A. (2000). Nomenclature of voltage-gated calcium channels [letter]. Neuron *25*, 533-5.

Finkbeiner, S., and Greenberg, M. E. (1998). Ca^{2+} channel-regulated neuronal gene expression. J Neurobiol *37*, 171-89.

Fleidervish, I. A., Friedman, A., and Gutnick, M. J. (1996). Slow inactivation of Na+ current and slow cumulative spike adaptation in mouse and guinea-pig neocortical neurones in slices [published erratum appears in J Physiol (Lond) 1996 Aug 1;494(Pt 3):907]. J Physiol (Lond) *493*, 83-97.

Forsythe, I. D., Tsujimoto, T., Barnes-Davies, M., Cuttle, M. F., and Takahashi, T. (1998). Inactivation of presynaptic calcium current contributes to synaptic depression at a fast central synapse. Neuron *20*, 797-807.

Fox, J. L., Burgstahler, A. D., and Nathanson, M. H. (1997). Mechanism of long-range Ca^{2+} signalling in the nucleus of isolated rat hepatocytes. Biochem J *326*, 491-5.

Franceschetti, S., Guatteo, E., Panzica, F., Sancini, G., Wanke, E., and Avanzini, G. (1995). Ionic mechanisms underlying burst firing in pyramidal neurons: intracellular study in rat sensorimotor cortex. Brain Res *696*, 127-39.

French, C. R., Sah, P., Buckett, K. J., and Gage, P. W. (1990). A voltage-dependent persistent sodium current in mammalian hippocampal neurons. J Gen Physiol *95*, 1139-57.

Frey, U., Krug, M., Reymann, K. G., and Matthies, H. (1988). Anisomycin, an inhibitor of protein synthesis, blocks late phases of LTP phenomena in the hippocampal CA1 region in vitro. Brain Res *452*, 57-65.

Frey, U., and Morris, R. G. (1998). Synaptic tagging: implications for late maintenance of hippocampal long- term potentiation [see comments]. Trends Neurosci *21*, 181-8.

Garaschuk, O., Yaari, Y., and Konnerth, A. (1997). Release and sequestration of calcium by ryanodine-sensitive stores in rat hippocampal neurones. J Physiol (Lond) *502*, 13-30.

Ghosh, A., and Greenberg, M. E. (1995). Calcium signaling in neurons: molecular mechanisms and cellular consequences. Science *268*, 239-47.

Goldbeter, A., Dupont, G., and Berridge, M. J. (1990). Minimal model for signal-induced Ca^{2+} oscillations and for their frequency encoding through protein phosphorylation. Proc Natl Acad Sci U S A *87*, 1461-5.

Grabner, M., Dirksen, R. T., Suda, N., and Beam, K. G. (1999). The II-III loop of the skeletal muscle dihydropyridine receptor is responsible for the Bi-directional coupling with the ryanodine receptor. J Biol Chem *274*, 21913-9.

Gutfreund, Y., yarom, Y., and Segev, I. (1995). Subthreshold oscillations and resonant frequency in guinea-pig cortical neurons: physiology and modelling. J Physiol (Lond) *483*, 621-40.

Gyorke, S., and Fill, M. (1993). Ryanodine receptor adaptation: control mechanism of Ca(2+)-induced Ca^{2+} release in heart [see comments]. Science *260*, 807-9.

Halliwell, J. V., and Adams, P. R. (1982). Voltage-clamp analysis of muscarinic excitation in hippocampal neurons. Brain Res *250*, 71-92.

Hanson, P. I., Meyer, T., Stryer, L., and Schulman, H. (1994). Dual role of calmodulin in autophosphorylation of multifunctional CaM kinase may underlie decoding of calcium signals. Neuron *12*, 943-56.

Hardingham, G. E., Chawla, S., Cruzalegui, F., and Bading, H. (1999). Control of recruitment and transcription-activating function of CBP determines gene regulation by NMDA receptors and L-type calcium channels. Neurosci. Meeting Abst. *25*, 1961.

Hardingham, G. E., Chawla, S., Johnson, C. M., and Bading, H. (1997). Distinct functions of nuclear and cytoplasmic calcium in the control of gene expression. Nature *385*, 260-5.

Heist, E. K., and Schulman, H. (1998). The role of Ca^{2+}/calmodulin-dependent protein kinases within the nucleus. Cell Calcium *23*, 103-14.

Heist, E. K., Srinivasan, M., and Schulman, H. (1998). Phosphorylation at the nuclear localization signal of Ca^{2+}/calmodulin- dependent protein kinase II blocks its nuclear targeting. J Biol Chem *273*, 19763-71.

Hell, J. W., Westenbroek, R. E., Warner, C., Ahlijanian, M. K., Prystay, W., Gilbert, M. M., Snutch, T. P., and Catterall, W. A. (1993). Identification and differential subcellular localization of the neuronal class C and class D L-type calcium channel alpha 1 subunits. J Cell Biol *123*, 949-62.

Helmchen, F., Imoto, K., and Sakmann, B. (1996). Ca^{2+} buffering and action potential-evoked Ca^{2+} signaling in dendrites of pyramidal neurons. Biophys J *70*, 1069-81.

Hessler, N. A., Shirke, A. M., and Malinow, R. (1993). The probability of transmitter release at a mammalian central synapse. Nature *366*, 569-72.

Hines, M. L., and Carnevale, N. T. (2000). Expanding NEURON's repertoire of mechanisms with NMODL [In Process Citation]. Neural Comput *12*, 995-1007.

Hines, M. L., and Carnevale, N. T. (1997). The NEURON simulation environment. Neural Comput *9*, 1179-209.

Hirschberg, B., Maylie, J., Adelman, J. P., and Marrion, N. V. (1998). Gating of recombinant small-conductance Ca-activated K+ channels by calcium. J Gen Physiol *111*, 565-81.

Hofer, G. F., Hohenthanner, K., Baumgartner, W., Groschner, K., Klugbauer, N., Hofmann, F., and Romanin, C. (1997). Intracellular Ca^{2+} inactivates L-type Ca^{2+} channels with a Hill coefficient of approximately 1 and an inhibition constant of approximately 4 microM by reducing channel's open probability. Biophys J *73*, 1857-65.

Hoffman, D. A., Magee, J. C., Colbert, C. M., and Johnston, D. (1997). K+ channel regulation of signal propagation in dendrites of hippocampal pyramidal neurons [see comments]. Nature *387*, 869-75.

Imredy, J. P., and Yue, D. T. (1994). Mechanism of Ca(2+)-sensitive inactivation of L-type Ca^{2+} channels. Neuron *12*, 1301-18.

Jacobs, J. M., and Meyer, T. (1997). Control of action potential-induced Ca^{2+} signaling in the soma of hippocampal neurons by Ca^{2+} release from intracellular stores. J Neurosci *17*, 4129-35.

Jaffe, D. B., and Carnevale, N. T. (1999). Passive normalization of synaptic integration influenced by dendritic architecture. J Neurophysiol *82*, 3268-85.

Jensen, K. F., Ohmstede, C. A., Fisher, R. S., and Sahyoun, N. (1991). Nuclear and axonal localization of Ca^{2+}/calmodulin-dependent protein kinase type Gr in rat cerebellar cortex. Proc Natl Acad Sci U S A *88*, 2850-3.

Jensen, M. S., Azouz, R., and Yaari, Y. (1996). Spike after-depolarization and burst generation in adult rat hippocampal CA1 pyramidal cells. J Physiol (Lond) *492*, 199-210.

Johnston, D., Hoffman, D. A., Colbert, C. M., and Magee, J. C. (1999). Regulation of back-propagating action potentials in hippocampal neurons. Curr Opin Neurobiol *9*, 288-92.

Jun, K., Piedras-Renteria, E. S., Smith, S. M., Wheeler, D. B., Lee, S. B., Lee, T. G., Chin, H., Adams, M. E., Scheller, R. H., Tsien, R. W., and Shin, H. S. (1999). Ablation of P/Q-type Ca(2+) channel currents, altered synaptic transmission, and progressive ataxia in mice lacking the alpha(1A)- subunit. Proc Natl Acad Sci U S A *96*, 15245-50.

Kargacin, G. J. (1994). Calcium signaling in restricted diffusion spaces. Biophys J *67*, 262-72.

Kawasaki, H., Morooka, T., Shimohama, S., Kimura, J., Hirano, T., Gotoh, Y., and Nishida, E. (1997). Activation and involvement of p38 mitogen-activated protein kinase in glutamate-induced apoptosis in rat cerebellar granule cells. J Biol Chem *272*, 18518-21.

Kirkpatrick, K., and Bourque, C. W. (1996). Activity dependence and functional role of the apamin-sensitive K+ current in rat supraoptic neurones in vitro. J Physiol (Lond) *494*, 389-98.

Lanini, L., Bachs, O., and Carafoli, E. (1992). The calcium pump of the liver nuclear membrane is identical to that of endoplasmic reticulum. J Biol Chem *267*, 11548-52.

Lee, A., Wong, S. T., Gallagher, D., Li, B., Storm, D. R., Scheuer, T., and Catterall, W. A. (1999). Ca^{2+}/calmodulin binds to and modulates P/Q-type calcium channels [see comments]. Nature *399*, 155-9.

Lipowsky, R., Gillessen, T., and Alzheimer, C. (1996). Dendritic Na+ channels amplify EPSPs in hippocampal CA1 pyramidal cells. J Neurophysiol *76*, 2181-91.

Llinas, R., and Moreno, H. (1998). Local Ca^{2+} signaling in neurons. Cell Calcium *24*, 359-66.

Mainen, Z. F., and Sejnowski, T. J. (1996). Influence of dendritic structure on firing pattern in model neocortical neurons. Nature *382*, 363-6.

Mainen, Z. F., and Sejnowski, T. J. (1998). Modeling Active Dendritic Processes in Pyramidal Neurons. In Methods in Neural modeling, C. Koch and I. Segev, eds. (Cambridge, MA: MIT Press).

Martin, K. C., Michael, D., Rose, J. C., Barad, M., Casadio, A., Zhu, H., and Kandel, E. R. (1997). MAP kinase translocates into the nucleus of the presynaptic cell and is required for long-term facilitation in Aplysia. Neuron *18*, 899-912.

Martone, M. E., Zhang, Y., Simpliciano, V. M., Carragher, B. O., and Ellisman, M. H. (1993). Three-dimensional visualization of the smooth endoplasmic reticulum in Purkinje cell dendrites. J Neurosci *13*, 4636-46.

Mayford, M., Wang, J., Kandel, E. R., and O'Dell, T. J. (1995). CaMKII regulates the frequency-response function of hippocampal synapses for the production of both LTD and LTP. Cell *81*, 891-904.

McDonald, T. F., Pelzer, S., Trautwein, W., and Pelzer, D. J. (1994). Regulation and modulation of calcium channels in cardiac, skeletal, and smooth muscle cells. Physiol Rev *74*, 365-507.

Meberg, P. J., Kinney, W. R., Valcourt, E. G., and Routtenberg, A. (1996). Gene expression of the transcription factor NF-kappa B in hippocampus: regulation by synaptic activity. Brain Res Mol Brain Res *38*, 179-90.

Meldolesi, J. (1998). Calcium signalling. Oscillation, activation, expression [news; comment]. Nature *392*, 863, 865-6.

Mermelstein, P. G., Bito, H., Deisseroth, K., and Tsien, R. W. (2000). Critical dependence of cAMP response element-binding protein phosphorylation on L-type

calcium channels supports a selective response to EPSPs in preference to action potentials. J Neurosci *20*, 266-73.

Mermelstein, P. G., Foehring, R. C., Tkatch, T., Song, W. J., Baranauskas, G., and Surmeier, D. J. (1999). Properties of Q-type calcium channels in neostriatal and cortical neurons are correlated with beta subunit expression. J Neurosci *19*, 7268-77.

Mickus, T., Jung, H., and Spruston, N. (1999). Properties of slow, cumulative sodium channel inactivation in rat hippocampal CA1 pyramidal neurons. Biophys J *76*, 846-60.

Mickus, T., Jung, H. Y., and Spruston, N. (1999). Slow sodium channel inactivation in CA1 pyramidal cells. Ann N Y Acad Sci *868*, 97-101.

Minta, A., Kao, J. P., and Tsien, R. Y. (1989). Fluorescent indicators for cytosolic calcium based on rhodamine and fluorescein chromophores. J Biol Chem *264*, 8171-8.

Mori, Y., Friedrich, T., Kim, M. S., Mikami, A., Nakai, J., Ruth, P., Bosse, E., Hofmann, F., Flockerzi, V., Furuichi, T., and et al. (1991). Primary structure and functional expression from complementary DNA of a brain calcium channel. Nature *350*, 398-402.

Murphy, T. H., Worley, P. F., and Baraban, J. M. (1991). L-type voltage-sensitive calcium channels mediate synaptic activation of immediate early genes. Neuron *7*, 625-35.

Nakai, J., Dirksen, R. T., Nguyen, H. T., Pessah, I. N., Beam, K. G., and Allen, P. D. (1996). Enhanced dihydropyridine receptor channel activity in the presence of ryanodine receptor. Nature *380*, 72-5.

Nakai, J., Sekiguchi, N., Rando, T. A., Allen, P. D., and Beam, K. G. (1998). Two regions of the ryanodine receptor involved in coupling with L-type Ca^{2+} channels. J Biol Chem *273*, 13403-6.

Nakamura, Y., Okuno, S., Sato, F., and Fujisawa, H. (1995). An immunohistochemical study of Ca^{2+}/calmodulin-dependent protein kinase IV in the rat central nervous system: light and electron microscopic observations. Neuroscience *68*, 181-94.

Nakazawa, H., and Murphy, T. H. (1999). Activation of nuclear calcium dynamics by synaptic stimulation in cultured cortical neurons. J Neurochem *73*, 1075-83.

Naraghi, M., and Neher, E. (1997). Linearized buffered Ca^{2+} diffusion in microdomains and its implications for calculation of $[Ca^{2+}]$ at the mouth of a calcium channel. J Neurosci *17*, 6961-73.

Neely, A., and Lingle, C. J. (1992). Two components of calcium-activated potassium current in rat adrenal chromaffin cells. J Physiol *453*, 97-131.

Neher, E., and Augustine, G. J. (1992). Calcium gradients and buffers in bovine chromaffin cells. J Physiol (Lond) *450*, 273-301.

Nguyen, P. V., Abel, T., and Kandel, E. R. (1994). Requirement of a critical period of transcription for induction of a late phase of LTP. Science *265*, 1104-7.

O'Malley, D. M. (1994). Calcium permeability of the neuronal nuclear envelope: evaluation using confocal volumes and intracellular perfusion. J Neurosci *14*, 5741-58.

Padua, R. A., Nagy, J. I., and Geiger, J. D. (1996). Subcellular localization of ryanodine receptors in rat brain. Eur J Pharmacol *298*, 185-9.

Pedarzani, P., Krause, M., Haug, T., Storm, J. F., and Stuhmer, W. (1998). Modulation of the Ca^{2+}-activated K+ current sIAHP by a phosphatase- kinase balance under basal conditions in rat CA1 pyramidal neurons. J Neurophysiol *79*, 3252-6.

Peng, Y. (1996). Ryanodine-sensitive component of calcium transients evoked by nerve firing at presynaptic nerve terminals. J Neurosci *16*, 6703-12.

Petersen, O. H., Gerasimenko, O. V., Gerasimenko, J. V., Mogami, H., and Tepikin, A. V. (1998). The calcium store in the nuclear envelope. Cell Calcium *23*, 87-90.

Peterson, B. Z., DeMaria, C. D., Adelman, J. P., and Yue, D. T. (1999). Calmodulin is the Ca^{2+} sensor for Ca^{2+} -dependent inactivation of L- type calcium channels [published erratum appears in Neuron 1999 Apr;22(4):following 893]. Neuron *22*, 549-58.

Pinsky, P. F., and Rinzel, J. (1994). Intrinsic and network rhythmogenesis in a reduced Traub model for CA3 neurons [published erratum appears in J Comput Neurosci 1995 Sep;2(3):275]. J Comput Neurosci *1*, 39-60.

Pittenger, C., and Kandel, E. (1998). A genetic switch for long-term memory. C R Acad Sci III *321*, 91-6.

Poolos, N. P., and Johnston, D. (1999). Calcium-activated potassium conductances contribute to action potential repolarization at the soma but not the dendrites of hippocampal CA1 pyramidal neurons. J Neurosci *19*, 5205-12.

Randall, A., and Tsien, R. W. (1995). Pharmacological dissection of multiple types of Ca^{2+} channel currents in rat cerebellar granule neurons. J Neurosci *15*, 2995-3012.

Regehr, W. G., and Tank, D. W. (1992). Calcium concentration dynamics produced by synaptic activation of CA1 hippocampal pyramidal cells. J Neurosci *12*, 4202-23.

Reyes, M., and Stanton, P. K. (1996). Induction of hippocampal long-term depression requires release of Ca^{2+} from separate presynaptic and postsynaptic intracellular stores. J Neurosci *16*, 5951-60.

Roberts, W. M. (1994). Localization of calcium signals by a mobile calcium buffer in frog saccular hair cells. J Neurosci *14*, 3246-62.

Ryan, T. A., and Smith, S. J. (1995). Vesicle pool mobilization during action potential firing at hippocampal synapses. Neuron *14*, 983-9.

Sabria, J., Pastor, C., Clos, M. V., Garcia, A., and Badia, A. (1995). Involvement of different types of voltage-sensitive calcium channels in the presynaptic regulation of noradrenaline release in rat brain cortex and hippocampus. J Neurochem *64*, 2567-71.

Sacchi, O., Rossi, M. L., and Canella, R. (1995). The slow Ca(2+)-activated K+ current, IAHP, in the rat sympathetic neurone. J Physiol (Lond) *483*, 15-27.

Sah, P., and Bekkers, J. M. (1996). Apical dendritic location of slow afterhyperpolarization current in hippocampal pyramidal neurons: implications for the integration of long- term potentiation. J Neurosci *16*, 4537-42.

Sah, P., and Clements, J. D. (1999). Photolytic manipulation of $[Ca^{2+}]i$ reveals slow kinetics of potassium channels underlying the afterhyperpolarization in hippocampal pyramidal neurons. J Neurosci *19*, 3657-64.

Santella, L., and Carafoli, E. (1997). Calcium signaling in the cell nucleus [published erratum appears in FASEB J 1997 Dec;11(14):1330]. Faseb J *11*, 1091-109.

Schwarz, J. R., and Eikhof, G. (1987). Na currents and action potentials in rat myelinated nerve fibres at 20 and 37 degrees C. Pflugers Arch *409*, 569-77.

Sham, J. S., Cleemann, L., and Morad, M. (1995). Functional coupling of Ca^{2+} channels and ryanodine receptors in cardiac myocytes. Proc Natl Acad Sci U S A *92*, 121-5.

Shao, L. R., Halvorsrud, R., Borg-Graham, L., and Storm, J. F. (1999). The role of BK-type Ca^{2+}-dependent K+ channels in spike broadening during repetitive firing in rat hippocampal pyramidal cells. J Physiol (Lond) *521 Pt 1*, 135-46.

Shepherd. (1999). Fundamental Neuroscience.

Sinha, S. R., Wu, L. G., and Saggau, P. (1997). Presynaptic calcium dynamics and transmitter release evoked by single action potentials at mammalian central synapses. Biophys J *72*, 637-51.

Smith, A. B., and Cunnane, T. C. (1996). Ryanodine-sensitive calcium stores involved in neurotransmitter release from sympathetic nerve terminals of the guinea-pig. J Physiol (Lond) *497*, 657-64.

Sossin, W. S. (1997). An autonomous kinase generated during long-term facilitation in Aplysia is related to the Ca(2+)-independent protein kinase C Apl II. Learn Mem *3*, 389-401.

Spruston, N., Jaffe, D. B., and Johnston, D. (1994). Dendritic attenuation of synaptic potentials and currents: the role of passive membrane properties. Trends Neurosci *17*, 161-6.

Spruston, N., Schiller, Y., Stuart, G., and Sakmann, B. (1995). Activity-dependent action potential invasion and calcium influx into hippocampal CA1 dendrites [see comments]. Science *268*, 297-300.

Stea, A., Dubel, S. J., Pragnell, M., Leonard, J. P., Campbell, K. P., and Snutch, T. P. (1993). A beta-subunit normalizes the electrophysiological properties of a cloned N-type Ca^{2+} channel alpha 1-subunit. Neuropharmacology *32*, 1103-16.

Stea, A., Tomlinson, W. J., Soong, T. W., Bourinet, E., Dubel, S. J., Vincent, S. R., and Snutch, T. P. (1994). Localization and functional properties of a rat brain alpha 1A calcium channel reflect similarities to neuronal Q- and P-type channels. Proc Natl Acad Sci U S A *91*, 10576-80.

Stevens, C. F. (1994). CREB and memory consolidation. Neuron *13*, 769-70.

Stocker, M., Krause, M., and Pedarzani, P. (1999). An apamin-sensitive Ca^{2+}-activated K+ current in hippocampal pyramidal neurons. Proc Natl Acad Sci U S A *96*, 4662-7.

Storm, J. F. (1989). An after-hyperpolarization of medium duration in rat hippocampal pyramidal cells. J Physiol (Lond) *409*, 171-90.

Storm, J. F. (1990). Potassium currents in hippocampal pyramidal cells. Prog Brain Res *83*, 161-87.

Stuart, G., and Sakmann, B. (1995). Amplification of EPSPs by axosomatic sodium channels in neocortical pyramidal neurons. Neuron *15*, 1065-76.

Stuart, G., Spruston, N., Sakmann, B., and Hausser, M. (1997). Action potential initiation and backpropagation in neurons of the mammalian CNS. Trends Neurosci *20*, 125-31.

Stuart, G. J., and Sakmann, B. (1994). Active propagation of somatic action potentials into neocortical pyramidal cell dendrites. Nature *367*, 69-72.

Sutton, K. G., McRory, J. E., Guthrie, H., Murphy, T. H., and Snutch, T. P. (1999). P/Q-type calcium channels mediate the activity-dependent feedback of syntaxin-1A. Nature *401*, 800-4.

Traub, R. D., Wong, R. K., Miles, R., and Michelson, H. (1991). A model of a CA3 hippocampal pyramidal neuron incorporating voltage- clamp data on intrinsic conductances. J Neurophysiol *66*, 635-50.

Tsien, R. W., Lipscombe, D., Madison, D. V., Bley, K. R., and Fox, A. P. (1988). Multiple types of neuronal calcium channels and their selective modulation. Trends Neurosci *11*, 431-8.

Usachev, Y. M., and Thayer, S. A. (1997). All-or-none Ca^{2+} release from intracellular stores triggered by Ca^{2+} influx through voltage-gated Ca^{2+} channels in rat sensory neurons. J Neurosci *17*, 7404-14.

Velumian, A. A., and Carlen, P. L. (1999). Differential control of three after-hyperpolarizations in rat hippocampal neurones by intracellular calcium buffering. J Physiol (Lond) *517*, 201-16.

Verkhratsky, A. J., and Petersen, O. H. (1998). Neuronal calcium stores. Cell Calcium *24*, 333-43.

Wang, Y., Rowan, M. J., and Anwyl, R. (1997). Induction of LTD in the dentate gyrus in vitro is NMDA receptor independent, but dependent on Ca^{2+} influx via low-voltage-activated Ca^{2+} channels and release of Ca^{2+} from intracellular stores. J Neurophysiol *77*, 812-25.

Wang, Y., Wu, J., Rowan, M. J., and Anwyl, R. (1996). Ryanodine produces a low frequency stimulation-induced NMDA receptor- independent long-term potentiation in the rat dentate gyrus in vitro. J Physiol (Lond) *495*, 755-67.

Warman, E. N., Durand, D. M., and Yuen, G. L. (1994). Reconstruction of hippocampal CA1 pyramidal cell electrophysiology by computer simulation. J Neurophysiol *71*, 2033-45.

Watanabe, Y., Johnson, R. S., Butler, L. S., Binder, D. K., Spiegelman, B. M., Papaioannou, V. E., and McNamara, J. O. (1996). Null mutation of c-fos impairs structural and functional plasticities in the kindling model of epilepsy. J Neurosci *16*, 3827-36.

Westenbroek, R. E., Hell, J. W., Warner, C., Dubel, S. J., Snutch, T. P., and Catterall, W. A. (1992). Biochemical properties and subcellular distribution of an N-type calcium channel alpha 1 subunit. Neuron *9*, 1099-115.

Westenbroek, R. E., Hoskins, L., and Catterall, W. A. (1998). Localization of Ca^{2+} channel subtypes on rat spinal motor neurons, interneurons, and nerve terminals. J Neurosci *18*, 6319-30.

Westenbroek, R. E., Sakurai, T., Elliott, E. M., Hell, J. W., Starr, T. V., Snutch, T. P., and Catterall, W. A. (1995). Immunochemical identification and subcellular distribution of the alpha 1A subunits of brain calcium channels. J Neurosci *15*, 6403-18.

Williams, M. E., Feldman, D. H., McCue, A. F., Brenner, R., Velicelebi, G., Ellis, S. B., and Harpold, M. M. (1992). Structure and functional expression of alpha 1, alpha 2, and beta subunits of a novel human neuronal calcium channel subtype. Neuron *8*, 71-84.

Xia, X. M., Fakler, B., Rivard, A., Wayman, G., Johnson-Pais, T., Keen, J. E., Ishii, T., Hirschberg, B., Bond, C. T., Lutsenko, S., Maylie, J., and Adelman, J. P. (1998). Mechanism of calcium gating in small-conductance calcium-activated potassium channels. Nature *395*, 503-7.

Yeckel, M. F., Kapur, A., and Johnston, D. (1999). Multiple forms of LTP in hippocampal CA3 neurons use a common postsynaptic mechanism. Nat Neurosci *2*, 625-33.

Yoshida, A., Oda, M., and Ikemoto, Y. (1991). Kinetics of the Ca(2+)-activated K+ channel in rat hippocampal neurons. Jpn J Physiol *41*, 297-315.

Zhang, J. F., Randall, A. D., Ellinor, P. T., Horne, W. A., Sather, W. A., Tanabe, T., Schwarz, T. L., and Tsien, R. W. (1993). Distinctive pharmacology and kinetics of cloned neuronal Ca^{2+} channels and their possible counterparts in mammalian CNS neurons. Neuropharmacology *32*, 1075-88.

Zuhlke, R. D., Pitt, G. S., Deisseroth, K., Tsien, R. W., and Reuter, H. (1999). Calmodulin supports both inactivation and facilitation of L-type calcium channels [see comments]. Nature *399*, 159-62.